Control of Joint Spacing During Fin Development and Regeneration

By

Cristobal Lopez-Jimenez

Thesis Submitted to the Faculty of Graduate and Postdoctoral Studies in Partial Fulfillment of the Requirements for the Degree of

Master of Science

In Biology

Department of Biology
Faculty of Science
University of Ottawa

TABLE OF CONTENTS

LIST OF TABLES

LIST OF FIGURES

LIST OF ABBREVIATIONS

dpf – Days post fertilization

dpa – Days post amputation

hpa – Hours post amputation

Fgf – Fibroblast growth factor

fgfr1 – Fibroblast growth factor receptor-1

Shh – Sonic hedgehog

Shha – Sonic hedgehog a

RA – Retinoic acid

Bmp – Bone morphogenetic protein

Hox – Homeobox gene

Ppmm – Pixels per millimetre

B000 – Time zero, before amputation

A000 – Time zero, after amputation

A028 – Twenty-eight days after amputation

A031 – Thirty-one days after amputation

A035 – Thirty-five days after amputation

A038 – Thirty-eight days after amputation

lof – Long fin mutation

alf – Another long fin mutation

sof – Short fin mutation

cx43 – *Connexin*43 gene mutation

RMSE – Root mean square error

Abstract

The zebrafish (*Danio rerio*) has emerged as a model to study vertebrate development due to rapid ontogenetic processes with external embryonic development. It is also an excellent model to study the mechanisms of regeneration and in this respect, the caudal fin is particularly convenient because it is easily accessible for experimental manipulation. Collection of quantitative data and postulation of theoretical models have become an attractive practice to explain complex biological problems. These models are used to test hypothetical mechanisms and predict results, but they also require calibration and validation with analysis of experimental data. This thesis aims at studying the developmental control of fin joint formation, which determines segment patterns of the rays in the caudal fin of zebrafish, before and after an amputation event, through a computational approach and imaging morpho-dynamics. We used a computational approach based on a quantitative framework developed for the analysis of fish fin development and regeneration and more specifically focused our analysis on the pattern of bone segments forming the ray. This allowed us to generate visual maps of the developing and regenerating caudal fins based on average fin data. The results from our experimental set show that bone segments at the amputation plane are longer after regeneration than segments at the same position in non-amputated fins. We also optimized a previously proposed morphogen driven model for fin growth and regeneration to accurately recreate segment numbers based on experimental data. Finally, we collected segment regression data that could be integrated into a new visual map method to analyse fin bony segment patterns.

Acknowledgements

I wish to thank my project supervisor, Dr. Anne-Gaelle Rolland-Lagan for all of her guidance, patience and support during my graduate project. Secondly, I thank Dr. Marie-Andree Akimenko for her feedback and time granted to help me completing this project. I thank Dr. Shelly Hepworth (Carleton University) for her time and feedback as my external committee member.

I extend my gratitude to Dr. John Lewis for providing critical feedback and comments on the manuscript, as well as Dr. Richard Blute for his support. I would like to thank my lab mates for encouragement, ideas and feedback through the duration of my graduate studies. I also thank Mathieu Paquette for his contributions in data collection.

I would also like to thank Vishal Saxena and Jing Zhang for their help regarding fish care and protocols. I thank CONACyT and the University of Ottawa for funding.
Special thanks to my aunt Norma and uncle Ricardo for feeding me and letting me stay at their home these last months while I was writing this thesis.

Finally, I thank my parents for their never-ending support, care and encouragement during every single moment of my life.

Los amo, padres míos!

Chapter 1 - Introduction

1.1 General Aspects About Development and Regeneration

Developmental biology can be simply defined as the branch of biology that studies the phenomenon occurring during embryonic and other developmental processes, although it is of utmost importance to understand that unlike embryology, development of a living being continues after birth. This definition however, could seem ambiguous without considering the questions it attempts to answer. Questions such as: how a single cell can produce a full array of different cell types? How can organs within an organism be accurately formed with such specific shape and function? How do cells know when they should start and stop dividing?

We notice then, that development of living beings is orchestrated in time and space, just as in a musical ensemble where each instrumental group enters at specific sections necessary to create a masterful composition. In the same way, each cell has the task to perform key biological functions following patterns, reacting and responding at different gradients of concentration of transcription factors and morphogens, all coordinated into a spatial-temporal symphony of developmental processes.

The development of an organism does not stop at birth, it continues to adulthood. In addition, some species such as the northern leopard frog (*Lithobates pipiens*) undergo the process of metamorphosis. Furthermore, a variety of animal species have the ability to restore missing or damaged body parts as a result of trauma by reactivation of development during post-embryonic life. This ability is called regeneration.

Traditionally, regeneration has been divided into four types: stem cell mediated, morphallaxis, compensatory regeneration and epimorphosis; each one of them with their own mechanisms and implications.

Stem cell-mediated regeneration permits an animal to regrow tissues or complete organs through pluripotent stem cells (Salo et al., 2009). The classical

animal model studied by Thomas Hunt Morgan (1905), the flatworm or planaria, can regenerate large portions of its body when cut in two or more pieces. The regenerating tissues form by specialized stem cells called neoblasts, which constitute more than 20% of total cell types found in the flatworm, and they are capable of regenerate every type of tissue from the flatworm (Aboobaker, 2011). Morphallaxis occurs when a new axis is formed after growth of new structures. This event can be seen in the hydra, which relies on cell organizers that provide molecular signals determining the polarity of the new structure (Broun & Bode, 2002).

During compensatory regeneration, the cells involved do not dedifferentiate to form a blastema, neither do they rely on stem cells to form the regenerate. Here cells divide to form identical cell types in order to compensate for lost parts of the organ through mitosis (White et al., 2005). Such process can be observed in the liver of some mammalian species after injury.

In the case of epimorphosis, that is happening in regenerating limbs of salamanders and fish fin regeneration as will be described in section 1.5, the regenerating blastema that gives rise to lost structures is made from adult cells that passed through dedifferentiation, followed by proliferation and then re-differentiation in new tissues (Brockes & Kumar, 2002; Gardiner et al., 2002).

Both development and regeneration hold great promise in the fields of regenerative medicine and stem cell biology, which could lead to novel therapies in diseases such as cancer and Alzheimer disease (Felsenstein et al., 2014).

1.2 Zebrafish as a Model Organism

A variety of biological models have been used to study both development and regeneration including but not limited to: flatworms, some urodele amphibians, hydra and some species of teleost (Spemann & Mangold, 2001). The zebrafish (*Danio rerio*) has emerged as a model to study vertebrate development due to its rapid ontogenetic process with external embryonic development. In addition zebrafish produce a large numbers of embryos per spawning. These embryos are transparent making them easy to observe and analyse and they develop rapidly. Zebrafish are also relatively easy to handle and to maintain.

The developmental characteristics mentioned above made the zebrafish an attractive model for molecular and genetic analyses, involving molecular tools to analyse specific mutants and to produce transgenic lines expressing fluorescent reporters (Brittijn et al., 2009). Results from mutant analysis revealed that the zebrafish is an excellent model to study vertebrate gene function including those involved in human genetic diseases. Furthermore, the zebrafish genome has been sequenced and revealed that approximately 70% of human genes have zebrafish orthologues, and that 82% of genes listed in the Online Mendelian Inheritance in Man (OMIM) database are related to at least one zebrafish orthologue. Genome analysis revealed that the zebrafish exhibits in average 2.28 genes for each human gene due to whole genome duplication that occurred during evolution in the teleost lineage (Howe et al., 2013). In addition, as other teleosts, the zebrafish presents a remarkable capability of regenerating several organs including its fins.

Fins are convenient for experimentation in regeneration studies because they are easily accessible for experimental manipulation and regeneration of the caudal fin following amputation is fast, as it can take between 21 to 38 days to regenerate at 28°C (Rolland-Lagan et al., 2012, Poss et al., 2000, Becerra et al., 1996).

1.3 Description of Caudal Fin Structure

The zebrafish (Figure 1.1A) caudal fin typically comprises 16 to 18 bony rays, which vary in length depending on their dorsal-ventral axis position (Figure 1.1B). The exoskeleton of the ray is divided into two components: lepidotrichia and actinotrichia (Becerra et al., 1983). Lepidotrichia, forming the rays, are composed of dermal bone segments that extend throughout the proximal-distal axis along the zebrafish fin and are separated by joints at regular intervals (Figure 1.1C) (Iovine & Johnson, 2000). Each lepidotrichium is formed of two facing un-fused hemirays separated on the lateral side (Figure 1.1D) (Montes et al. 1982). Actinotrichia consists of thin unmineralized spicules and are located at the distal edge of the rays (Becerra et al., 1983).

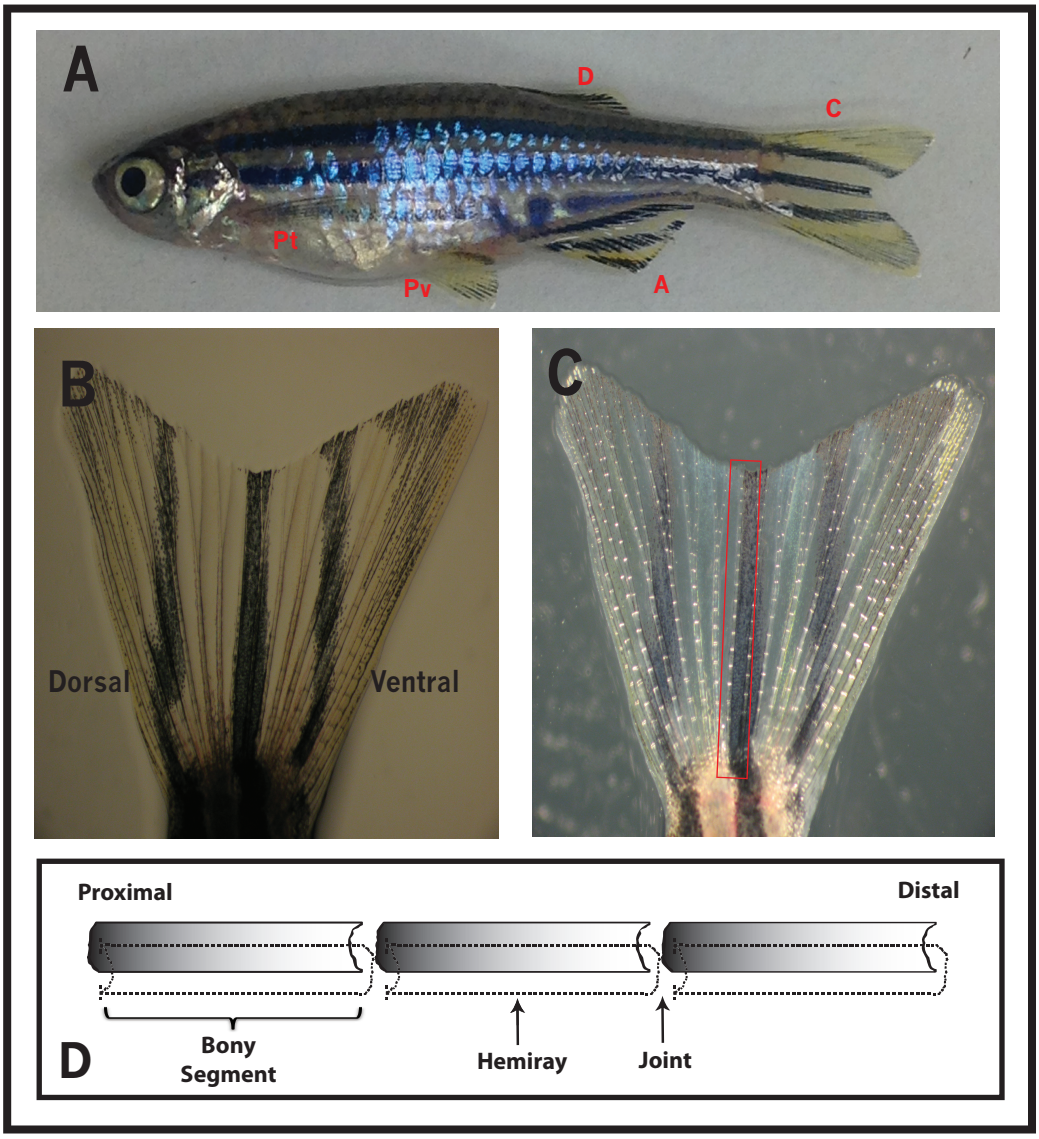

Figure 1.1 General aspects of the zebrafish fin external anatomy. **(A)** Lateral view of a nine months old (279 dpf) female, pectoral fins (Pt), pelvic fins (Pv), dorsal fin (D), anal fin (A) and caudal fin (C). **(B)** Bright-field image of the caudal fin disposed in the same orientation used during this thesis; left-dorsal, right-ventral. **(C)** Dark-field image of the caudal fin showing fin bony rays, as well as the joints. Red square area identifies an individual ray. **(D)** Representation of the bony segments (Lepidotrichia) within a single ray, adapted from of Rolland-Lagan and colleagues (2012). Dotted lines represent the corresponding hemi-ray for that segment.

1.4 Caudal Fin Development

During larval development, the first fin rays originate on the ventral side of the caudal end of the notochord (Géraudie et al. 1995).

Fin rays start to form approximately in 21 dpf juvenile fish (Laforest et al., 1998). Lepidotrichia (fin bony rays) are forming by the successive addition of bone segments as multiple bursts of cell proliferation occur in the caudal fin with higher rates and numbers on the lobes compared to those in the cleft, thus achieving the bi-lobed shape of the caudal fin (Goldsmith et al., 2003). Lepidotrichia develop through intramembranous ossification, where the mesenchymal cells differentiate into osteoblasts and then direct mineralization of the bone matrix without the need of a cartilage intermediate (Franz-Odendaal, 2011).

1.5 Caudal Fin Regeneration

Upon amputation of zebrafish caudal fin, regeneration of the fin is activated which permits the fish to regenerate all the tissues and structures of a functional fin. Appendage regeneration of the caudal fin requires the successful formation and organization of the blastema. Stages of blastema formation will be described in the following section.

1.5.1 Stages of Caudal Fin Regeneration in Zebrafish

Blastema formation through dedifferentiation and proliferation after injury is the hallmark of epimorphic regeneration in the zebrafish fin. Several steps have been identified and will be described in this section emphasising in the cellular types as well as the known molecular signals.

Wound healing

Following fin amputation, the first step consists in the covering of the wound by a thin epidermal layer within the first three hours post amputation (hpa). The epidermal layer thickens during the first 12-18 hpa as a consequence of cell migration

instead of cell proliferation. During this time period epidermal cells start to express *β*-catenin (Poss et al., 2002), which is involved in epithelial cell adhesion as well as in the *Wnt* signaling pathway. Additionally, the Retinoic acid (RA)-synthetizing enzyme (aldh1a2) is up-regulated as soon as 6 hpa, and it has been demonstrated that RA signalling is an early and essential step in forming the wound epidermis during fin regeneration (Blum & Begemann, 2012).

Later, an apical epidermal cap (AEC) is formed between 18-24 hpa (Figure 1.2); this structure is comprised of different layers in the wound epidermis, including the cuboidal cells that appear in the basal epidermal layer (Poss et al., 2000).

Blastema formation

The blastema starts to form when the mesenchymal cells between the amputation plane and the wound epidermis begin to disorganize (Poleo et al., 2001). There is strong evidence that the fin blastema is formed from at least two lineages, osteoblast and fibroblast-like cells which de-differentiate before they can start proliferating (Johnson & Weston, 1995). The expression of the *msx* homeobox genes (Figure 1.2) has been reported during blastema formation (Thummel et al., 2006; Koshiba et al., 1998; Akimenko et al., 1995) and some of these genes have been proposed to be involved in cell dedifferentiation and maintaining the undifferentiated cell state (Odelberg et al., 2000).

Mature osteoblasts dedifferentiate and form part of the blastema. Then these dedifferentiated osteoblasts proliferate in a fibroblast growth factor (Fgf) concentration-dependent manner (Knofp et al., 2011). During this period, Fgf signalling is essential for blastema formation and maintenance, as blastema formation is blocked in absence of Fgf signalling (Poss et al., 2000). Moreover, mesenchymal cells highly express fibroblast growth factor receptor 1 (*fgfr1*) at this stage (Poss et al., 2000). More recently, Fgf signalling has been proposed to be involved in a mechanism to assign positional-dependent properties to the forming blastema (Lee et al., 2005).

Regenerative outgrowth

By 48 hpa, the blastema has typically already formed at 28°C, and regenerative outgrowth is initiated. Mature blastema can be divided in distal and proximal blastema, the distal blastema contains non-proliferative or slow-proliferative cells (Nechiporuk & Keating, 2002). In contrast, cells from the proximal blastema have high levels of proliferation. Both proximal and distal blastema are positive for *msxb* expression (Smith et al., 2008).

The limit between the proximal blastema and the patterning zone (located beneath the proximal blastema) is characterized by the expression of *shha* in the basal epidermal layer (Laforest et al., 1998). Re-differentiation of tissue occurs below the proximal blastema and in the vicinity of the *shha* expression domain (Figure 1.2) and results in initiation of osteoblast differentiation (Laforest et al., 1998). Functional analysis suggests that hedgehog signalling is involved in bone patterning (Quint et al. 2002).

There is evidence that the FGF receptor *fgfr1* plays a significant role during regenerative outgrowth. Thummel and colleagues (2006), showed that knockdown of this receptor by electroporation of fgfr1-morpholino at 72-hpa causes the inhibition of regenerative outgrowth in a dose-dependent manner, causing a 20% to 70% reduction of outgrowth. Recent functional analysis has provided evidence that RA is essential for maintenance of the formed blastema by providing a pro-survival mechanism in blastema cells against cell-death mechanisms (Blum, & Begemann, 2012).

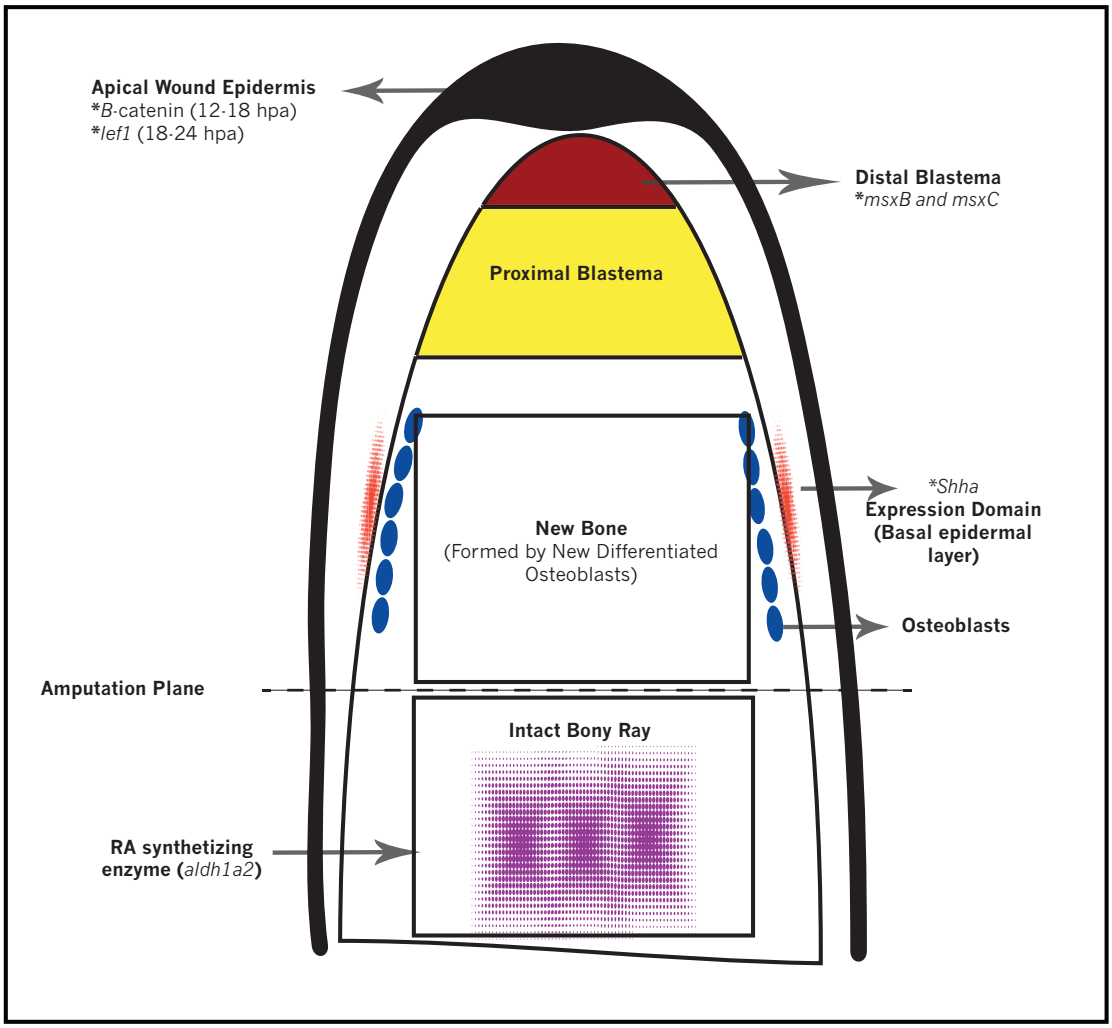

Figure 1.2 Representation of the fin regenerate, summarizing the events described in section 1.5.1. "Stages of caudal fin regeneration in zebrafish".

1.6 Tissue Patterning

One of the main challenges for developmental biology as a discipline lies in unveiling the mechanisms responsible for determination of correct size, shape and structural patterns resulting in fully functional structures.

Changes in shape can be achieved when variations of the growth rates of different tissues occur (Wolpert 2002). According to classic studies of patterning, it has been considered that typically pattern formation precedes cell movement in order to specify which cells will move and what will be their destination (Wolpert 1972). There are two main components in shape alterations of an organ or group of cells: molecular differentiation and patterning.

Molecular differentiation controls the synthesis of specific macromolecules necessary for that particular cell group, while patterning dictates the spatial organization of such activities. Wolpert considers that the interaction between these two components can be explained by the fact that cells possess previously assigned positional information, which provides their position in a coordinate system. Then this positional information determines the molecular activity of those cells and allows for cyto-differentiation.

1.6.1 Basis for Tissue Patterning

The concept that developing organisms require regulation of molecular expression, in order to achieve the appropriate structural shape, was established by the Driesh-Spiegelman Law: “The amount of material capable of developing into a particular region is always greater than the presumptive region” (Waddington, 2012). Currently this statement suggests the molecular mechanisms, transcriptional factors and biochemical pathways involved in most developmental processes have the capacity to create greater proliferative and cytological responses than what is observed in living organisms. Therefore restriction mechanisms are required in order to obtain anatomically correct structures.

This allowed setting the basis for gradient models, which are attractive explanations for regulation of several developmental processes.

The French flag model was proposed to explain how cells can achieve a specific fate, based on the concentration of substances involved in pattern formation (morphogens) (Wolpert, 1969). In this model, cells can become three types of cells: (Blue, White or Red), depending on the concentration of a hypothetical substance based on their position on an axis, creating the three equally distributed color bands of the flag. If, the mechanisms ruling the distribution of the patterning substance are changed, the resulting pattern will be affected, creating different outcomes with alterations on the width of the color bands.

This model can also be used to explain epimorphic regeneration, in which cells of the blastema acquire positional information corresponding to the new regenerated tissues and are able to restore the pattern of the original organ. Failure in obtaining these values would result in an altered pattern of the structure.

During bone morphogenesis of the fin ray, joints are distally formed in space intervals. The amount of bone deposited between each joint determines the length of bony segments (Haas, 1962). Patterning trends can be observed in the distribution of bony segments across the proximal-distal and medial-lateral axes of the fin (Figure 1.3), such as longer segments are present in the proximal part compared to those in the distal region; also segments located in lobe rays are longer than those in the cleft rays (Iovine & Johnson 2000, Rolland-Lagan et al., 2012).

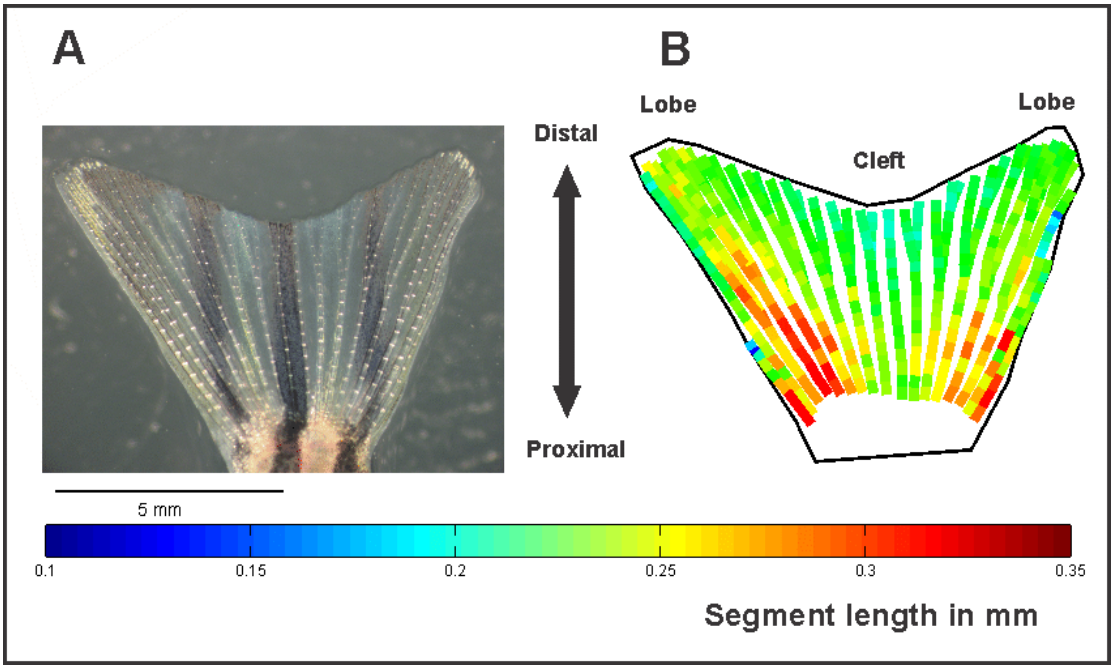

Figure 1.3 Caudal fin and segment trends **(A)**: Image of a caudal fin with dark field. **(B)**: Graphic representation of the caudal fin showed on the left, depicting the observed segment lengths within different positions of the fin. Color-bar shows segmental length in mm. Left and right lobes are dorsal and ventral respectively.

1.6.2 Segment and Overall Fin Length

Recent studies have been made to elucidate the mechanisms responsible for initiation, regulation and patterning of fish caudal fin during development and regeneration. One of the main aspects that have been studied is the genetic control of the mechanisms that initiate the formation of new segments and the determination of elements that control size of new segments. It has been proposed that the dynamics of segment growth involves multiple and periodic pulses of cell proliferation, with divisions occurring at approximately 60 microns of separation (Jain et al., 2007).

Zebrafish, as other teleosts has the potential to grow indefinitely. During juvenile stages, fin growth is not proportional to body size (allometric) (Goldsmith et al., 2006) but, as the individual enters the adult stage its growth rate slows down and becomes proportional to body growth rate (isometric) in wild-type fish (Goldsmith et al., 2003).

Analysis of the zebrafish *longfin* (*lof*) mutants, showed that the fast rate of growth is maintained, even after reaching the typical size which triggers a decrease in growth rate on wild-types, resulting in longer fins by increasing the number of bony segments. The *shortfin* (*sof)* mutants on the other hand, show isometric growth resulting in fins with lower number of segments as well as fins with only half the length of fins from wild-type fish (Iovine & Johnson, 2000). From these studies, the authors suggest that *lof* mutants bypass the mechanisms that limit bony segments initiation, while the *sof* gene product regulates segment length.

It was later demonstrated that this *sof* phenotype is the result of a mutation in the *connexin43* (*cx43*) gene causing reduced *cx43* mRNA and protein levels (Iovine et al., 2005); on the other hand, higher levels of *cx43* can be found on the *another-longfin* (*alf)* mutant, which exhibits longer fins and segments of irregular length due to joints pattern that seems to be random (Iovine et al., 2009). Connexins are subunits of gap junctions, which allow the exchange of small molecules (lower than 1200 Daltons) between two adjacent cells. In the developing and regenerating fins of wild type zebrafish, *cx43* is expressed at the level of the joints of the bone segments (Iovine et al., 2005).

The molecular identifications of lesions in *cx43* suggest that gap junctional intercellular communication is required during mammalian bone morphogenesis (Paznekas et al., 2003). In the fin, it is suggested that *cx43* activity coordinates regulating signals for cell division as well as joint formation by allowing communication between *cx43*-expressing mesenchymal cells with those surrounding new forming joints (Iovine et al., 2009). These findings strongly indicate that: "local direct cell-cell communication plays a critical role for the regulation of bony segment growth and size" (Iovine et al., 2005). This is the first reported gene mutation having a direct effect on fin length.

It is important to note however, that although manipulation of *cx43* expression will affect segments length, the manipulation of fin growth rates alone is not enough to alter segment length (Iovine et al., 2009). This is supported by the results of experiments in which, *shh* signalling or *fgfr1* are blocked using inhibitors, causing reduction in cell proliferation but segment length is unaffected (Lee et al., 2005; Quint et al., 2002). As a result, fin growth rate is inhibited in a dose-dependent manner resulting in small fins with ray segments of normal size (Lee et al., 2005). This seems to suggest, that there exists a mechanism that controls segment joint patterns, which could act independently of fin growth.

Most studies on detailed fin segment patterns have focused on quantifying the number of bony segments along rays, or comparing the segment length in specific locations of the fin (such as only on the most distal segments or only the segments of the third lateral ray). The lack of detailed segment data in the literature, combined with the evidence of a joint pattern mechanism, which can act independently of cell proliferation, serve as part of the basis of this study. One of the elements of my work aims to study bony segment patterns and assess the joint formation mechanism through a computational approach. This will be further explained in section 1.8.

1.6.3 Fin Shape and Differential Rates of Growth Between Rays

As it was mentioned in section 1.4 Caudal Fin Development, it is thought that the key factor for the bi-lobed shape of the caudal fin lies in differential growth rates among rays, where the rays located in the lobes of the fin should have a higher proliferation rate compared to cleft rays (Goldsmith et al., 2003). An alternative explanation could be that rays in the cleft simply "opt-out" or stop adding new bony segments at specific time points during fin development. These two hypotheses were further tested using bromodeoxyuridine (BrdU) incorporation in juvenile caudal fins to label proliferating cells *in vivo* (Goldsmith et al., 2006).

All fin rays from the lobes showed BrdU labeled cells in the distal mesenchyme, while the cleft rays only showed an insignificant amount BrdU positive cells during juvenile fin development. The amount of proliferating cells were approximately 25% higher in the lobes than in the cleft rays (Goldsmith et al., 2006). In addition authors of this study predicted that the difference in proliferation between lobes and cleft during juvenile development would disappear at the adult stage when fish adopt synchronous growth. Effectively, they showed that adult caudal fins present no difference in the amount of BrdU labeled cells between the lobes and cleft.

These results suggest that the caudal fin bi-lobed shape is established during juvenile development (asynchronous growth) and the fin simply continues to grow following that pattern at the adult stage (synchronous growth).

Results from other experiments involving oblique fin amputation and grafting blastema to another ray positions suggest that local interactions between ray and inter-ray tissue can control growth rates through the dorso-ventral axis during caudal fin regeneration (Mari-Beffa & Murciano, 2010).

1.6.4 Ray Bifurcations

As bony rays and segment lengths constitute one of the components of fin patterning, a second component is ray bifurcations or branching. With the exception of the most-lateral rays of the caudal fin, bifurcations can be seen multiple times in a single ray.

Bifurcations of structures is observed in many organs such as the vasculature or the lungs and is necessary for the supply of nutrients, and adequate gas exchange for the whole organism. It occurs by creating extensions of tissues or cell groups, which ultimately increase the surface area of the organ in question. Bifurcations can occur at the cellular level such as in neurons, when creating dendrites to communicate with neighbouring cells or at the tissue level such as in the vasculature, which allows the delivery of nutrients and removal of metabolic wastes. In the case of the fin, they allow the proper shape necessary for an efficient thrust during locomotion of teleost fish achieved by sideways movement of the caudal region (Dowis et al., 2003).

Ray branches have a pattern which is defined by the length, width, shape and spacing. We can identify two main elements that specify the bifurcation patterns: a) number and location of branching points, and b) appropriate size and shape of the bony segments within each branch.

In order to achieve the previous mentioned elements, a genetic control is required for the inductive and restrictive signals that initiate cell proliferation, migration and to determine cell orientation as well as maintain the branch outgrowth in a specific direction during branching morphogenesis (Metzger et al., 1999).

Studies in lung branching patterns during morphogenesis, indicate that the fibroblast growth factor (Fgf) pathway acts as an axis-signalling provider that works as an iterative genetic program each time a new generation of bifurcations appears (Metzger et al., 1999). Furthermore, the Fgf pathway can create feedback at different branching stages to launch a different bifurcation outcome. For example, at the early stages of morphogenesis, Fgf-10 is diffused to mesenchymal cells promoting their proliferation and expanding the endoderm (Bellusci et al., 1997); lung buds are then created distally, which provide direction for outgrowth. A single peak of expression

of Fgf-10 is observed at the bud tips during their elongation, in contrast to the terminal bifurcation stage, which exhibits two splits spots localized between the lung border and the bud tips (Hirashima et al., 2009).

In addition, mice NPAS3-null mutants (diminished alveorization) exhibit decreased production of *shh*, Fgf-9, Fgf-10 and Bmp4 and die by respiratory distress (Zhou et al., 2009). All these signalling molecules play a specific role during bifurcations, especially *shh* which acts along the transforming growth factor-β (TGFβ) as major negative and positive regulators of Fgf-10 synthesis respectively.

Their activities provide long-range activation and short-range inhibition of Fgf-*10* expression ensuring localized peak expression of this factor at a specific distance, thus creating the necessary spatial pattern of bifurcations during morphogenesis (Li-Y et al., 2004).

In the zebrafish caudal fin, the mechanisms responsible for bifurcations patterns are not completely understood. It is known however, that bifurcation occurs as rays grow, and the patterns vary between each ray resulting in rays which never bifurcate to rays that can have multiple bifurcations (Haas, 1962). One hypothesis regarding the absence of bifurcations in the most lateral rays, is that rays require inter-ray tissue on both sides of the ray in order to trigger bifurcations. As a result, outermost rays do not bifurcate (Murciano et al., 2002). Indeed, it has been shown that grafting fragments of the most lateral rays into a medial ray position within the caudal fin results in bifurcation induction of the grafted rays, indicating that all rays have a bifurcation potential, but they branch only if there is an inter-ray tissue on both sides of the ray (Murciano et al., 2002). More recently, it was shown through analysis of transgenic lines and cell ablation experiments that *shha* may direct localized cell proliferation and branching morphogenesis of the fin rays. Indeed, it has been shown that ablation with a laser beam of the *shha*-expressing cells leads to a delay in the events of ray bifurcation without affecting ray growth (Zhang et al., 2012).

With all previous aspects considered, the caudal fin is an excellent organ to study morphogenesis during development and regeneration at the molecular and signalling level, including the mechanisms involved for patterning and organ shape.

1.7 Morphogens and Morphogen Gradients

Morphogens can be defined in the most general sense, as mobile substances that are produced at a specific site of origin and migrate towards a target site creating gradients of concentration. They provide differential cues for gene expression along the axis between the source point and final destination, thus creating different types of tissue by cell differentiation (Lee et al., 2005). It has been proposed that diffusion and interaction of morphogens contribute to the development of spatial patterns of biological tissues and structures (Turing 1952).

The balance between production and decay of substances and signals that control patterning is necessary to establish gradients of concentration. It is essential that these substances are able to successfully diffuse through boundaries that limit transport and provide compartmentalization (Kicheva et al., 2012).

When the gradients are established, each differential morphogen gradient trigger specific signaling cascades, resulting in differential transcriptional gradients. The effectors of these signals can target specific genes that can regulate other genes as positive or negative feedback; this relationship has been described as a gene regulatory network.

In their review, Kicheva and collaborators (2012) hypothesize that morphogen kinetics can vary in spatial and temporal manner, in terms of events occurring at subcellular to tissue levels; or from seconds to hours, during pattern formation, which they describe as: “An emergent behaviour that results from the coordination of events occurring across molecular, cellular, and tissue scales”. For this, cell growth and proliferation, production from a source point, and type of transport trough tissues, should be addressed as the main determinants of morphogen gradients.

1.8 Systems Biology

Systems biology is one of the most promising approaches in order to understand the mechanisms underlying the physiology of living organisms. This field aims to study living organisms at systems level. Systems are the combination and integration of quantitative data of individual components (nodes) in order to understand the resulting behaviour of a natural phenomenon (Kholodenko et al., 2005).

It consists in the collection, analysis and comparison of biological pathway networks, as well as in the study of abnormal conditions such as individuals affected by diseases and/or mutations. These biological systems however, have significant differences between them; not only for their components but also in the way these components are distributed in the architecture of the network and also in the way they interact. These differences determine specific form and function of living beings. Therefore, "living organisms cannot be fully understood by merely analyzing individual components" (Zhang et al., 2008).

The basis of this approach lies on the application of the available quantitative data to postulate a theoretical model, which functions as the backbone of a biological problem. One of the most common examples is constituted by the gradually growing "omics" databases, where each genotype and phenotype represent individual nodes; subsequently more complex pathways are integrated creating a network which can be used to predict a theoretical model to explain the whole system. Finally, perturbations (such as mutant individuals or other conditions) are introduced in the system, in order to test the robustness of the model as well as to collect new experimental data, which in turn, will improve and will be used to modify the existing model.

As a result, systems biology works as an iterative discipline in which new and more accurate models are generated at each cycle. The feedback obtained in each cycle grants several properties to the system. These properties are: 1) Robustness to internal variations and external conditions, 2) Linear response between input and output signals and 3) Evident effect caused by an increase in magnitude over the input signal (Kholodenko et al., 2005).

This thesis uses a computational approach in order to study developmental mechanisms. A hypothetical ray growth model (Rolland-Lagan et al., 2012) was previously proposed based on information from the literature and experimental data. The system biology approach requires constant data collection which is further used to adjust the theoretical model by calibration of its parameters. Data collection relies on imaging morpho-dynamics (in our case imaging fin development or fin regeneration) and the development of custom computational tools as a way to accurately measure and track developmental processes in space and time.

1.8.1 Computational Models for Caudal Fin Patterning

A model was proposed by Rolland-Lagan and colleagues (2012) in order to explain the basic mechanism underlying growth and segment patterns of the zebrafish caudal fin. This model is based on the action of three hypothetical morphogens named "G", "X" and "S". Series of compartments are distributed through the proximal-distal axis of the ray, and they represent a single cell or group of cells. Morphogens are transported from their source to their destination through these compartments, and their concentration varies from one compartment to another due to production rate and decay.

The first component of the model accounts for ray growth during development and regeneration after amputation, and it involves the interaction of the two hypothetical morphogens "G" and "X". The main activity of morphogen G is to stimulate and drive outgrowth at the most distal compartment of the developing fin ray and in the blastema during fin regeneration. Since outgrowth only occurs distally as experimental data has shown (Jain et al., 2007) it is assumed that "G" is only produced in the most distal compartment. In addition, the levels of "G" during regeneration are higher if the last compartment is located proximal to the ray base than if the amputation occurs at a more distal position. Regarding morphogen "X", it is assumed that it activates the production of "G" directly proportionally to the level of "X" present; also its source point of production is located at the basal compartment of the ray and its production increases over time.

The second component of the model accounts for segment length and joint patterns. A third morphogen is proposed, arbitrarily named “S” and it determines where a joint will be made in the growing ray. Morphogen “S” is supposed to inhibit the formation of new joints until the level of this morphogen falls to a threshold that triggers the formation of a new joint. It is assumed that “S” is produced when a new joint is formed, creating a peak of concentration in that compartment thus preventing the formation of joints in the vicinity. As the ray grows distally, morphogen “S” starts to diffuse and decays until it reaches the threshold to trigger another joint and repeat the cycle. Similarly to morphogen “G”, “X” regulates morphogen “S” concentration as the peaks generated at each joint are proportional to the level of “X” in that compartment. In other words the peaks of “S” are higher in proximal positions compared to distal positions, and as a result, distal joints tend to be placed closer to each other as rays become larger (Figure 1.4A).

In summary, this model can account for the simulation of the fin as a whole, the differential rate of growth between juvenile and older fish, as well as the growth rate of individual rays (Figure 1.4B).

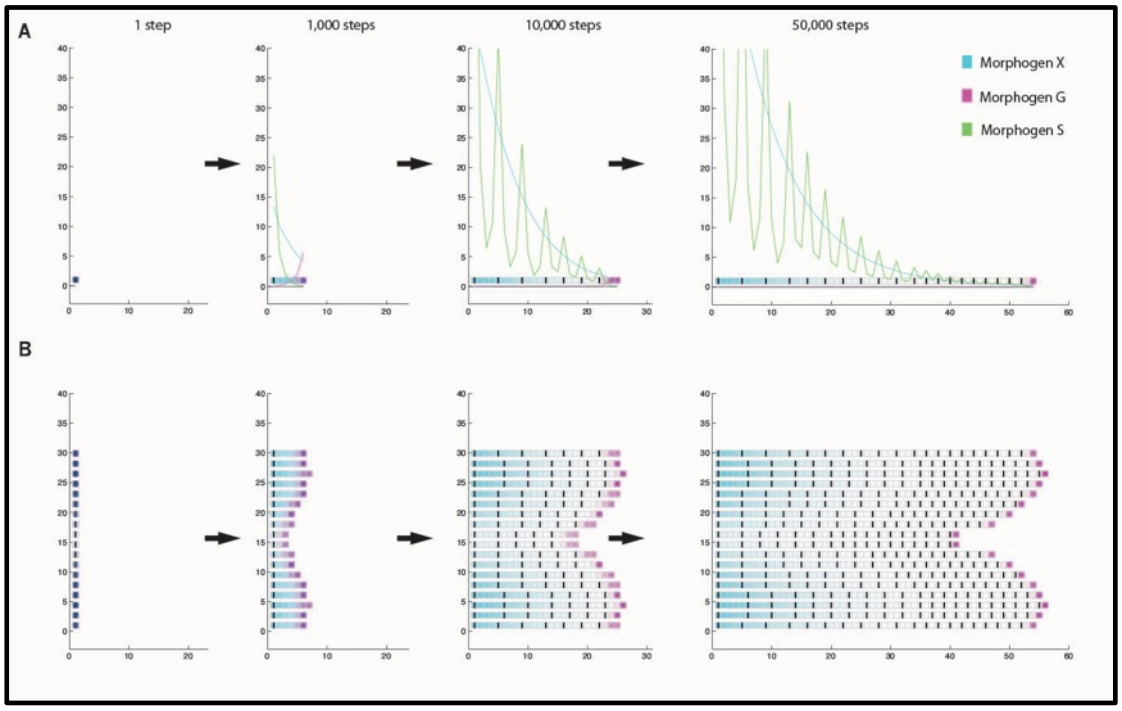

Figure 1.4 Morphogen driven model postulated by Rolland-Lagan (2012) for zebrafish caudal fin growth and patterning. **(A):** Time sequence of morphogens concentrations in function to the position of the last compartment in the proximo-distal axis of a single ray. Vertical axis is the morphogen level of concentration. Horizontal axis is the number of compartments. Values are arbitrary. **(B):** Multi-ray representation of caudal fin at the respective time-points shown in (A), differential ray lengths, bony segment lengths and joints positions are determined by morphogens concentrations. Small squares represent cell compartments and black lines indicate the presence of a joint. Horizontal axis is number of compartments. Values are arbitrary.

In addition to this model, colleague Valerie Tweedle (2012) postulated for her Master's thesis a second model, which aims to explain how bifurcation pattern occurs (Figure 1.5). This model is based on *shha* expression using particle modeling, and involves two sets of points: source and bone points.

In this model, source points represent *shha* expression domains located distally and are responsible for growth. Bone points on the other hand, represent newly differentiated osteoblasts and are localized proximally to each source point. As osteoblasts differentiate, source points move distally as well as bony points below them, matching the formation of new bony segments.

Formation of bifurcations depends on a hypothetical bifurcation forming substance, which is produced at the distal end of the ray tip. This bifurcation forming substance is distributed across the medial-lateral axis and decreases over time.

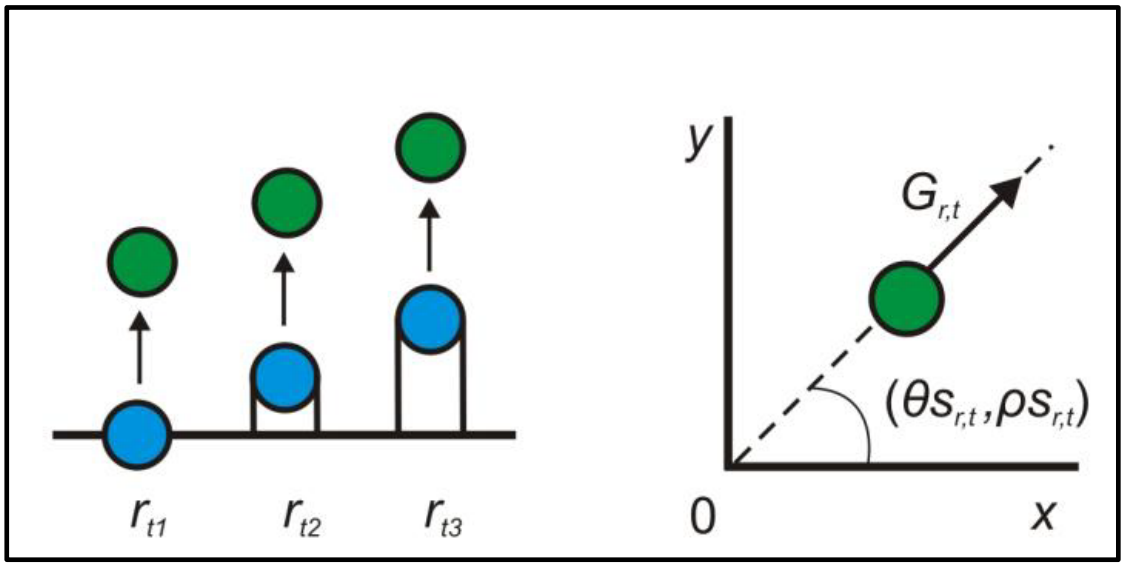

Figure 1.5 Left: Schematic drawing representing the association between source (green) and bone (blue) points and the formation of bony segments as they migrate distally in three timepoints, as envisioned by Valerie Tweedle (2012). **Right** Polar coordinate system used to assign values to source points positions at any time in the system. Where $\theta s_{r,t}$ represents the angle of the source point at time (t), and $\rho s_{r,t}$ is the distance from the origin at time (t). *Courtesy of Valerie Tweedle* (2012).

Chapter 2 – Proposed Research

2.1 Systems Biology Approach

As previously mentioned in section 1.8, systems biology is an iterative approach in which the ultimate goal lies in understanding complex biological problems by developing theoretical models and testing their predictions by performing quantitative experiments. In turn, this allows us to calibrate and validate the original model using the new data, and complete the cycle by making new predictions.

Although the amount of information regarding the cellular, genetic and molecular mechanisms that control differentiation and patterning in fin regeneration has been increasing over the last 20 years, multidisciplinary approaches are needed to obtain new insights in this field of research (Akimenko et al., 2003). Systems biology can further provide the necessary perspectives to expand the current knowledge about these topics. In addition, most studies have focused on measuring fin length, the regeneration of a single ray, or number of bony segments, and in the case of segments only measuring the first most proximal segment and the final segments on the tips (Iovine & Johnson, 2000). Very few studies have focused at the level of individual segments and their potential pattern differences before and after regeneration.

2.2 Objectives

This thesis aims at studying the developmental control of fin joint formation, which determines segment patterns of the rays in the caudal fin of zebrafish, before and after an amputation event, through a computational approach and imaging morpho-dynamics, as a part of the systems biology field.

To do so, we used an image database (obtained by Mathieu Paquette) comprising images of 17 fish during fin development and regeneration. However, these samples required preparation, extraction and analysis of segment data.

In addition, a morphogen driven model for simulation of fin development and regeneration was proposed by Rolland-Lagan and colleagues (2012). Calibration of the model parameters was still necessary in order to validate it with the results obtained from this present experimental analysis.

Another objective was to test the predictions from the morphogen-driven model. One of the predictions was changes in segment patterns after an amputation event. Indeed, it predicted that the first few segments regenerating after amputation would be longer than the original segments and then segment lengths would gradually decrease in size. The model was also showing longer segments at some locations distal to the amputation plane.

Lastly, we assessed and adapted a quantitative framework (Rolland-Lagan *in preparation*) for analysis of the caudal fins from fish samples showing non-homogeneous number of rays and same age, by developing "likely fin maps" to analyse ray patterns from samples with variations in size and ray numbers.

Chapter 3 - Methods

3.1 Animal Care

3.1.1 Housing

The zebrafish micro-environment consisted of individual tanks of three liters and ten liters distributed in racks inside the fish facility. Tanks contained circulating water and a small amount of air volume under their respective tank cover. Groups of fish from the same age were kept in the same tank. Fish tanks are made of transparent polycarbonate to allow easy observation, their capacity varied depending on the number of animals and their developmental stage. However, three liters tanks were used primarily to keep non-breeding adult fish. The number of fish kept in this type of tank was between 11 to 15 fish per tank, that is within the recommended density for adults which is 5 individuals per liter. The temperature was set at 28.5°C, the photoperiod in the facility was 14 hour of light and 10 hours of darkness; these settings are widely used for developmental studies (Matthews, 2002). Feedings occurred two times per day on weekdays, while during weekends and holidays they were fed only one time per day.

3.1.2 Breeding

For breeding fish, a group of two females and one male was separated from the rest in the afternoon and placed overnight in breeding tanks containing 1 liter of water, egg traps or marbles were used to prevent the consumption of eggs by breeding adults. The fish were fed with brine shrimp in addition to the regular dry food prior to every breeding event. Breeding attempts did not exceed two events within the same week.

Embryos were collected during the morning of the next day and rinsed in a bowl containing 1 ml of 5% sodium hypochlorite with 170 ml of system water for two minutes, then placed in a petri-dish containing E3 growth medium 1x. Petri dishes containing embryos were placed in an incubator at 28.5°C for 5 days, and were

periodically checked to remove dead embryos or debris using a pipette, in order to prevent growth of mold and the decay of zebrafish embryos.

After this period, larvae were moved to small 1-liter tank containing system water with 3ml of 0.01% methylene blue (methylthioninium chloride) per liter of system water for fungus control. Water had to be replaced every third day, as these tanks were placed on baby stations (1-litter tanks) and were not linked to the system. Half spoon-tip of dry food with very small particle size (zm000) was used during the first week and gradually increasing to larger sizes until the juveniles were able to digest adult flakes approximately at 60dpf, although it is considered that they could start to eat adult food after 21dpf (Westerfield, 1995). Juveniles were then transferred to three liter tanks when they were big enough for the grid preventing the fish falling through the water recycling system.

3.1.3 Amputation Procedures

For fin amputations, fish were temporary placed in a separate container and transported out of the fish facilities into the lab. The tank was stored in a water bath at approximately 28.5°C during the whole experimental period. In addition to the tank with the samples, another tank with system water was set in the bath to allow fish to recover after experimental manipulation and was labeled as “recovery tank”. Fish used for amputations were 167 dpf old for reproducibility with the previous experiments carried out by undergraduate student Mathieu Paquette.

Fish were anesthetised by placing them in a bowl containing system water with 0.17mg/ml of tricaine (ethyl 3-aminobenzoate; Westerfield, 1995). Right after fish gills stopped moving, fish were placed over a petri-dish previously marked with the desired distance from the caudal peduncle to the amputation plane (2 mm or 4 mm for proximal and distal amputations, respectively). Amputations were performed with a single cut parallel to the dorso-ventral axis using a surgical scalpel. After amputation, amputated fish had their fins imaged and then placed in the recovery tank. Fish were kept anesthetised for no more than five minutes.

3.1.4 Imaging

Fish caudal fins were imaged at different developmental stages ranging from 24 dpf to 205 dpf. Prior to any imaging procedure, the organisms had to be anesthetised with tricaine as previously described in the amputation section. Concentrations of the drug were adjusted because the juveniles grew in age and size, by addition of more drops of tricaine to the solution. Ideally, fish had to assume a relaxed state within 30-40 seconds of immersion into the tricaine solution. Due to their small size juveniles at early stages (24-70 dpf) were imaged in petri-dishes prepared with agar containing canals to hold the juveniles.

Adult fish were imaged in petri-dishes without the canals. Fish at 167 dpf were imaged before and after the caudal fins were amputated. Fish that underwent fin regeneration were imaged until 38 dpa (days post amputation).

Imaging was performed using a mounted Canon Powershot A640 digital camera on a Zeiss V8 discovery microscope; all imaging events took place two times per week at regular time periods (every third and fourth day of the week). The imaging process consisted of obtaining a set of three images generated by exposing the samples to bright and dark fields, achieving a better observation of fin structures such as rays, joints and individual bony segments. These three images contained the imaged samples with 1) Full Bright field, 2) Dark field and 3) An intermediate position between bright and dark field.

3.2 Computing Tools

This thesis uses a computational approach and imaging morpho-dynamics to quantify and analyse fin ray patterns in a process conceptually similar to (Rolland-Lagan et al., 2009). There are two main phases for this approach and each phase is further divided in several sub-steps. The first phase is the data extraction of the digital images and the second phase consists of generating visual maps to analyse trends and perform statistical analyses.

3.2.1 Data Extraction

In order to work with imaged fin samples, an image morpho-dynamic framework consisting of a series of programs is created to organize, extract and assign extracted data constituted by five main components; 1) Folder architecture, 2) Shape and dimensions, 3) Identification of ray joints and segments, 4) Assignment of ray positions and trajectory and 5) Matching bony segments between time-points. These programs were developed by Dr. Rolland-Lagan on MATLAB platform (The Mathwoks, Inc., Natick, MA) version R2012a.

1) *Folder architecture*

Fin images were organized in specific folder directories in order to be recognized for the next programs. In addition, image files are named based on their developmental time-point, amputation status, number of sample and type of image.

For example an image named: "A028F01**B**" means:

- First letter corresponds to before (B) or after amputation (A).
- Three digit number indicates the time-point (in days post-amputation)
- Letter "F" with a two-digits number is the fish sample
- Last letter corresponds to the type of image: Bright field (B), dark field (D) or intermediate (K).

This example indicates that this sample is from an amputated fish, at 28 days after amputation, fish sample number 1 and that the image was taken using bright field.

2) *Shape and dimensions*

The second step involved obtaining the dimensions and shape of the fin samples within the images. Using our Matlab custom program we set the scale bar to calculate the image resolution in pixels per millimetre (ppmm). Then using a mouse or digital pen, we outlined the fin perimeter, and traced fin length and width (Figure 3.1).

Length of the fin (Figure 3.1, L) was determined by measuring the third rightmost ray on the ventral lobe of the fin, while fin width (Figure 3.1, W) was obtained by measuring the dorsal-ventral axis of the fin at the widest point (approximately one or two segments below the tips).

Perimeter was set by placing two-points, one in the cleft and the other at the middle of the base of the fin to keep the fin orientation, then points are distributed along the outline of the fin and recorded in a matrix of (x,y) Cartesian coordinates. Finally, the area of the fin was obtained with the sum of the pixels enclosed within the outlined area and divided by the square value of the image resolution (Rolland-Lagan *in prep*).

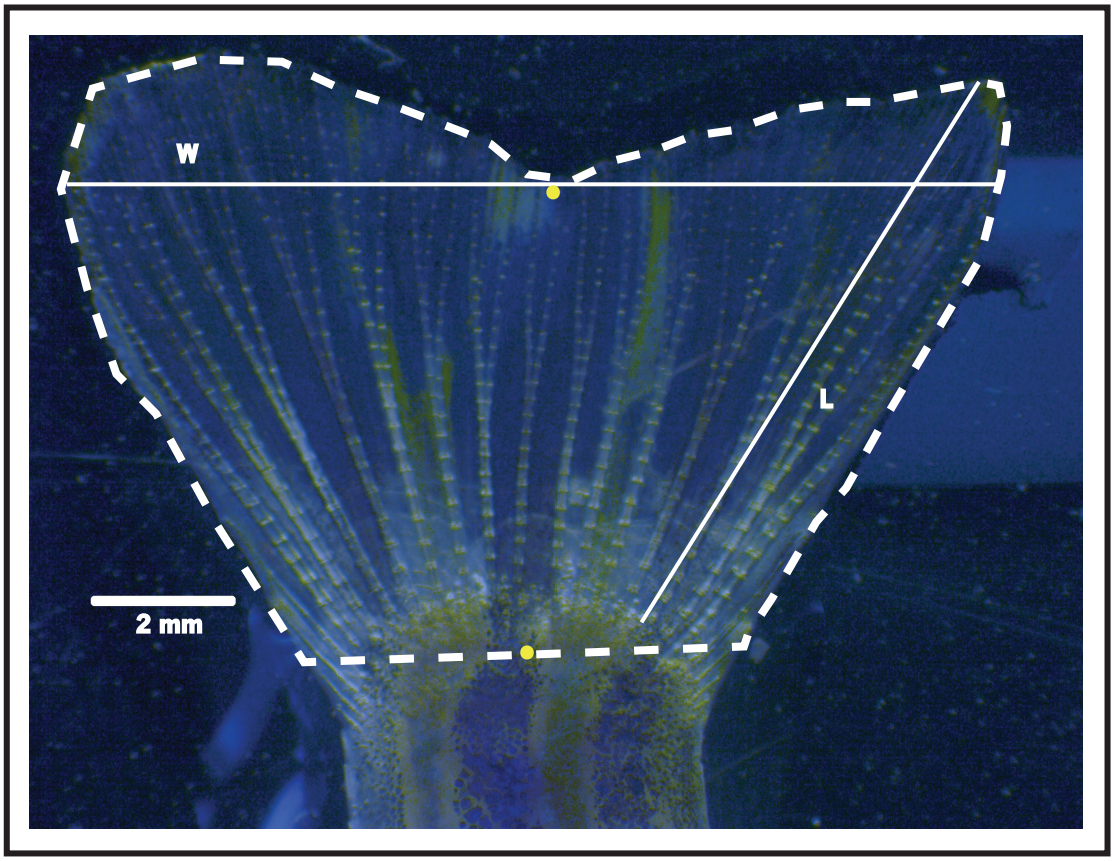

Figure 3.1 Fin shape and dimensions. Left lobe is dorsal, right lobe is ventral; W: Fin width, L: Fin length. Yellow points are used to keep the same fin orientation for all the samples. Dashed lines delimitates the fin perimeter.

3) *Identification of ray joints and segments*

The previous step set fin shape and dimensions. In order to extract bony rays and individual segments data, we had to digitize each sample. Digitizing consisted in assigning positional values (nodes) to structural fin elements such as the ray joints in the images collected during the experimental stage at different developmental time-points (Figure 3.2A), and record them in a matrix. The name of this matrix is "segmenta" (Figure 3.2B).

4) *Assignment of ray positions and trajectory*.

After digitizing fin joints, the next step consisted in identifying and classifying each node, as well as removing erroneous single points (Figure 3.3). Nodes were classified as:

a) Joint point: The main and most frequent type of node. They are distributed along the ray, representing fin joints and delineate each bony ray segments.

b) Ray base point: They are located at the most proximal position of the fin and indicate the start of each fin ray.

c) Free ending tip: They are the most distal points of the last segment from each branch of every ray.

d) Bifurcation point: Indicate the start of two new branches derived from the same parental ray.

5) *Matching bony segments between developmental time-points*

This step required the tracking of all previously classified nodes in the assignment step, and is accomplished by a custom ray-tracking program. Here we verified that the nodes were correctly assigned and set a ray as reference (Figure 3.3B). We chose a ray in the cleft as reference ray consistently in every time-point, to number ant rack all rays. This allowed us to match every node in all time-points. The criteria for numbering consisted of assigning increasing numbers to rays starting from the cleft of the fin and progressing to the ventral lobe, and then decreasing numbers from the fin cleft to the dorsal lobe (i.e: 1, 2, 3, 4, etc. and -1, -2, -3, -4, etc. for rays on ventral and dorsal lobes, respectively).

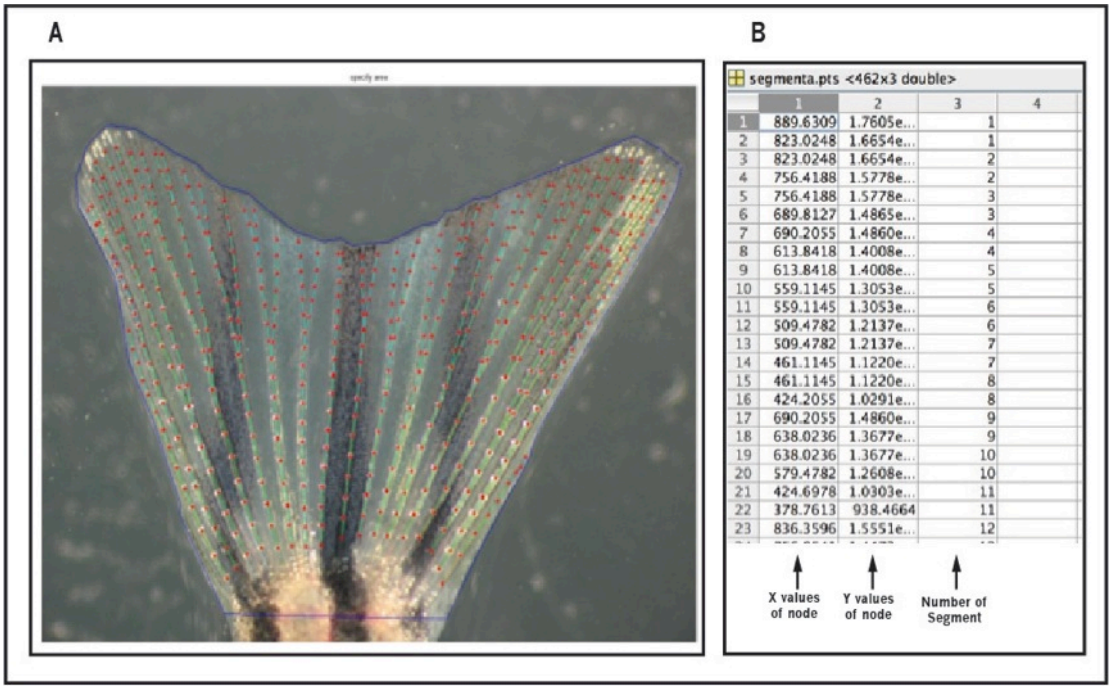

Figure 3.2 Digitizing process **(A)** Appearance of fully digitized fin, red dots are the nodes that represent the joints. **(B)** Variable "segmenta" matrix, which stores the coordinate values of each node in the two first columns, the third column indicates the number of the segment; a set of two rows represents a segment.

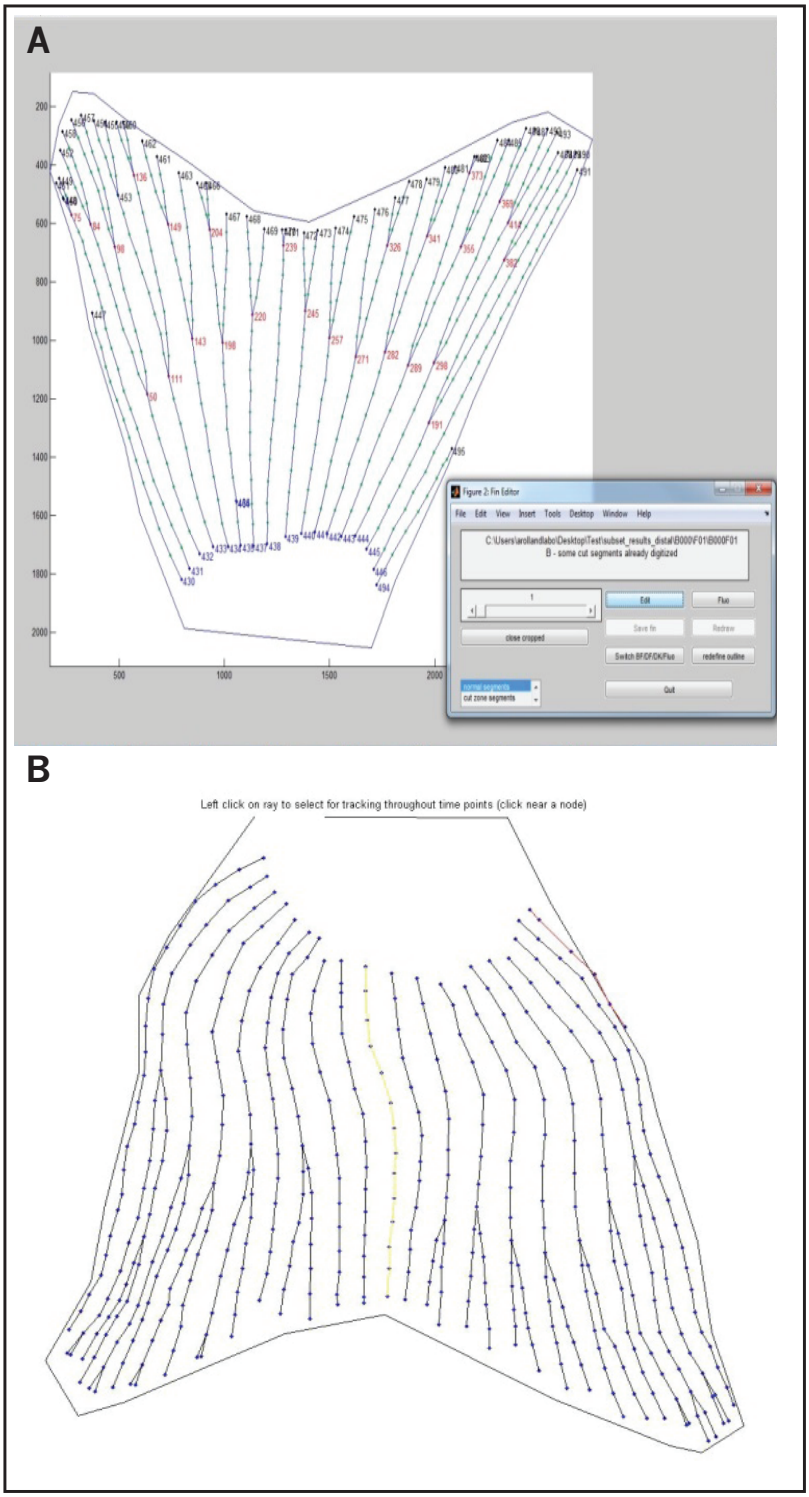

Figure 3.3 Step of node assignment and data extraction. **(A)** Screen of a sample with all its nodes identified, blue nodes are assigned to ray bases, green nodes to joint points, red nodes to bifurcation points and black nodes correspond to free ending tips. **(B)** Tracking rays across time-points, yellow ray is set as the reference ray on each digitized sample belonging to the same individual, allowing accurate extraction of ray and segment data during growth and regeneration.

3.2.2 Generation of Files for Graphic and Statistical Analysis

A custom-made computational framework developed in the Rolland-Lagan lab was used to analyse extracted fin data with up to 3 bifurcations per ray. A section hierarchy was established based on the presence of a bifurcation in a given ray (S1, S2, S3 and S4), where (Figure 3.4);

S1: Section from the base to the free ending tip if there is no bifurcation, or to the first bifurcation (bp1).
S2: Section from bp1 to the free ending tip or to the second bifurcation (bp2).
S3: Section from bp2 to the free ending tip or to the third bifurcation (bp3).
S4: Section from bp3 to the free ending tip.

The files generated are the following:

-Wholefin: Contains the number of segments of the whole fin at a particular time-point, the average segment length, the amount of branching points in each ray section, number of ray base points as well as the number of free ending tips (See appendix 8.1).

- Ray S1, S2, S3 and S4: These files contain the following variables.

*"Parentray": indicates the parental ray to which each section belongs, the ordering for rays depends on the original order assigned by the user in the digitizing step.

*"x,y_posbase": specifies the coordinates for the proximal node of a specific segment.

*"x,y_postip": Specifies the coordinates for the position of the distal node of a specific segment.

*"dleft, dright": specifies the distance from a segment mid-point to the adjacent rays along a perpendicular projection.

*"opstate": Indicates the presence of an upper segment.

*“xref”: Is the distance from the base of a segment to a horizontal reference line at the base of the fin. This is due to the fact that bony rays do not start at the same level.

-Seg S1, S2, S3 and S4: Four files are generated to contain the numbering of each ray based on digitized order and the distance from middle segment point to the reference line at the base of the ray.

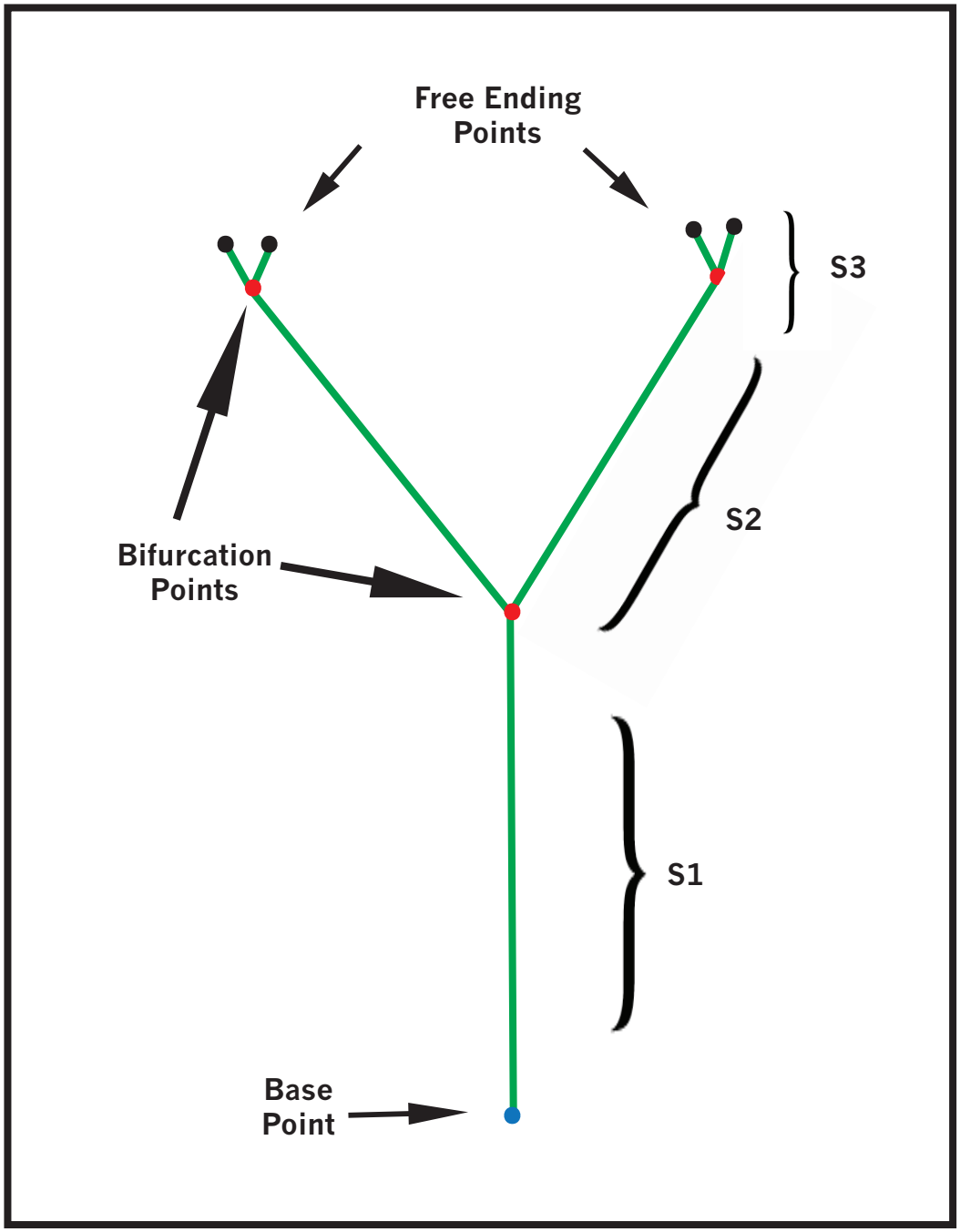

Figure 3.4 Diagram of ray sectioning. Registered rays can have between one to four sections. Each section consists in all the bony segments located between a bifurcation point and a base point or ending point. Segment data are grouped by section, including all branches within a given section. S1, S2, S3 on this image represent sections 1, 2 and 3 respectively.

Control checkpoint for screening and correction of errors

To proceed with the generation of bony ray and segment data analysis, it was necessary to perform a control checkpoint in every sample for correction of possible issues with the arrangement such as erroneous ray tracking, wrong detection of ray bases (such as the example shown in Figure 3.3A), bad branching or fusion of end points at the tips; which could lead to inappropriate data analysis.

This was accomplished with a couple of custom-made program. The first program searched for inconsistencies in ray tracking. These inconsistencies can include:

- Merging two different rays or branches.
- Duplications in base or ending points.
- Incomplete ray tracking. This happens when the program cannot find the next joint.
- Joint points can sometimes be skipped if the ray trajectory is not straight enough, or due to user error.

After the program identifies issues, it displays a list of rays that need correction. A second program was then used to access each specific fish on a specific time-point to individually fix the problem. The corrective measures include, re-digitizing a problematic segment, increase the area of joint points detection to solve skipped nodes or decreasing the area to avoid fusion of nodes between neighbouring rays. After correction of issues, re-assignment of segment positions and ray tracking data must be performed. When all issues are fixed we can now use programs for generating ray and segment data files for analysis with proper track positioning.

3.2.3 Visual Maps from Average Segment data

Elaboration of the Likely Fin

In order to prepare the average fin data to create the "likely fin" visual maps, sample data needs to be re-coded. Likely fin map outlines were generated for each time-point. Reference points were assigned to the outlines in a counter clock-wise fashion, resulting in a series of outline-maps for every sample (Figure 3.5A). These

outlines were grouped for a specific time-point and then overlapped to create a likely fin outline based on the average outline from all samples (Figure 3.5B).

For the next step, it was necessary to re-scale individual fin samples to the average outline through image warping. To represent the likely fin maps, a horizontal reference line ("X-position") was set at the base of the outlines generated in the previous step. Then, points were distributed on this reference line to represent the position of the rays in the dorsal-ventral axis of the fin, as well as the average position of these points (reference likely ray); this allowed the likely rays to be referenced within all average outlines for every time-point (Figure 3.5C).

After re-scaling, individual samples were then compared to a reference likely ray. As previously mentioned, this dataset consisted of samples that presented anatomical differences in the number of rays. For this reason, rays after re-scaling did not completely match the same position between different individuals (Figure 3.6A). Data from individual rays were re-assigned to their closest reference likely ray (Figure 3.6B). In this way, we were able to process and analyse data from fins with heterogeneous ray numbering. New warped image data were stored in files containing fin, ray and segment information.

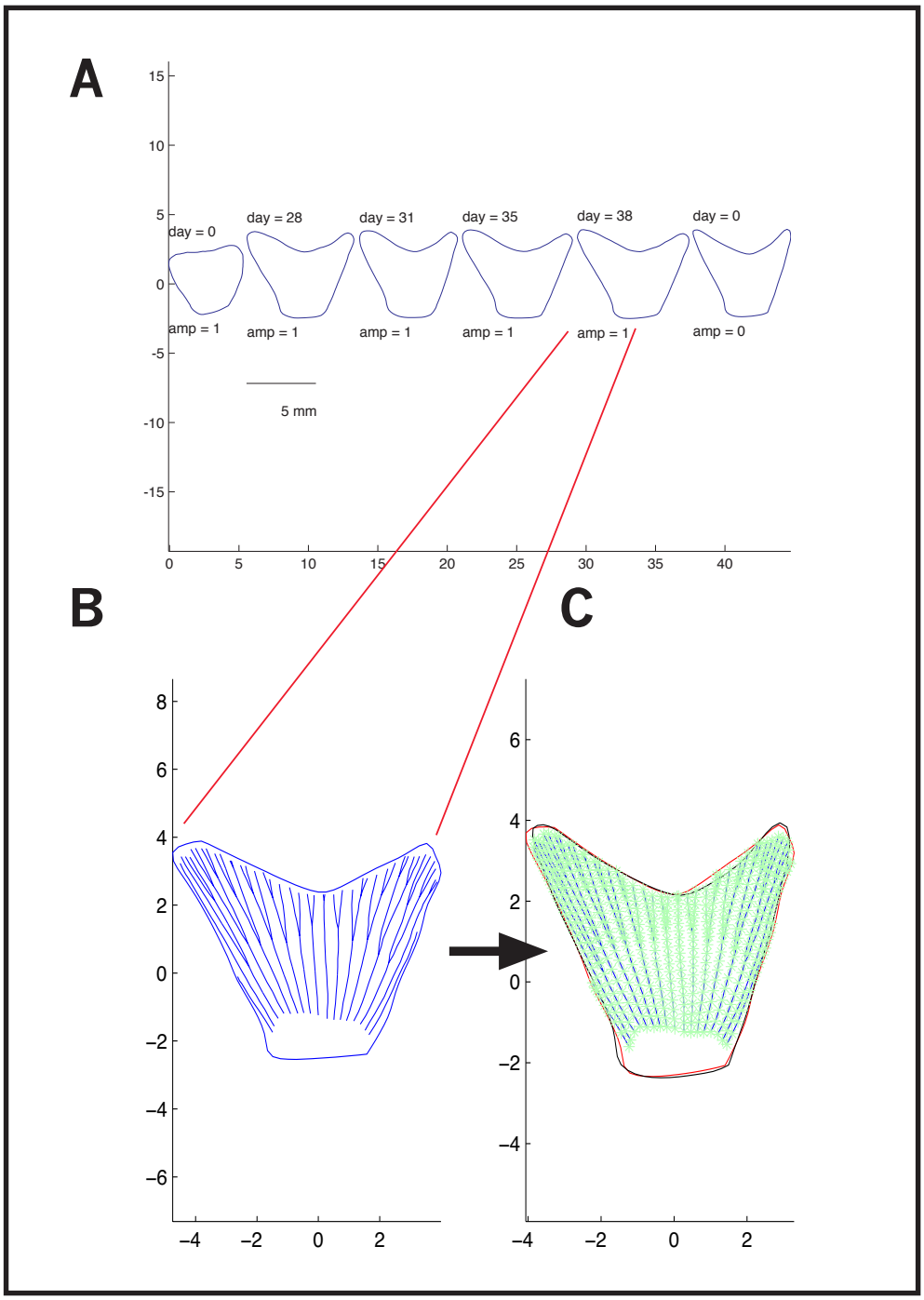

Figure 3.5 Obtaining average outlines and re-scaling of individual samples. **(A)** Average fin outlines for every time-point; the number of days after amputation is indicated above; the number below each figure indicates whether or not amputation occurred (1 or 0 respectively). **(B)** Average fin outline at one specific time-point; 38dpa. **(C)** Overlapping of all the samples at the same time-point as (B), and re-scaling within the average outline dimensions.

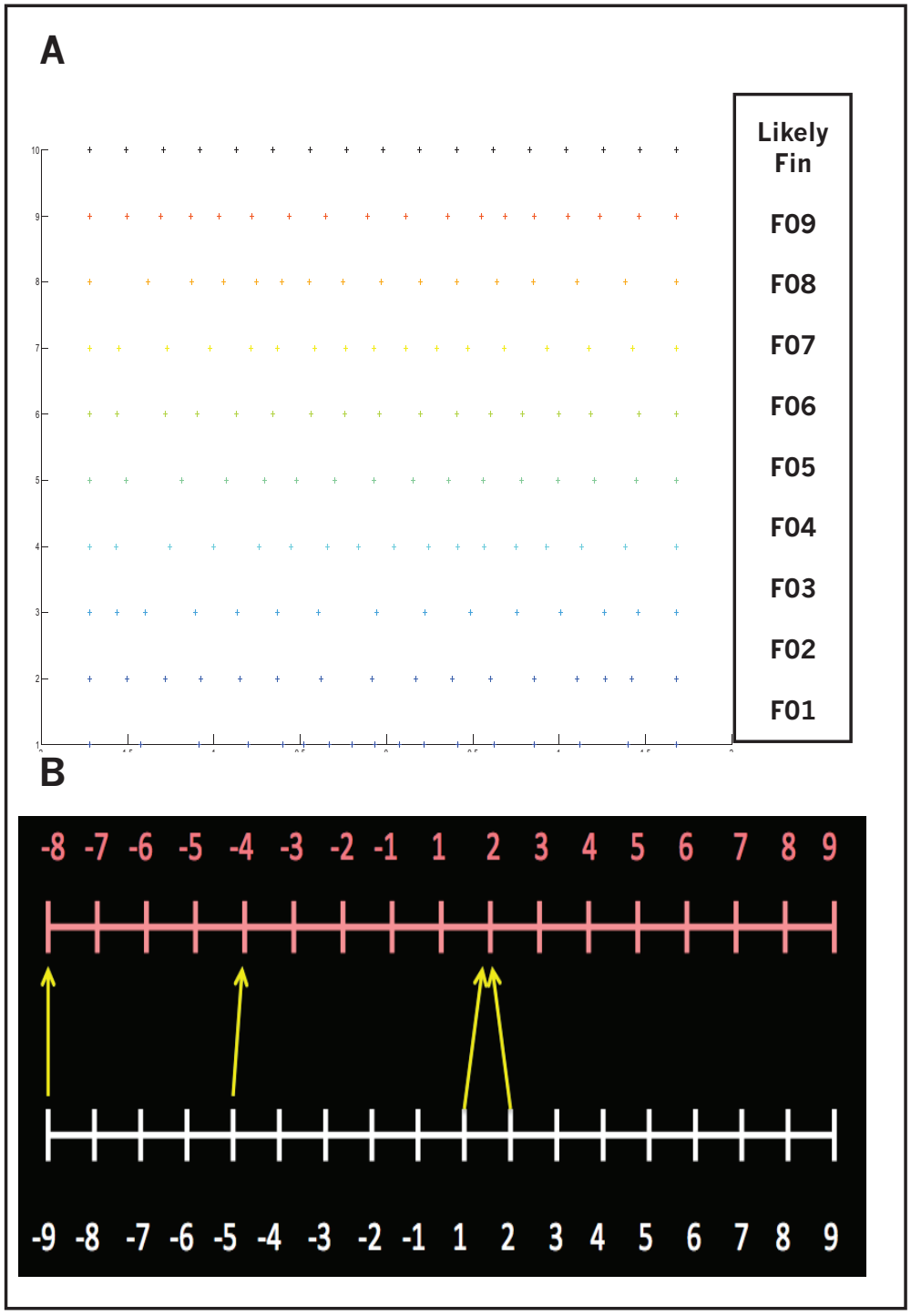

Figure 3.6 Re-assigning of ray data to likely fin reference rays. **(A)** Dots array showing ray spacing of the likely fin compared to individual samples of the distal subset after re-scaling; each individual dot represents a ray and a row of dots represents a fin sample. **(B)** Schematic representation of ray numbering distributed in the dorsal-ventral axis of the fin, arrows show how rays at the same position have different ray number when comparing samples with 17 (pink) and 18 (white) rays, respectively.

We merged individual files to create complete sheets with likely fin for analysis and for generating graphic maps using the average ray data from the longest branch of each ray. To verify that all rays between time-points match after the warping procedure, another checkpoint program allows tracking rays and segments across files to verify that data after warping is correctly stored in the files. This checkpoint is similar to that performed before image warping.

With all the necessary files, we generated a series of matlab figures (.fig) and their corresponding graphic file format (.eps) to represent maps of: a) Segment lengths, b) Number of samples per ray, c) Segment ID distributed through bony rays; in addition to maps with the d) Standard errors of segment lengths and e) Standard error maps of segment ID positions; made from average data.

Finally, we compared two sets of average maps created in the last step using a custom made program to compare likely fin maps. The program output generated three new figures:

1) Showing the differences in segment lengths between two sets of maps of different developmental time-points.

2) Displaying the differences in the segments IDs at specific regions of the fin rays between two maps of different developmental time-points.

3) Comparing two maps of different developmental time-points and showing the difference in the number of samples.

3.2.4 Testing Segment Differences at the Amputation Plane

We performed segment measurement at the amputation plane of a new sample set of 11 fish, after distal amputation (4mm from caudal peduncle). Measurements were carried out before amputation and after regeneration using the software for measuring digital images ImageJ.

The reason for using this method was to corroborate observations from likely fin visual map comparisons. By using ImageJ, we measured the amputation plane in a faster way without the need of extracting the detailed segment data of the samples at each time-point required in the custom digitizing programs. However, full segment

and ray data is not obtained in this way. The original distal amputation sub-group was also measured with ImageJ for comparison.

Scale pictures were taken at several magnifications (1.0x, 1.25x, 1.6x, 2.0x, 2.5x, 3.2x and 4.0x) and were used as a reference to measure distances on an image at a specific magnification.

To determine where the amputation plane would correspond in images of fins still not amputated (before amputation or B000) and in fully regenerated fins, the distance of each sample after amputation (A000) was measured. These distances allow identifying which segments were located at the amputation plane. Segment lengths at the level of amputation are obtained with ImageJ and recorded in excel files, and numbered from left to right (dorsal to ventral) for a given sample (see appendix 8.2).

3.2.5 Optimization of Ray Growth Model

The ray growth model postulated by Rolland-Lagan and colleagues (2012) accounts for final ray length and segment patterns (see section 1.8.1) during a given amount of simulation steps depending on the concentration of the interacting morphogens (Figure 3.7).

Parameters in this model are:

- Initial production of hypothetical morphogens “X”, “G” and “S”. Morphogen “X” is produced proximally and its concentration determines the concentration level of “G” and “S” in the distal compartment. “G” promotes growth, and “S” inhibits the formation of joints, hence controlling segment patterning.
- Compartment lengths. Simulated rays are made from compartments that can represent an individual cell or group of cells.
- Diffusion rate of hypothetical morphogens from one compartment to another.
- The rate of increase of morphogen “X” production in the first compartment in function of time (beta).

- Number of simulation days (A single day represents 1,000 simulation steps in this model).
- Amputation level in millimeters, if any.
- Time at which amputation will be simulated, in days.

The output from the program for ray growth model (Figure 3.7) created a file with a matrix that stores simulation data. The name of this matrix was labeled “segL” and it contains three columns:

a.- Compartment number where a joint is present.

b.- Distance in compartments between current joint and the previous recorded joint (Length of the bony segment in number of compartments).

c.- Ray number on which the joint is located (useful when modeling multi-ray simulations in whole fins).

A brief summary of the methods is shown in Figure 3.8.

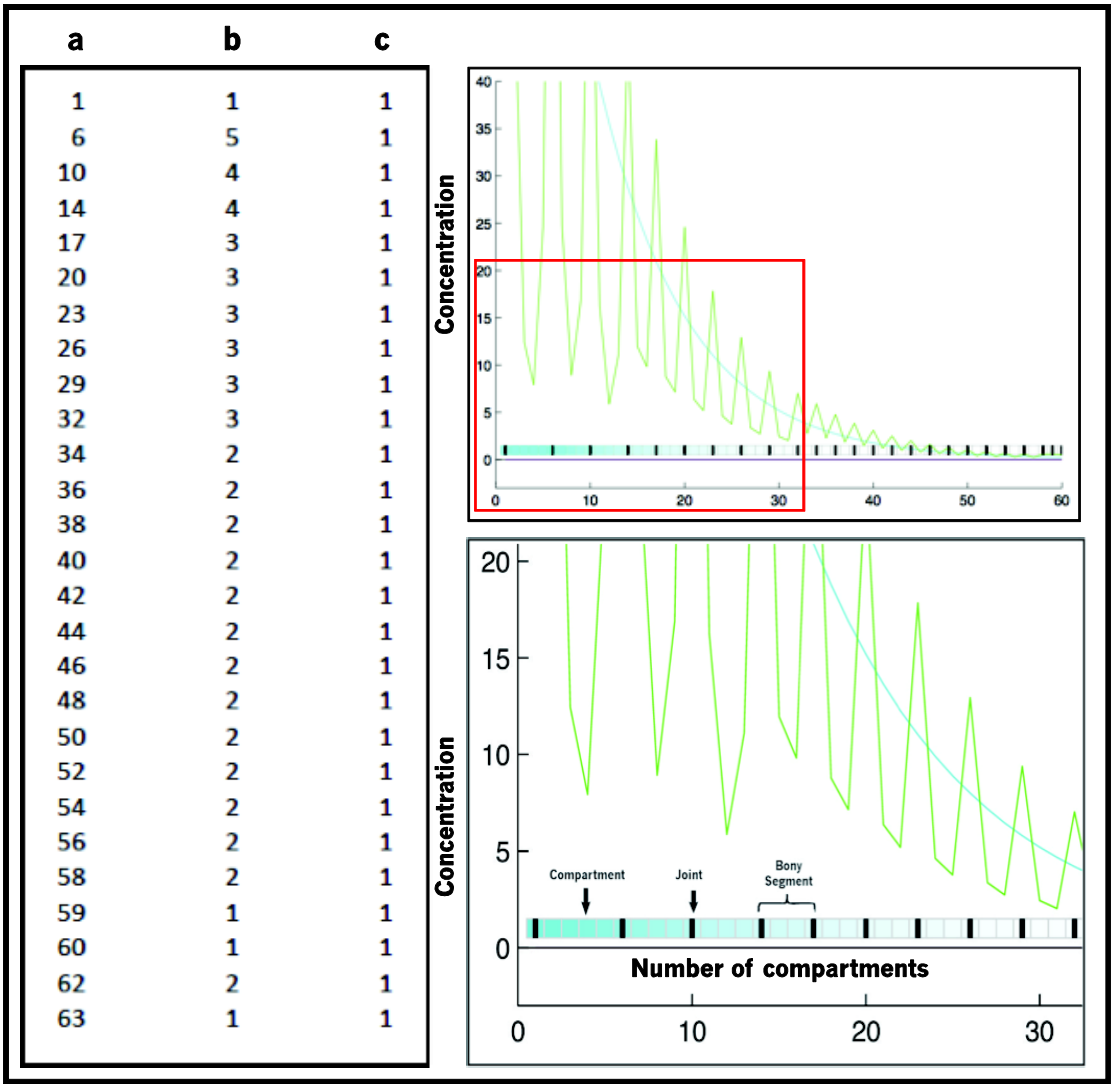

Figure 3.7 Output of ray growth model. **(Left)** Matrix "segL" which records joints spacing in terms of number of compartments as previously described: column "*a*" is the compartment number where a joint is present, column "*b*" is the distance in compartments between previous and current joint, column "*c*" is the ray number in which the segment being recorded is located. **(Top right)** Graphic from ray model output showing the different levels of morphogen concentrations in arbitrary numbers (Y axis) and length of the simulated ray in number of compartments (X axis). **(Bottom left)** Detailed section from top right image; blue squares represent compartments, black lines indicate the presence of a joint, green peaks show the concentration of morphogen "S" and blue curve is the concentration of model morphogen "X".

Calibrating the Model Parameters

In order to validate the ray growth model, changes in the individual parameters had to be made, as originally the values were arbitrary. Using stepwise regression we determined which parameters (section 3.2.5) had a better predictor effect over the growth curve from the simulation (see appendix 8.3). To find the best values for these parameters we relied on data available from the amputation experiments, and different ranges of values were systematically tested over hundreds of simulations.

We compared the ray growth curve output from the simulation model using a given set of parameter values against the expected growth curve from experimental data. Then we used the Root Mean Square Error (RMSE) to quantify error. To optimize the supervision of results, we only kept the results of 30 sets with the lowest RMSE obtained.

The RMSE has been used in other studies to evaluate model predictions for example, in crop simulation models growing under specific conditions. One particular study concluded that a process-oriented model was a good predictor to simulate biomass and grain yields over a wide range of conditions by testing the RMSE of population densities, grain maturity and aerial biomass (Villalobos et al., 1996).

Calibration of ray growth

As it was previously mentioned, it was necessary to compare the growth curves from the model output against experimental values. However, some of the parameters above are involved in growth while others control joint spacing. For the case of ray growth, we used a custom calibration program to calculate the RMSE after the simulation output with a specific set of values.

Simulation results were stored in excel files where each recorded event consists in the total ray length (in mm) and the elapsed time (in days) occurring every 250 simulation steps. This means that four events are recorded per day of simulation. In addition, the first simulation event was set to start at 26.25 days of development as seen in experimental results previously obtained prior to my graduate studies.

Finally, a simulation curve was obtained which was compared to the experimental curve. To calculate the RMSE, every point from the experimental curve was subtracted from the model curve, and then we obtained the square of the differences. The sum of all values was divided by the number of elements and the square root is then calculated from the resulting value.

Calibration of segment lengths and patterns

The model also accounts for bony segment and joint patterning. For this reason it was necessary to optimize the model so the number of segments would represent what we have seen experimentally. This was achieved by increasing the level of production of morphogen "S" as well as its diffusion rate (Ds) in the ray growth model. As previously explained, these elements are responsible for inhibiting the formation of joints and thus joint spacing and segment length.

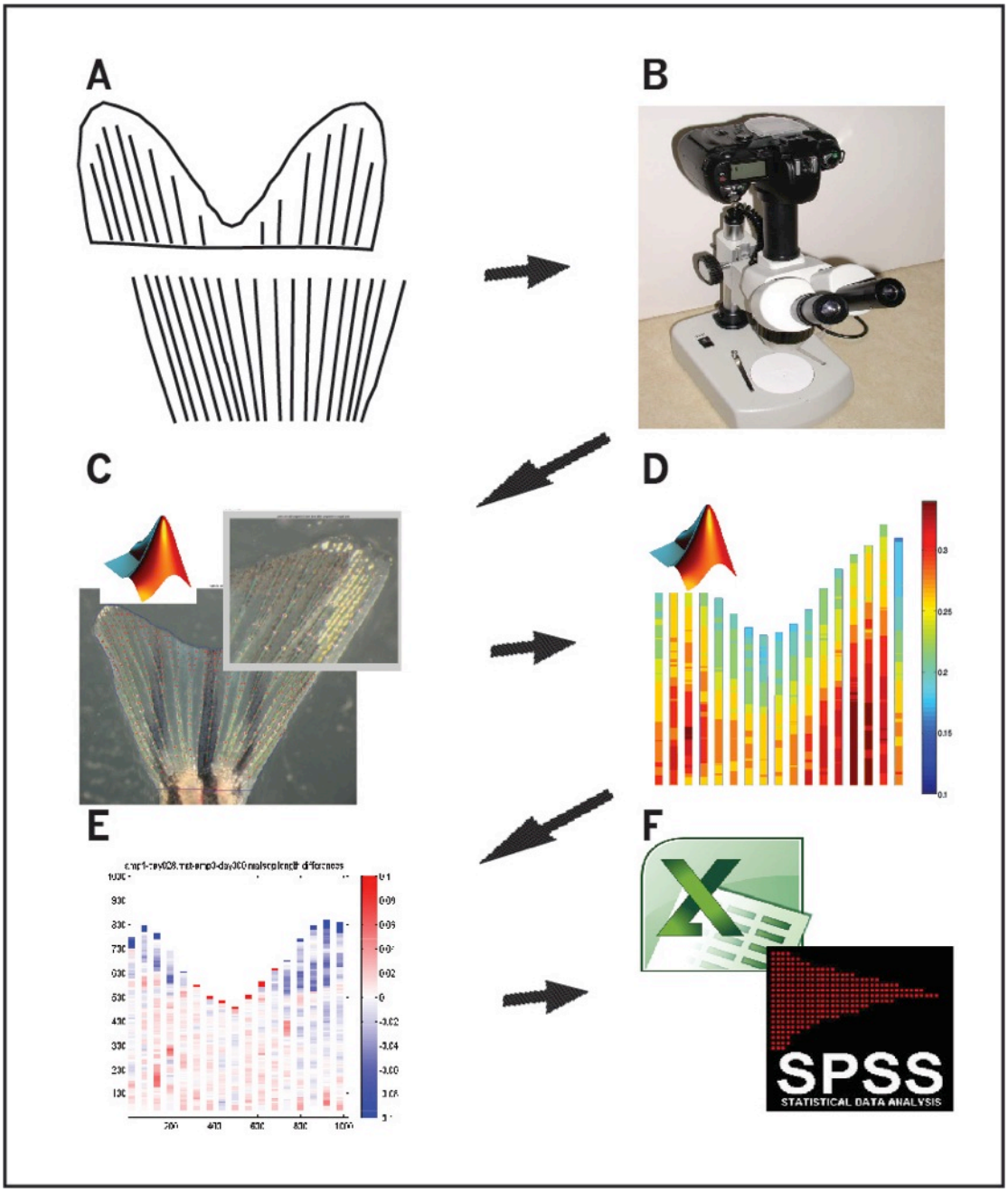

Figure 3.8 Summary of methodology used in this thesis. **(A)** Fin amputation experiments. **(B)** Samples imaging during development and regeneration. **(C)** Data extraction. **(D)** Elaboration of Likely Fin maps. **(E)** Maps comparisons at different time-points. **(F)** Data and Statistical Analysis.

Chapter 4 – Results

We used a computational approach following a quantitative framework developed for the analysis of fish fins (Rolland-Lagan *in prep*). This allowed us to generate "likely fin" maps based on average data, and systematically use them to compare the results obtained using raw data. We analyzed fish fin development and regeneration based on dpf although, ideally fish size is a better parameter for this purpose. By using age instead of size we tested the performance and reproducibility of the likely fin method. We observed reported segment trends and then further validated the likely fin maps by the obtaining of standard error maps.

We observed changes in specific areas of the fin after regeneration. In addition, we used statistical analysis to test segment length differences by performing Friedman's test and post-hoc analysis using the data from the proximal-distal amputation experiments, as well as using a new batch of samples in which the distal amputation was repeated for corroboration.

4.1 Proximal-distal Amputation Experiment Results

4.1.1 Extraction of Fin Data Before Amputation

Images of fish at 167 dpf were obtained and recorded just before amputation took place (B000). After imaging, fish were placed in a recovery tank and then re-anesthetised in order to perform the amputations. Three images per sample were taken for each time-point (Figure 4.1), and organized as described in the methods section. Dark field images allowed us to easily identify bony segments and joints from the fin ray, and to digitize these images using our custom programs. Fish were re-imaged right after amputation at 0 dpa (A000).

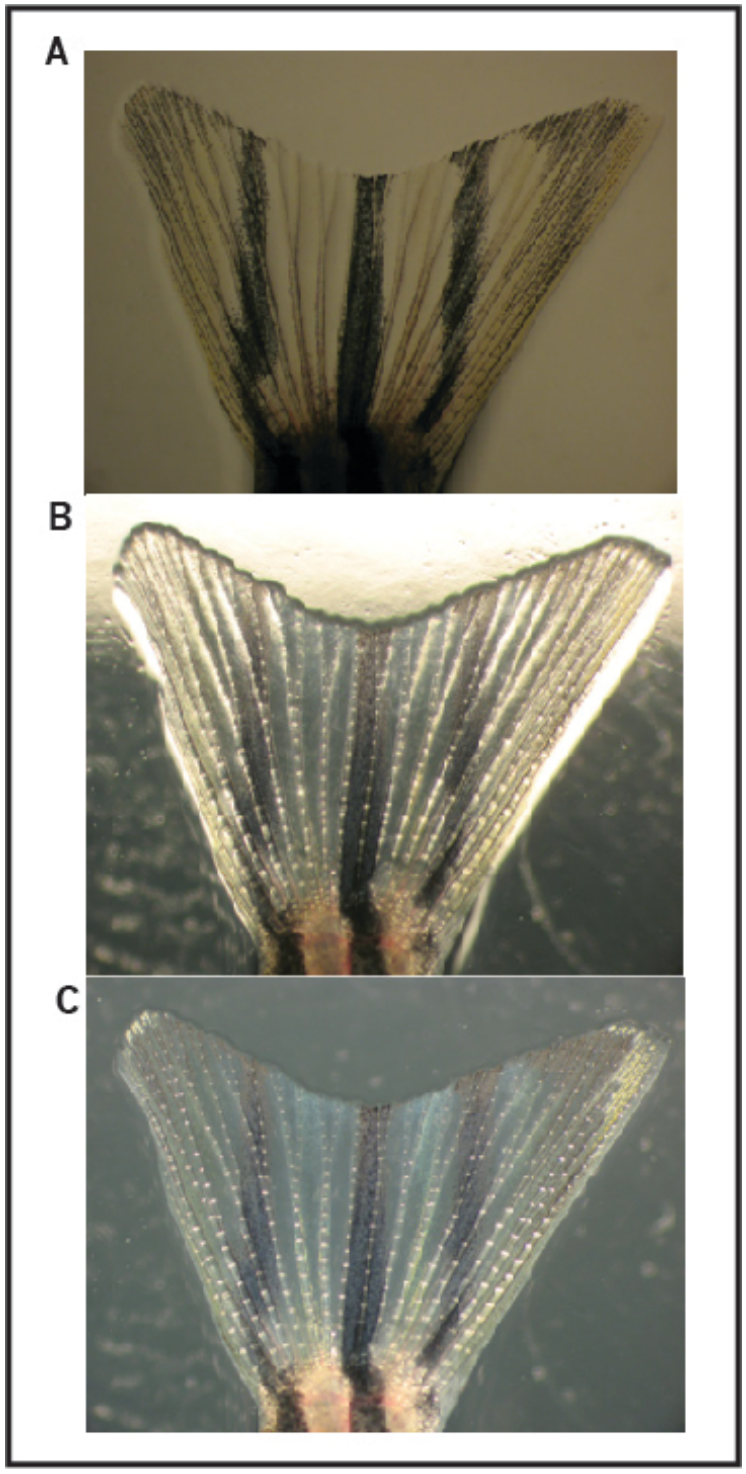

Figure 4.1 Fins imaged with different lighting field for joint identification. All images correspond to the same sample at the same developmental stage (167 dpf) before amputation. **(A)** Bright field. **(B)** Intermediate. **(C)** Dark field. *Images, by Mathieu Paquette*

The digitizing process allowed us to extract fin length before amputation (B000). This analysis showed that the average fin length was 6.05 $\pm$ 0.78 mm (n= 17), width was 7.06 $\pm$ 1.21 mm, and fin area was 24.62 $\pm$ 7.04 mm^2 (Figure 4.2A,C).

Ray lengths at 167 dpf (Figure 4.2B) ranged from 3 mm to 6 mm depending on ray number, and the number of segments per ray varied from 12 to 24 segments (Figure 4.2D); standard error bars were larger in lateral rays [-10, -9, 9, 10] than in medial rays [-8 to 8] (please see explanations for ray numbering under section 3.2.1 in the chapter Materials and Methods). Average segment length ranged from 0.23 mm to 0.30 mm (Figure 4.2E). As in the case of ray length, segment length of the most lateral rays, rays [-10 and 10], presented the highest variations and, with the highest level of error.

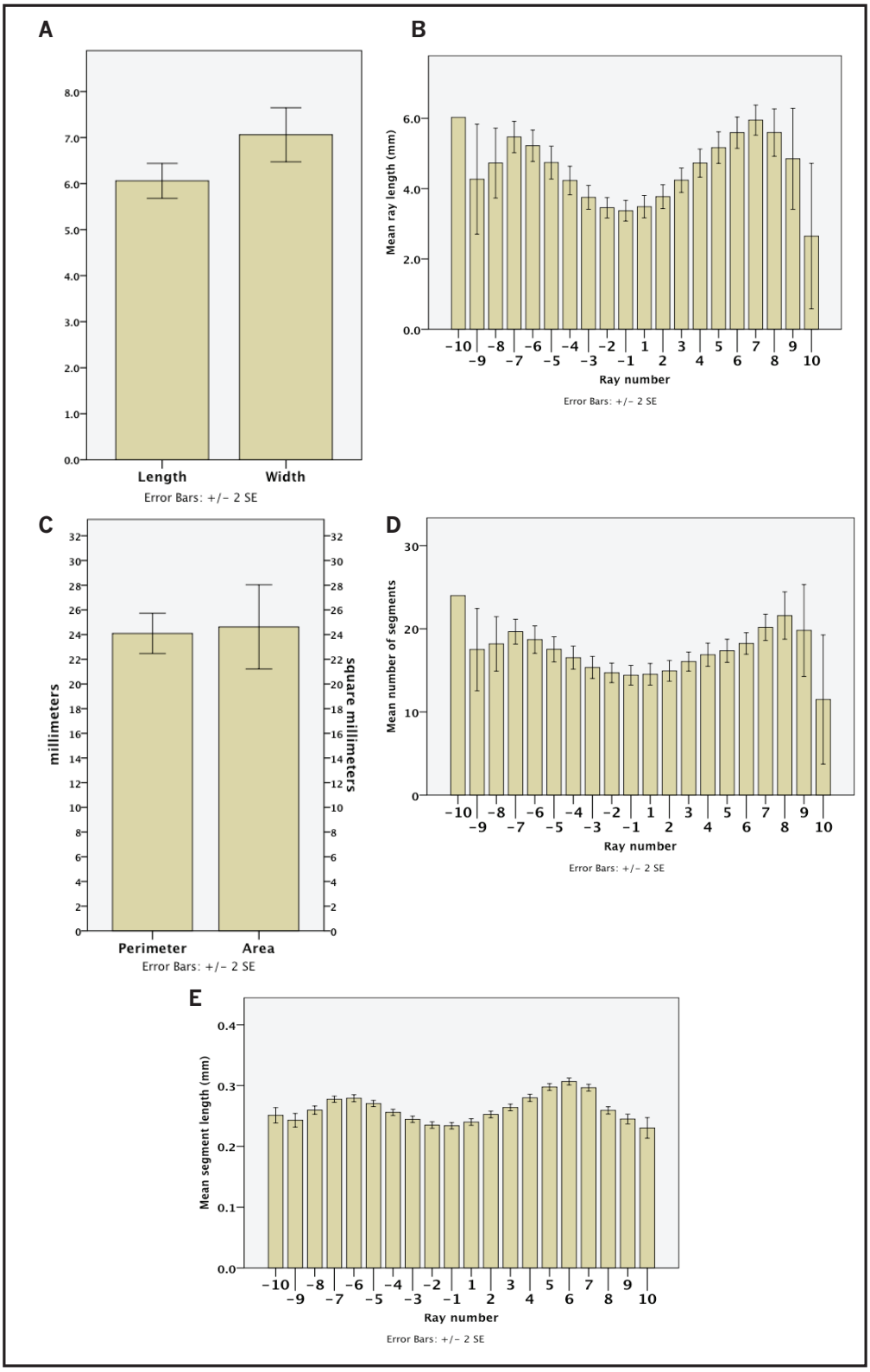

Figure 4.2 Data overview of the caudal fin samples (n=17) before amputation (167 dpf). **(A)** Mean fin length and width (in mm) of the fish before amputation. **(B)** Mean ray length by ray number. **(C)** Mean fin perimeter and area before amputation. **(D)** Number of segments by ray number. **(E)** Average segment length by ray number before amputation.

4.1.2 Extraction of Fin Data After Amputation

To analyse bony segment patterns after regeneration we performed two types of amputation based on their distance from the caudal peduncle. Amputations at 2 mm (proximal) and 4 mm (distal) were performed (see appendix 8.4) to evaluate and compare differences in fin, ray and segment lengths as well as segment numbers and their positions within the fin. Following distal or proximal amputation, fish were imaged and then returned to the fish room. These fish will be referred as distal and proximal subgroup, respectively. Imaging took place two times per week from 0 dpa until 80 dpa.

For the analysis of fins "after regeneration", we analysed fin ray and segment patterns at 38 dpa (A038). This was considered as the "after regeneration" time-point, although in some instances some fish were able to regain their pre-amputation length as soon as 28 dpa. This is consistent with the times reported in the literature for fin regeneration which vary from three weeks to more than 38 days to fully regenerate at 28°C (Poss et al., 2003; Rolland-Lagan et al., 2012), as well as with the results obtained from colleague Valerie Tweedle (2012).

Since it is not possible to amputate at exactly 2 or 4 mm from the caudal peduncle in every sample, small variations in length are observed for amputated fins at 0 dpa (A000). As such, the average fin length after distal amputation was 4.24 $\pm$ 0.28 mm (n=8), and the average fin length for the proximal subgroup was 2.67 $\pm$ 0.33 mm (n=9). The average fin widths at this time-point were of 6.24 $\pm$ 0.93 mm and 4.89 $\pm$ 1.27 mm for distal and proximal groups, respectively. The average fin areas were 21.06 $\pm$ 4.92 mm^2 for the distal and 12.63 $\pm$ 3.73 mm^2 for the proximal group.

Original fin length is recovered after 28 days of regeneration following proximal and distal amputation

Original fin length recorded before amputation (B000) was 6.05 ± 0.78 mm. After 28 dpa (A028), fins (of both subgroups) had regenerated to achieve an average total fin length of 6.23 ± 0.46 mm. As fin regeneration progresses, it is observed that the average length of both subgroups at A028 is closely similar to the length at A038 (6.23 ± 0.46 mm and 6.34 ± 0.42 mm respectively). The average fin length after regeneration (A038) was 6.33 ± 0.41 mm and 6.35 ± 0.46 mm for distal and proximal subgroups respectively (Figure 4.3A). Fin lengths obtained between the time-points between 28 dpa to 38 dpa was consistent (Figure 4.3A). This validates the results obtained by the custom digitizing programs.

In the case of fin width and area we observed that they both are larger in regenerates than in fish before amputation and this is more evident in the distal subgroup (Figure 4.3B,C). In addition, both fin width and area showed significant variability within the same subgroup at different time-points (Figure 4.3B,C). The inconsistencies in fin area and width can be attributed to fin spreading at the time of imaging. This indicates that fin width and area are not ideal parameters for measuring fin growth in comparison to length while using these kinds of imaging tools.

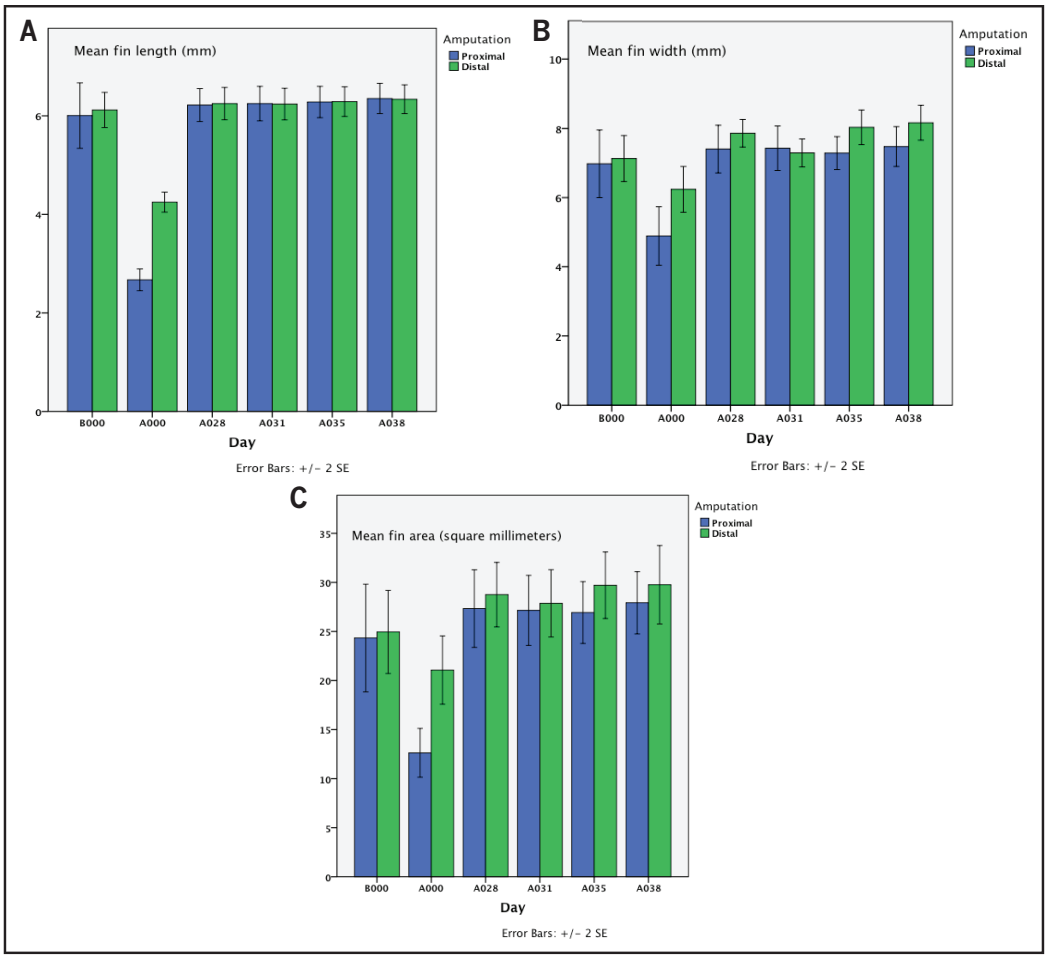

Figure 4.3 Fin lengths, widths and areas at all time-points by amputation type (n=17). **(A)** Fin length progression from B000 to A038. **(B)** Fin width progression from B000 to A038. **(C)** Fin area progression from B000 to A038.

Lobe rays have faster regeneration rate than cleft rays

Comparison of individual ray length in both subgroups shows that even when all ray lengths are very similar just after amputation (A000), lobe rays grow significantly larger than cleft rays at the end of regeneration (A038). In other words cleft rays regenerated more slowly compared to lobe rays (Figure 4.4C,D). In accordance with these data, we also observe in general that ray number [8] (ventral lobe) reflects total fin length and grows linearly in comparison to ray number [1] (cleft) (Figure 4.5A). Ray [1] shows lengths between 2 mm to 4 mm even when the whole fin has already regenerated between 3 mm to 7 mm (Figure 4.5B). We also observe that most lateral rays show high length variability (large error bars) before amputation (B000) as well as at all time-points after amputation.

Segment patterns after regeneration

The numbers of segments were also quantified at all time-points after amputation (Figure 4.4E,F). In the distal group, average number of segments ranged between 10 to 14 segments in non-lateral rays, while in the proximal group the range of number of segments ranged from 6 to 9 in average for non-lateral rays at the moment of amputation (A000). After regeneration at A028, the number of segments ranged from 15 to 23 on the proximal group and 15 to 21 in the distal depending on the ray. When comparing before amputation (B000) and after regeneration (A038) the average number of segments was similar (22 and 23 segments respectively for 3rd longest ray). Lateral rays showed larger variations from these values (Figure 4.4E,F).

In addition, we measured the segment length (Y) as a function of distance from the base (X), obtaining regression values from every ray in the form of the equation (Y= b + aX) using the IBM SPSS v22 Statistical software; where (a) is the segment regression slope and (b) the constant. In average, the length of the segments was decreasing linearly for most rays (although not always) as they approached to the tips (Appendix 8.5). As in the case of ray length, segment regression slope (a) and constant (b) of lateral rays were inconsistent with the results observed in the other rays more medially located in the fin (Figure 4.6).

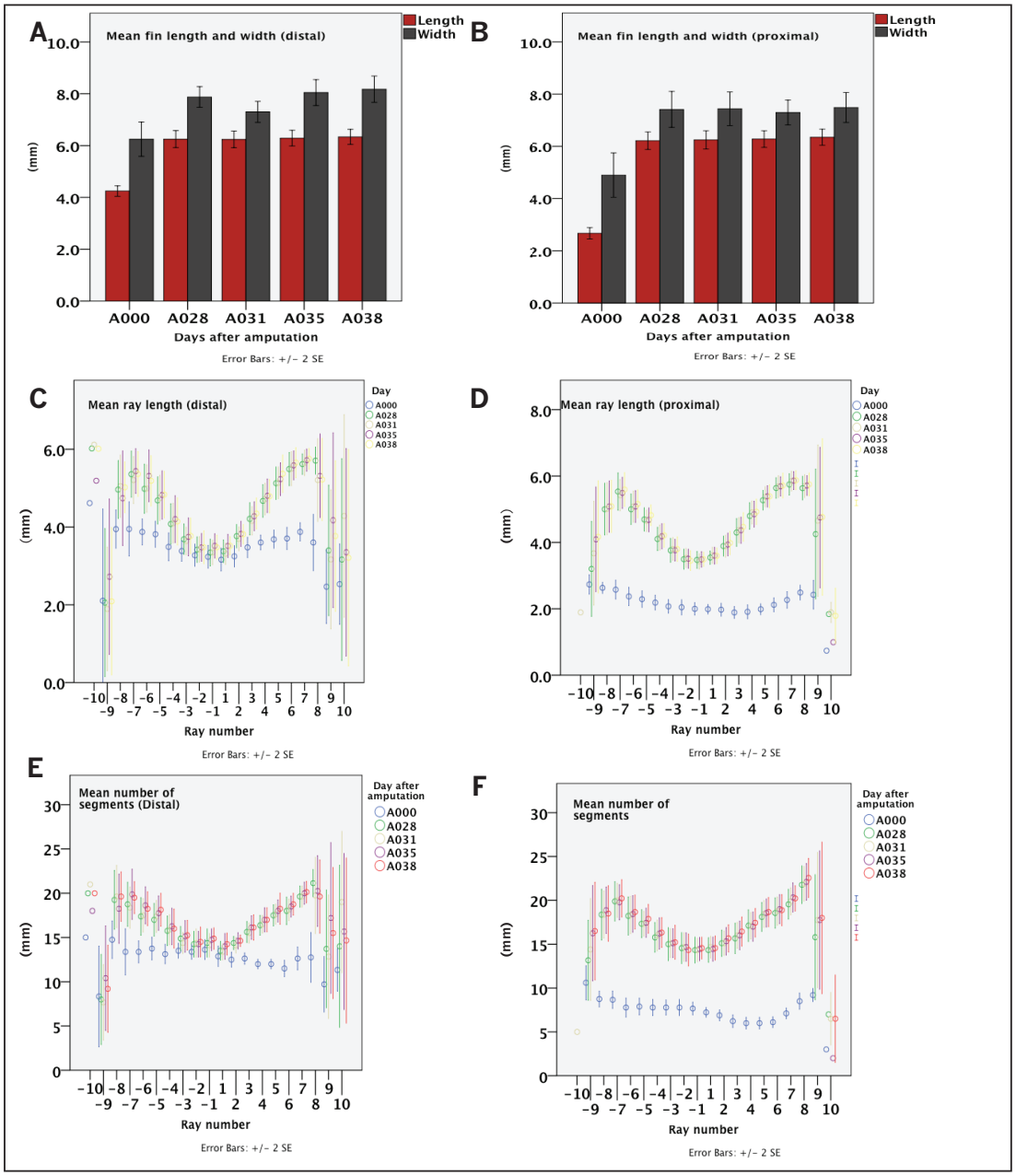

Figure 4.4 Quantitative analysis of fin regeneration. **(A)** Mean length and width of the fins after amputation at 28, 31, 35, and 38 days post amputation in the proximal subset, **(B)** and in the distal subset. **(C)** Mean ray length of the fins at each time-point after distal amputation, **(D)** and after proximal amputation. **(E)** Mean number of segments at each time-point after distal amputation, **(F)** and after proximal amputation. Blue dots correspond to the time-point right after amputation (A000).

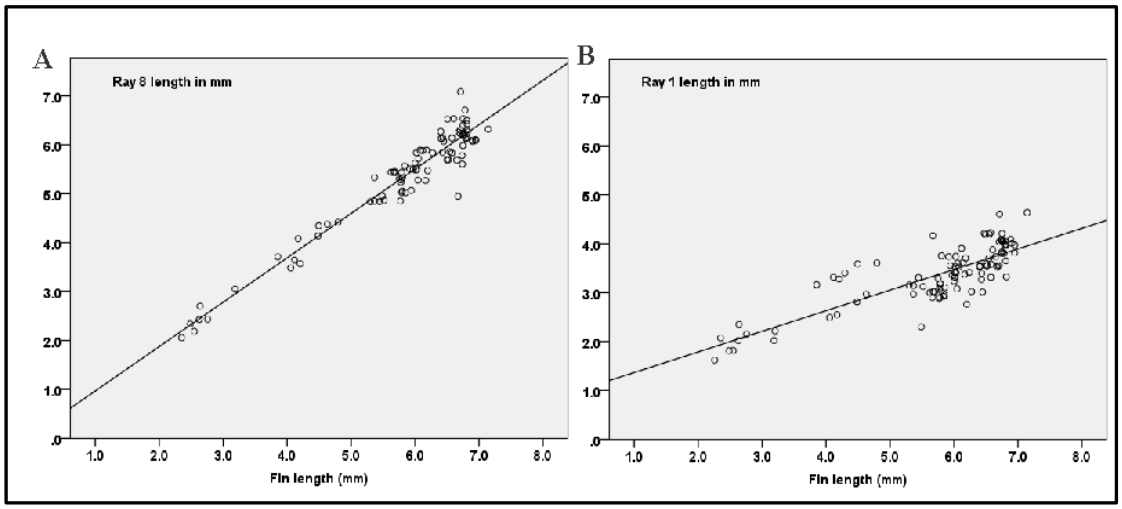

Figure 4.5 (A) Ray [8] length in function of fin length. **(B)** Ray [1] length in function of fin length. Time-points evaluated were 167 dpf, 0 dpa, 28 dpa, 31 dpa, 35 dpa and 38 dpa, (n=17).

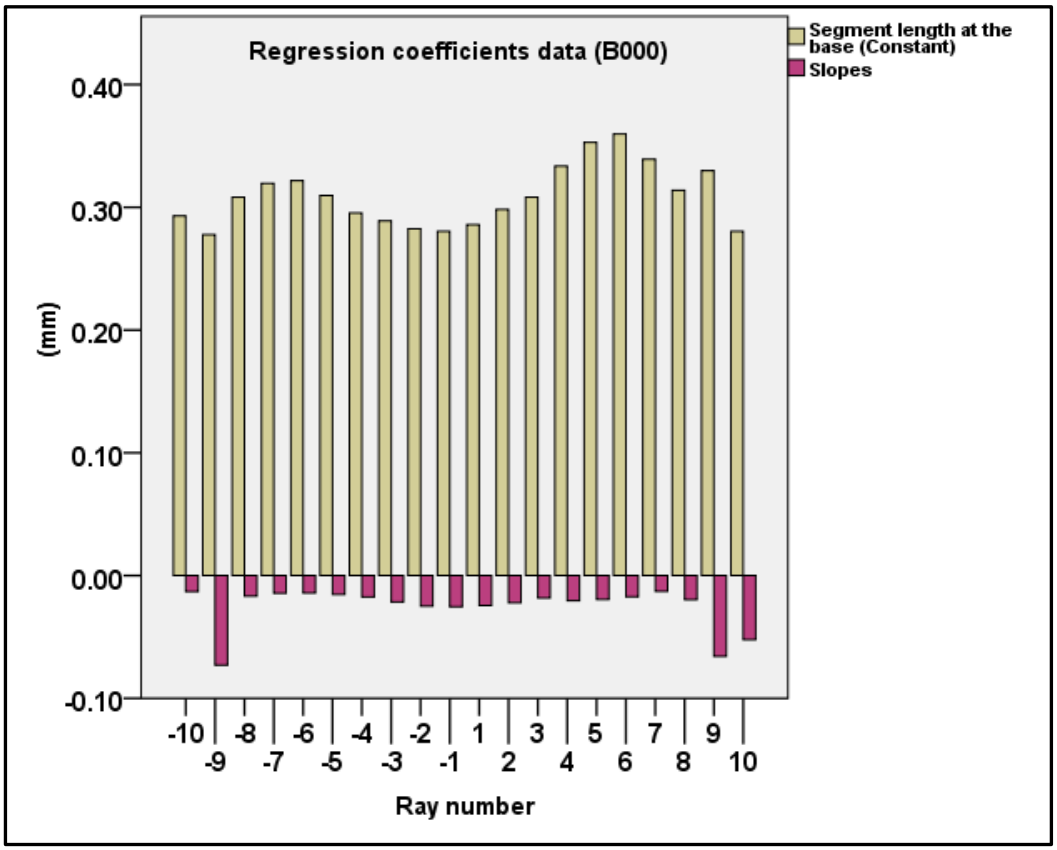

Figure 4.6 Mean regression coefficients of segments before amputation by ray number. Yellow bars represent the regression equation constant (b) or mean length of the first segment at the fin base, and pink bars represent the slope (a) or decrease of segment length as segments locate closer to the tip.

Analysis by fin section

Ray data were divided into sections based on the bifurcation positions within a ray, as described in the methodology chapter. Each section corresponds to the portion of a ray located between two bifurcation points, or for the first section (S1) between the ray origin to the first bifurcation, and for the last section between the last bifurcation to the tip of the ray.

We noticed that section 1 (S1) represents the largest section of the rays. For the cleft rays, S1 contributes to at least 75% of the whole ray, and for lobe rays they represent roughly 45% to 50% of the whole ray (Figure 4.7A,B). The following sections become progressively smaller, section 2 (S2) being larger than section 3 (S3) and section 4 (S4). Moreover, not all rays have S4 and most-lateral rays only have S1 due to the fact that those rays do not present any bifurcation. In addition, S1 average length ranged between 2.2 mm to 4.1 mm.

Consistently with full ray data, S1 sections of rays closer to the lateral sides of the fin (positions [-9 and 8]) before amputation showed larger error bars compared to more inner rays, as observed with the average total ray length and the average segment lengths (Figure 4.7C). Furthermore, inconsistencies in S1 lengths were observed when results are presented as proximal and distal subgroup at 38 dpa, especially in lateral rays where we can observe differences in average lengths up to 2mm for the same ray position between distal and proximal subgroup (Figure 4.7D).

Average segment lengths obtained from S1 portions of the rays (Figure 4.8A) were similar to the segment averages obtained from the whole ray. In the whole ray, the values ranged from 0.24mm to 0.31mm (Figure 4.2E). However average segment lengths for S1 were larger than segment length average from the full ray, as the average for the full ray included smaller segments from more distal sections (S2, S3, S4). The difference is more evident for the rays in the lobes where the ranges varied from 0.24 mm to 0.33 mm (Figure 4.8B).

In accordance to published data (Iovine & Johnson, 2000; Rolland-Lagan et al., 2012), the overall segment length decreased from the proximal to the distal position along the ray (Figure 4.8C). This pattern is ray-specific and these results are similar to those obtained prior to my study with another fish group that showed that cleft segments were shorter than lobe segments at the same proximal-distal position (Rolland-Lagan *in prep*.).

Data of bony segment patterns showed that segments presented average ranges of 0.2 mm (cleft) to 0.3 mm (lobes) and that segment lengths decreased from proximal to distal, with segments as long as 0.4 mm at the base and as short as 0.1 mm near the tip of a single lobe ray. This is consistent with the general observation that cleft rays have fewer and shorter segments than the lobes (Goldsmith, 2006), and that segments located at the base of a ray are longer than segments of the tip of any given ray (Iovine & Johnson, 2000; Haas, 1962). This pattern however, does not seem to be affected by bifurcations. Analysis of the segment length along the proximal-distal axis in non-bifurcating rays (most-lateral rays) shows that segments still decrease in length as they are more distally positioned within the ray (Figure 4.8D).

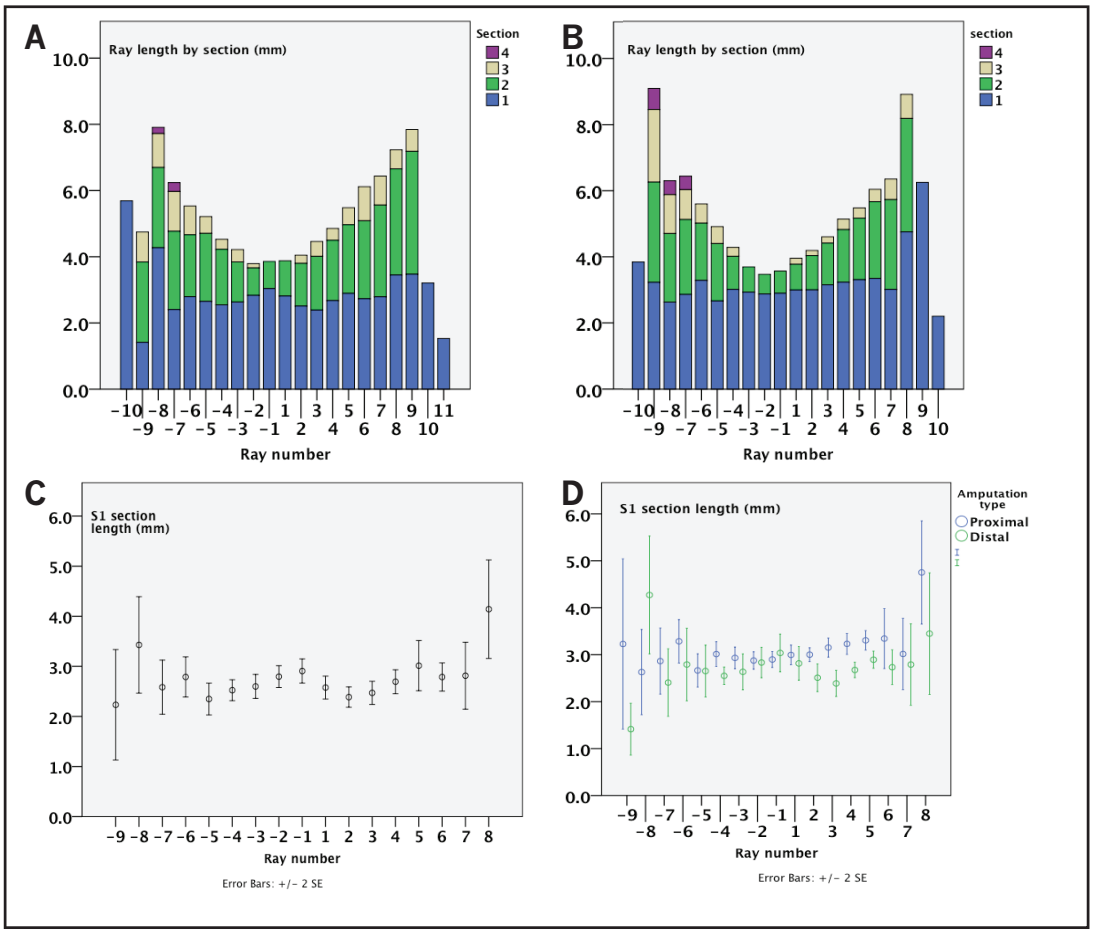

Figure 4.7 Ray patterns. Ray sections (color coded in A and B) and their corresponding average sizes within the distal **(A)** and proximal **(B)** amputation sub-groups at 38 dpa. Lengths of section-1 (S1) by ray number without including most lateral rays before amputation **(C)** and after regeneration **(D)**.

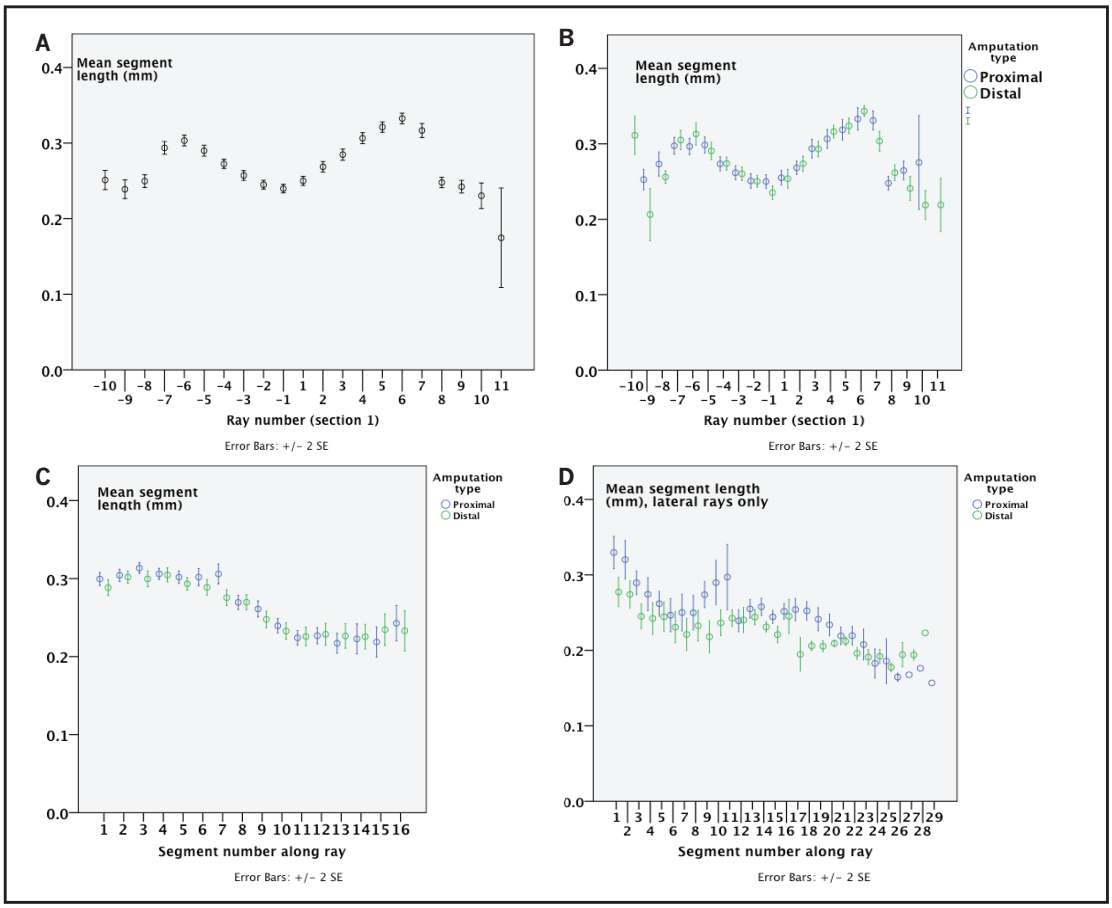

Figure 4.8 Segment patterns in section 1 (S1). **(A)** Average S1 segment lengths in each ray at B000. **(B)** Average S1 segment lengths in each ray at A038. **(C)** Mean S1 segment lengths in function of the segment position along the proximal-distal axis at A038. This graph does not include lateral rays. **(D)** Mean segment lengths in function of segment position along the proximal-distal axis at A038 of lateral rays only. Linear decrease can be observed in individual rays (please see appendix 8.5).

Problem with the analysis of ray data

Digitizing and data extraction of regenerating fins after two types of amputation allowed us to track the progression of fin regeneration until 38 dpa and to compare the rates of regeneration between fins following distal and proximal amputations. Ray patterns, as well as detailed individual segment data were also evaluated as described above.

A problem arises however due to the variability of the number of rays per fin: most of the fins have between 16 to 18 rays and in one case, there were only 15 rays (Figure 4.9A,B). Large variations and error bars can be observed when analyzing individual ray and segment patterns when these data are grouped and categorized by ray number, as ray numbers do not always match between samples due to ray number differences.

For instance a fin sample can present nine rays in the ventral lobe while another sample shows only seven. In this case grouping and analyzing ray and segment pattern data for "ray number 7" (ray [7]) counting from the cleft position in all samples is not appropriate, as in the first case the ray in question is the longest ray of the ventral lobe, while in the second case that ray would correspond to the most lateral ray. For this reason we created the "Likely Fin" visual maps on average data, which allowed analyzing ray patterns from fin samples with variations in ray number (see methods 3.2.3; Figure 3.6).

The Likely fin was set as a fin with 17 rays

Visual maps from average segment data (likely fin maps) were created to analyze segment patterns (see methods 3.2.3). In order to create the likely fin maps from our samples, all ray data had to be uniformly re-arranged in 17 ray-zones as this was the most common number of rays (Figure 4.9).

Ray data was re-arranged within these 17 ray-zones for analysis using average segment results from all samples (see appendix 8.6). For the generation of the likely fin, we only took into account the segments contained in the longest branch when dealing with bifurcations, as there was no difference if we used both branches to analyze ray lengths (see appendix 8.7).

Ray numbers in the likely fin were set as [-8 to 9], with eight rays in the dorsal side and nine on the ventral. Ray mean lengths re-arranged within the 17 ray-zones of our likely fin show that ray number [8] is the longest in both subgroups and ray [-1] and ray [1] are the shortest in the proximal and distal groups, respectively.

Unlike our raw data analysis, average length of the most lateral rays are no longer larger than the rays in the middle of the lobes, which is consistent with observations in individual fin samples (Figure 4.9C,D). Individual fin samples show longer rays in the middle of the lobes compared to most lateral rays or in the cleft.

It is important to mention that the creation of likely fin maps through image warping and ray re-arrangement only distributes ray data based on the dorsal-ventral position rather than ray number, and it does not modify fin length. Small changes (around 0.1 to 0.3 mm) are observed in individual rays after re-arrangement compared to raw data results. Although raw data shows lateral rays that seem longer than other rays (Figure 4.9C,D), this is the result of non-homogeneous samples in which the values of medial rays include the average of several samples and the lateral rays only show a sample with particular long rays [-10 and -9]. For this reason we decided to warp and re-arrange fin data when dealing with samples with variation in ray numbers.

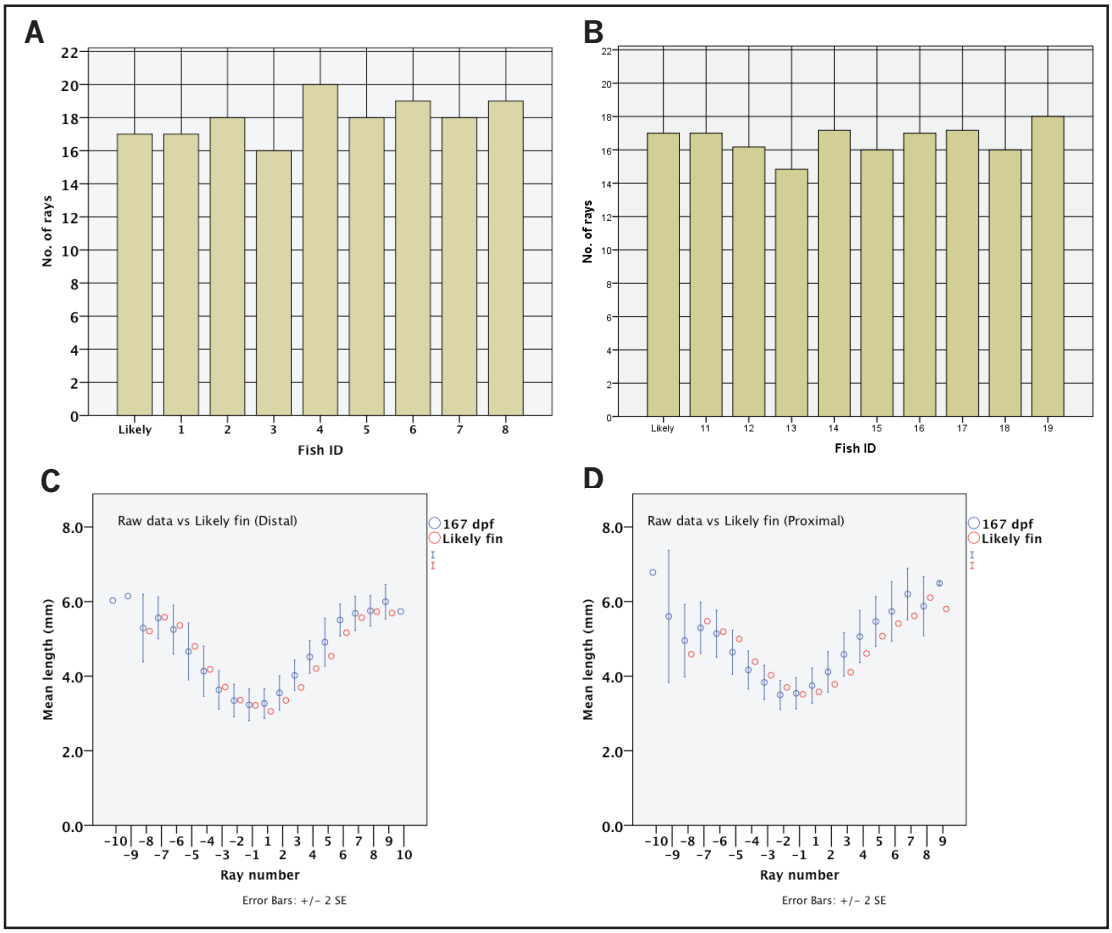

Figure 4.9 Number of rays per fin before amputation. **(A)** Number of rays in the distal subgroup. **(B)** Number of rays in the proximal subgroup. Comparison of ray lengths in raw data results and the re-arranged 17 ray zones of the likely fin of the distal **(C)**, and the proximal subgroups **(D)**.

4.2 Likely Fin Maps From Average Data

4.2.1 Maps of all Extracted Time-points

Similar to trends observed in individual rays and reported in the literature, longer segments are located in rays [-7, -6, 6, 7 and 8] in proximal regions. Shorter segments on the other hand are observed in medial rays and in distal areas of any given ray (Rolland-Lagan et al., 2012; Goldsmith et al., 2006; Iovine & Johnson, 2000).

Segment lengths for our likely fin ranged from 0.35 mm to 0.15 mm in most cases (Figure 4.10A). Segment ID maps were also obtained at every time-point, which allowed categorizing the average positions of the bony segments within a fin, by assigning ID numbers to each likely segment from base to tip (Figure 4.10B). A third set of maps shows the sample sizes used to generate a given ray for that map. Due to the fact that fin samples had variable number of rays, ray data was re-arranged within the ray-zones created to elaborate the likely fin average maps. This means that some likely rays were generated from different sample sizes. For example, there were cases in which as low as 5 samples were used while other cases had 9 samples (Figure 4.9C). A set of maps for the proximal subset at B000 is shown in Figure 4.10. Maps for the distal subset are similar and hence not shown.

Lastly, we obtained standard error maps for both segment lengths and segments ID. Standard error for segment lengths ranged from 0.005mm to 0.025mm (see appendix 8.8A). This provides estimation of how mean segment values are deviated from the whole population mean. For example red areas observed in a given standard error length map (appendix 8.8A) indicate that the segment mean in that zone are estimated to show a 0.025mm deviation from the population mean.

Similarly standard error maps for segment ID show that segment average positions within the likely fin were constant, except for the most lateral dorsal ray (ray [-8]) that showed un-matching segments within the likely fin maps in the distal part of the ray (see appendix 8.8B).

This variation in ray [-8] of the standard error maps (appendix 8.8B) can be the result of using samples with different number of rays, which caused that some segments in different ray number from fins do not match well when overlapped and re-arranged in the same ray-zone, when the likely fin was created. Despite this, the maximum difference in segment positions showed a deviation of two segments from the average segment ID in the distal section of ray [-8], while all other segments within the fin had very consistent positions (see appendix 8.8B). Altogether, these data indicate that the method is reliable and has high level of reproducibility for extracting and quantifying segment length and positions within the fin.

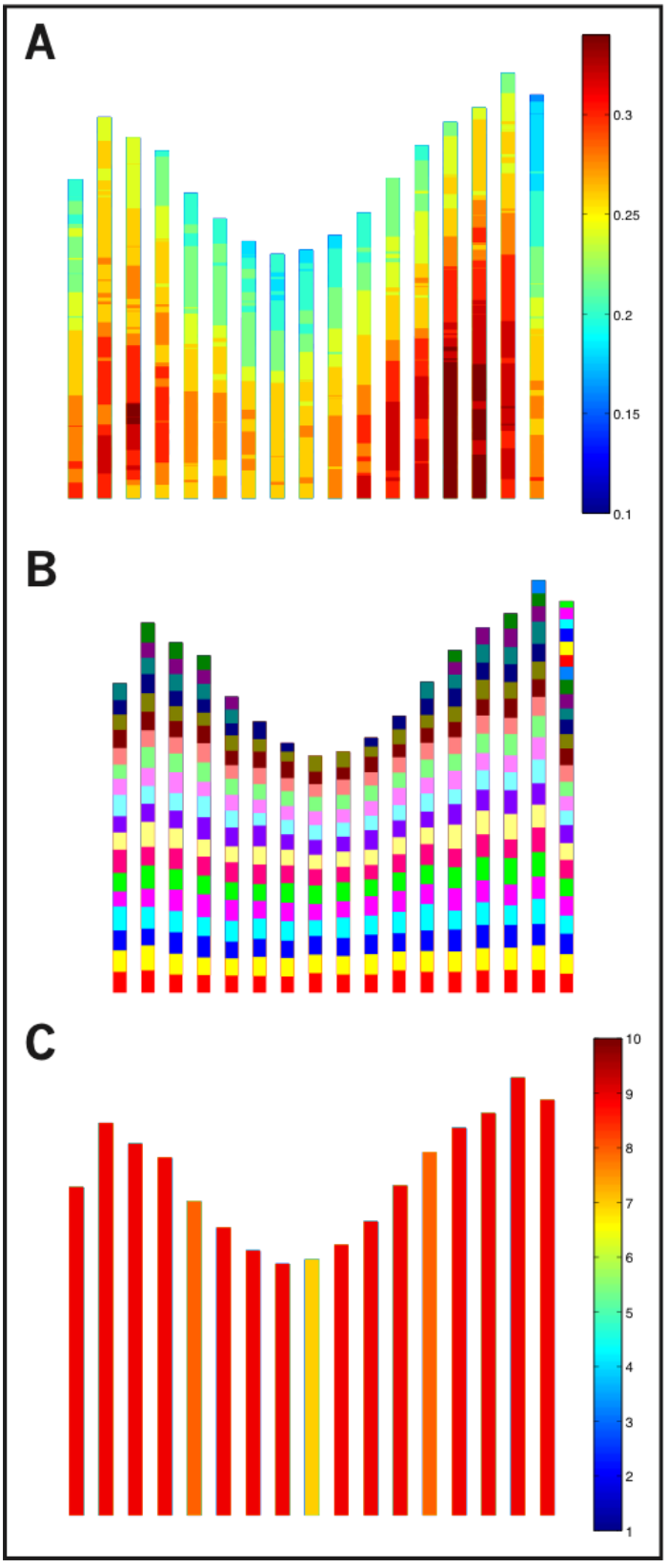

Figure 4.10 Likely fin visual maps from average data of the proximal sub-set at B000. **(A)** Graphic representation of the likely fin rays showing the average segment lengths. Color-band is in mm. **(B)** Map displaying the average segment ID distribution within the likely fin. **(C)** Number of samples (rays) used to calculate values of each likely ray-zone, after ray re-assignment.

4.2.2 Maps Comparison Before Amputation and After Regeneration

A comparison between the likely fin segment length maps at different time-points was performed. Through this comparison we obtained real differences (both positive and negative differences) in segment length that were shown as Blue-red graphic maps. Blue color indicates a negative difference between segment length maps at B000 and a time point after amputation, and red color indicates a positive difference between these two time points.

Figure 4.11A shows the differences between the likely fin before amputation (B000) and after 28 days of proximal amputation (A000). By overlapping both maps, we get the difference of the later time-point in a particular segment position ("before amputation map" subtracted from "28 days after amputation map"). Positive differences (longer segments) after regeneration are displayed in red while negative differences (shorter segments) are displayed in blue. (No difference is indicated in white).

In the particular case shown in Figure 4.11A, differences displayed in dark blue distally to the amputation plane in the tips of the rays, indicate the presence of segments at B000 which do not exist at A028 anymore effect of the amputation, hence a negative difference. This method allowed us to track segment patterns and to test model predictions regarding segment pattern differences after regeneration.

Proximal amputation subgroup

When comparing the differences in segment length for the proximal amputation group, we observe that most of the rays present a negative difference in their most distal regions at 31 dpa (Figure 4.11B). Then, there is an increase number of fin rays showing a positive difference at their tips at 35 and 38 dpa (Figure 4.11C,D). In other words these results indicate that for the proximal group, the likely fin did not quite regain the pre-amputation length in most rays before 35 dpa (A035).

In addition, longer segments appear at the amputation plane at A028 and all subsequent time-points (Figure 4.11A,B,C,D), which is consistent with the model presented by Valerie Tweedle (2012) and observed by Mari-Beffa and collaborators (1999) in goldfish experiments.

Distal amputation subgroup

Analysis of the progression of segment length differences before and after distal amputation shows a large positive difference on most ray tips after A031 (Figure 4.12C,D), which indicates a ray outgrowth compared to their original length at B000. Unlike the proximal amputation group, no segment length difference is seen at the amputation plane in the distal group at any time-point compared to before the amputation.

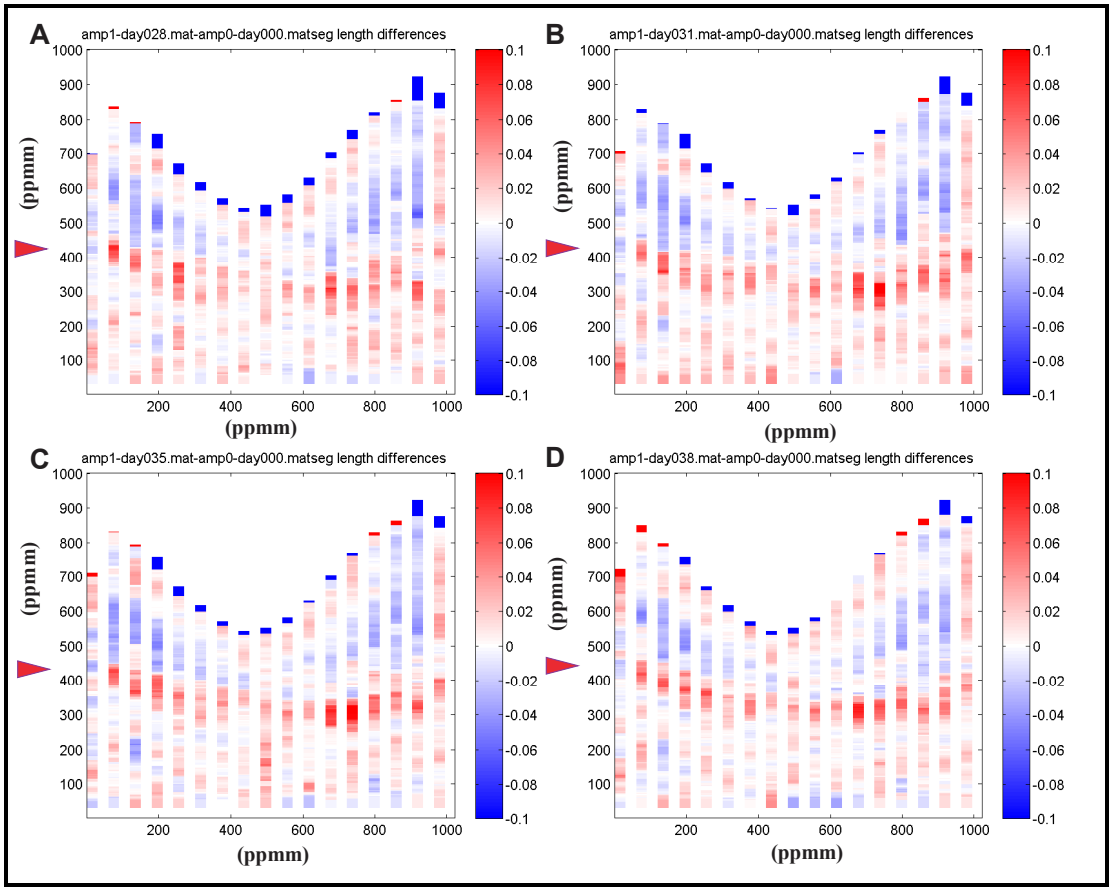

Figure 4.11 Segments length differences between the likely fin before amputation, and at 28, 31, 35 and 38 days, respectively after proximal amputation. Blue areas represent negative differences and red areas positive differences between maps. **(A)** Likely fin map at B000 subtracted from a fin map at A028. **(B)** Differences between maps at B000 and A031. **(C)** Differences between maps at B000 and A035. **(D)** Differences between maps at B000 and A038. Red arrowheads indicate the plane of amputation. Numbers on both axes indicate pixels per millimeter (ppmm). Color-band scale indicates difference in mm.

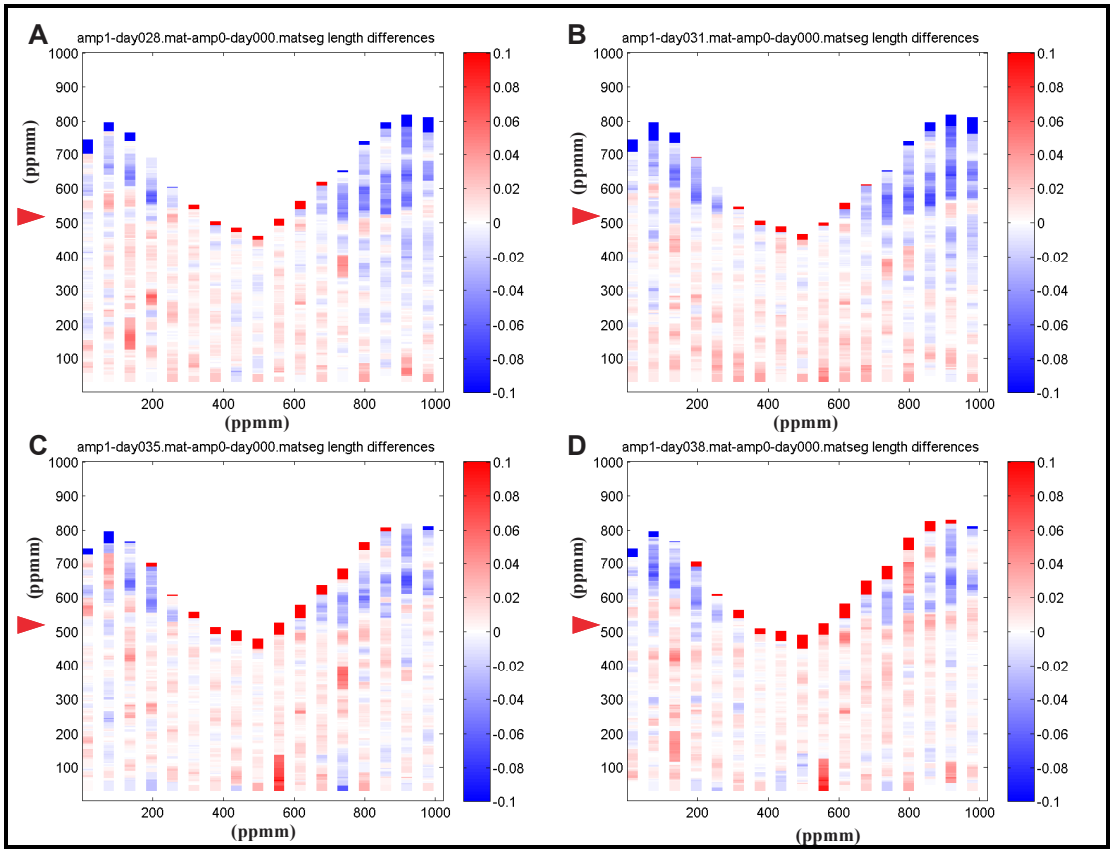

Figure 4.12 Progression of segments length differences between the likely fin before amputation, and at 28, 31, 35 and 38 days respectively after distal amputation. Blue areas represent negative differences and red areas positive differences between: B000 and A028 **(A)**, B000 and A031 **(B)**, B000 and A035 **(C)**, B000 and A038 **(D)**. Red arrowheads indicate the plane of amputation. Numbers on both axes indicate pixels per millimeter (ppmm). Color-band scale indicates difference in mm.

Generation of "Heat maps"

In both subgroups, we observed small differences (both positive and negative) within the maps after comparisons. These small differences are the result of user error at the moment of digitizing the segments, as they also appear in segments that were not amputated. In order to distinguish and better visualize large differences that may not be due to user error, we generated "heat maps" based on the comparison maps from the previous section.

First, we obtained absolute differences between the lengths before amputation and after regeneration by setting all differences to positive values (Figure 4.13A). The next step consists in eliminating the differences below the standard error in segment length for each map combination (the differences below an established threshold are displayed in black). Absolute differences above the established threshold are displayed in red and progressively change to white as they increase in value. This allows generating "heat-maps" using this color scheme, which only show large differences (Figure 4.13B).

These heat-maps more easily show those areas with larger segment length differences when comparing the likely fins before amputation (B000) and after regeneration (A038) for both subsets.

It results from the heat-maps that both proximal and distal groups show large differences at the tips of the rays when comparing before amputation and after regeneration as a result of fin regenerate outgrowth, and the proximal group only shows differences at the amputation plane (Figure 4.13B).

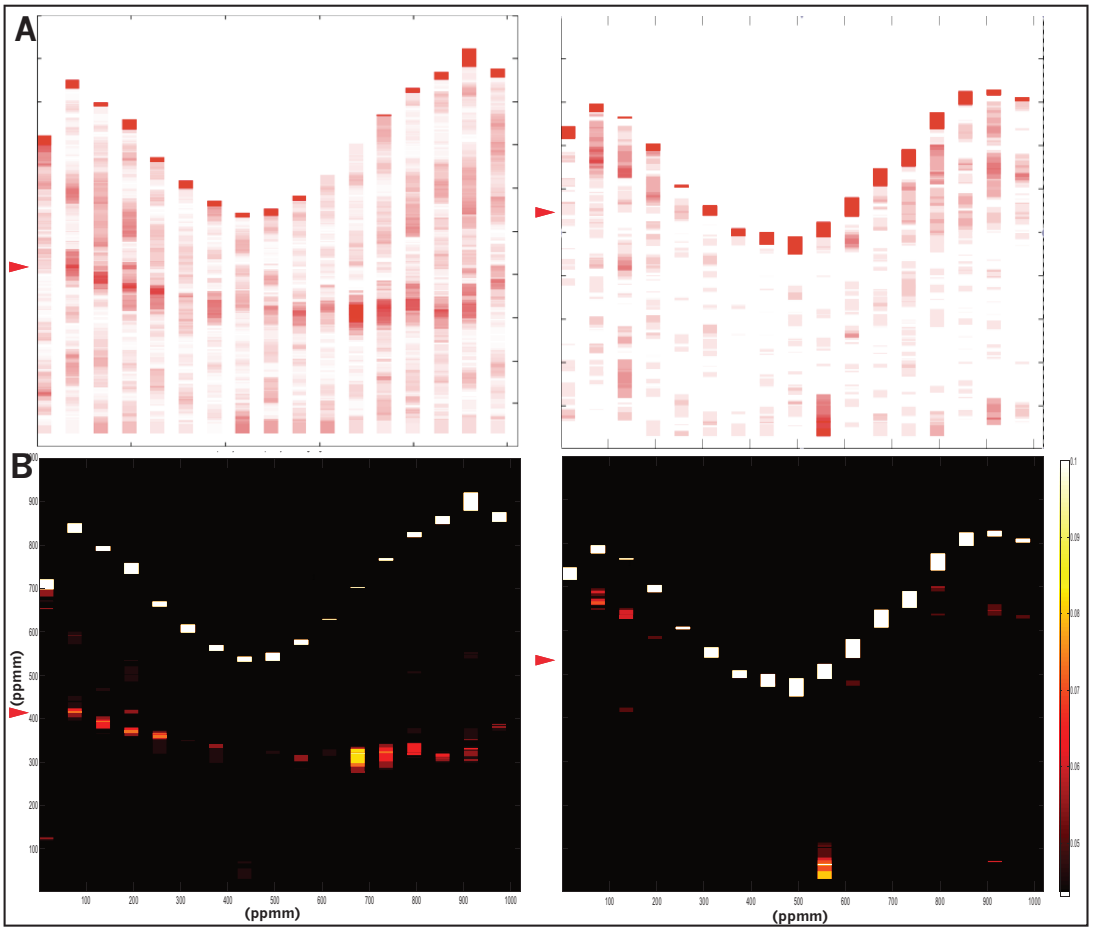

Figure 4.13 Generation of heat-maps. **(A)** Comparison of the likely fin maps using absolute values. Left: proximal subgroup. Right: distal subgroup. **(B)** Heat-maps generated by changing color scheme and removing segment differences below the assigned threshold. Left: proximal subgroup. Right: distal subgroup. Both proximal and distal subgroups are from the comparison of B000 and A038. Red arrows indicate the plane of amputation.

4.2.3 Segment Differences at the Amputation Plane

There is a statistically significant difference before amputation and after regeneration of the segment length at the amputation plane.

Statistical analysis was carried out in the original samples to compare segment differences before amputation (B000), 28 dpa (A028) and 38 dpa (A038) with both proximal and distal amputations (Table 2).

Comparison of segment measurements at the amputation plane at these three time-points was performed using non-parametric Friedman's test. This analysis shows that there is a statistically significant length difference before amputation and after regeneration ($p < 0.05$). Post-hoc analysis by Wilcoxon signed-ranks test with Bonferroni correction applied, resulted in significance level set at $p \leq 0.017$.

As expected, the proximal amputation group shows segment differences at the amputation plane when comparing fins before amputation and after regeneration (Table 1A), in accordance to differences observed on the visual maps. Although visual maps do not show changes in segments in the case of distal amputation, statistical analysis reveals that the segments at the amputation plane are longer after regeneration than before amputation in the distal group (Table 1B).

Analysis of a new distal amputation experiment

In order to confirm these observations, the distal amputation experiment was repeated, using a new set of 11 fish under the same conditions. However as we were only interested in the segments located at the amputation plane we did not perform the full digitizing procedure for extracting segment data, and used the software ImageJ (see section 3.2.4) instead to only measure the length of the segments at the amputation plane at B000, A028 and A038 (Table 1C).

Average segment lengths at the amputation plane at B000, A028 and A038 were 0.234 $\pm$ 0.01 mm, 0.203 $\pm$ 0.02 mm and 0.207 $\pm$ 0.01 mm, respectively (n=11). Differences were observed when comparing B000 against both A028 and A038 (Z=-2.756, p=0.006 and Z=-2.580, p=0.010; respectively). There was no statistical significant difference between the two time-points after amputation A028 and A038 (Z=-0.622, p=0.534).

Using ImageJ to measure the original subgroup

Taking into account that, measurements from the original set were performed using Matlab custom programs, while the new distal amputation experiment with new fish was measured using ImageJ, the original distal amputation group was also re-measured with ImageJ for comparison.

Segment averages at B000, A028 and A038 were 0.249 $\pm$ 0.016 mm, 0.253 $\pm$ 0.026 mm and 0.256 $\pm$ 0.031 mm respectively (n=8) in the original distal amputation group using ImageJ (Table 1D). Surprisingly the non-parametric Friedman's test ($p < 0.05$) reported that there is no statistical significant difference ($X^2 = 0.250$, p=0.882) between the segments length of the original distal amputation group at B000, A028 and A038 when measured with ImageJ (Table 2).

Due to the fact that statistical significance is the probability that the observed difference between two groups is caused by chance, effects sizes (Table 3) were obtained using Cohen's d estimate to determine the magnitude of differences between groups (Sullivan & Feinn, 2012).

$$d = \frac{\mu_1 - \mu_2}{\sigma} \qquad (4.1)$$

where:
μ_1 = Group 1 mean
μ_2 = Group 2 mean
σ = Pooled standard deviation

Depending on the d value obtained, four categories are used to classify the type of effect: large, medium, small and trivial.

Type of effect	Value of d
Large	0.81 - 2
Medium	0.51 – 0.8
Small	0.21 – 0.5
Trivial	0 – 0.2

Segment differences at the amputation plane from the proximal amputation sub-group show differences of small magnitude (d= 0.32, r=0.15). Cohen's d estimates of the original distal subgroup measured with Matlab reveals that the differences at the amputation plane before and after regeneration, although statistically significant, are trivial (d= 0.11, r=0.05).

		N	Mean	Std. Deviation	Minimum	Maximum
A)	**B000**	9	.27978	.044362	.213	.357
	A028	9	.34444	.040887	.259	.402
	A038	9	.34622	.040143	.265	.401
B)	**B000**	8	.24962	.025690	.213	.298
	A028	8	.26838	.027614	.220	.300
	A038	8	.26250	.027077	.218	.303
C)	**B000**	11	.23434	.016180	.207	.255
	A028	11	.20346	.024663	.162	.241
	A038	11	.20713	.017911	.186	.246
D)	**B000**	8	.24999	.016899	.220	.275
	A028	8	.25334	.026991	.206	.293
	A038	8	.25660	.031548	.197	.292

Table 1 Descriptive Statistics. **(A)** Proximal amputation group. **(B)** Distal amputation group. **(C)** New distal amputation experiment. **(D)** Original distal group using ImageJ

	Proximal (Matlab)	**Distal (Matlab)**	**New distal experiment (ImageJ)**	**Distal (ImageJ)**
Chi-Square	8.4	11.806	11.091	0.250
Significance	0.015	0.003	0.004	0.882

Table 2 Friedman test. Significance set p=0.05

Time-point comparison	**Proximal**	**Distal (Matlab)**	**New distal experiment (ImageJ)**
B000 vs A028	*0.31*	*0.11*	*-0.21*
B000 vs A038	*0.32*	*0.07*	*-0.20*

Table 3 Cohen's d estimates for effect size. Differences below d=0.2 are considered trivial.

Segment differences before amputation (B000) and after regeneration (A038) in the repeated distal amputation experiment with new fish and measured by ImageJ are at the borderline of small and trivial in the criteria of Cohen's d estimates for effect size (d=0.20, r=0.1).

Altogether these results indicate that following regeneration, fins present longer segments at the amputation plane compared to the length of the original segment before amputation.

According to Cohen's d estimation, segment differences were small in the proximal amputation group but trivial in the distal amputation group. As a result, differences can be identified by visual maps comparisons in the proximal subgroup but cannot be detected if the amputation plane is located in a distal position.

Using two different methods for measuring segments at the amputation plane resulted in small discrepancies on segment measurements. These discrepancies are not negligible as observed with the results from the original distal subgroup where the differences found by measuring the same samples with ImageJ, were non statistically significant between all three time-points (B000, A028 and A038). In addition, the results from the new group of 11 fish showed shorter segments when regenerated after distal amputation using ImageJ, while the other groups consistently showed larger segments at the amputation plane after regeneration (Table 1). Obviously, user accuracy becomes more important for distal segments than for proximal segments (due to their short size) when digitizing bony segments, where errors of 0.02 mm in these very short distal segments lead to important changes in bony segment length pattern analysis.

Our results show that the first regenerated segment at the amputation plane is longer than the original segment. In contrast, there was no detection of longer segments in the following regenerated segments more distally located from the amputation plane. This observation contradicts one of the predictions of the original morphogen driven model (Rolland-Lagan et al., 2012). This prediction accounted for longer lengths in some regenerated segments positioned distally to the amputation plane (Figure 4.14).

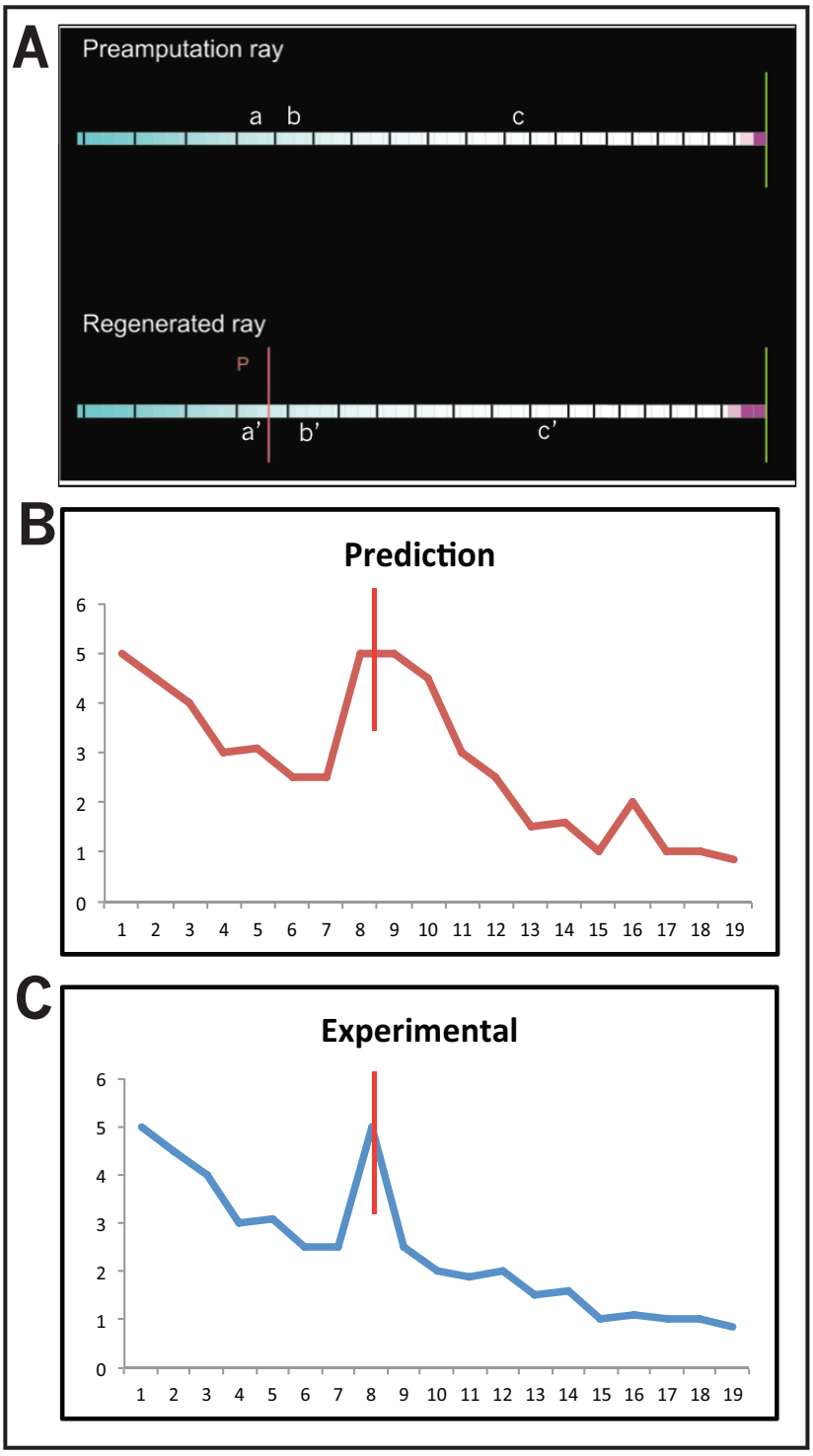

Figure 4.14 Ray model of bony segments after amputation. **(A)** Comparison of pre-amputated ray and after regeneration ray simulated by the original model (Rolland-Lagan et al., 2012). Letters indicate segment at the same position with difference in length. **(B)** Predicted segment length in function of proximal-distal position. Some segments display longer dimensions distally to the amputation plane. **(C)** Representation of observed progression of segments length after regeneration. Only the amputated segment is longer. Vertical lines indicate amputation. Segment length and ray distance values are arbitrary.

4.3 Validation of Ray Growth Model

4.3.1 Calibration of the Model Output with Experimental Feedback

Comparison of the model output for fin development and regeneration with experimental data indicates the need of changing parameter values.

Using growth data of fish during regeneration and also growth rates during development of younger fish (data not shown), a simulation curve was previously obtained by undergraduate student Mathieu Paquette. Development and regeneration growth rates were obtained by plotting fin length in function of time and selecting the best curve based on R^2 values. A logarithmic curve is inferred from the developmental data and compared to the output from the model simulation. The combination of this data allows simulating developmental growth from 26 dpf to 167 dpf (time of amputation) and fin regeneration until 50 days of regeneration.

However, the developmental and regeneration growth curves were based on data obtained from two different sets of samples. On average, the length of the fins used to calculate the growth curve for development were longer than the samples used for the regeneration curve. As a result, parameter values of the growth model (Rolland-Lagan et al., 2012) result in caudal fin lengths of 6.93mm at 167dpf and after amputation regrow to a length of only 6.3 mm after 50 dpa. This means that fish are unable to regain their pre-amputation length even after 50 dpa (Figure 4.15A). Experimental samples used in this thesis on the other hand, were on average able to regain their pre-amputation length after 28 dpa, as shown in section 4.1.2.

The first part of the curves shown in Figure 4.15A, represent fin growth from development until their day of amputation (167 dpf), then the second part of these curves indicate regeneration growth until 205 dpf (38 dpa). Yellow curve in this figure is a logarithmic curve for growth and regeneration obtained from old experimental data. It was obtained from two different datasets as mentioned above.

The red curve is the growth curve from the simulation, using an old set of parameters. When we compared this simulation curve with the results from the samples in the proximal-distal amputation experiments used in this thesis, we observed that the simulation curve does not fit anymore (green curve in Figure 4.15A).

In addition to fin length, the number of segments needed to be adjusted to that seen in experimental results. Previous parameters yielded a number of segments much higher than seen experimentally (appendix 8.9) before amputation and after regeneration (98 and 80 segments, respectively).

For the reasons stated above it was necessary to change the values of the model parameters in order to obtain an optimized fit regarding fin length, as well as number of bony segments observed experimentally.

Calibration of Model Parameters

A series of tests were run to evaluate the model performance based on different sets of parameters (methods 3.2.5). In order to obtain the optimal parameters for the fin growth model, we recorded length data at every 500 simulation steps (0.5 days) from both the inferred logarithmic curves and growth simulation curve (Figure 4.15A) and compare the error between them using the Root Mean Square Error (RMSE) as explained in section (3.2.5).

Due to the high number of parameters involved in the model output for regeneration, finding the right combination is particularly challenging. The initial productions of morphogen “X”, production of morphogen “G”, rate of diffusion of morphogen “X” and the increase of morphogen “X” production in the first compartment in function of time (beta), were set as independent variables (all these variables are explained in sections (1.8.1 and 3.2.5)). It was identified through stepwise regression that the best predictor of the RMSE from the logarithmic and simulation curves, is the parameter beta (see appendix 8.3).

Changing the values of a single parameter allows modifying the output of the simulation curve (Figure 4.15B). The specific effects of these parameters are explained in section 3.2.5. Although a combination of parameters was systematically tested, the lowest amount of RMSE obtained was 0.36 resulting in a growth simulation of 7.04 mm at 167 dpf and 6.14 mm at 38 dpa respectively. In comparison the previous set of parameter values used in the original model yielded 6.93 mm and 5.82 mm at 167 dpf and 38 dpa, respectively, with a RMSE of 0.69. Nevertheless, these new parameters do not still fit with the growth curve obtained from the proximal and distal experimental data described in the present study.

On the other hand, the number of segments obtained from the model simulation was reduced to the segment numbers observed experimentally by increasing the production of the hypothetical morphogen "S" which is produced at the joints and acts by inhibiting the formation of new joints in the vicinity of its production site.

The second parameter that controls joint spacing in the theoretical model is the diffusion of "S" (Ds) from one compartment to another. Ds was increased to reach the level of the hypothetical morphogen concentration necessary to reduce the resulting number of segments in the simulation. Experimental data show 22 segments in average at 167 dpf in the longest rays, and 23 segments at 38 dpa.

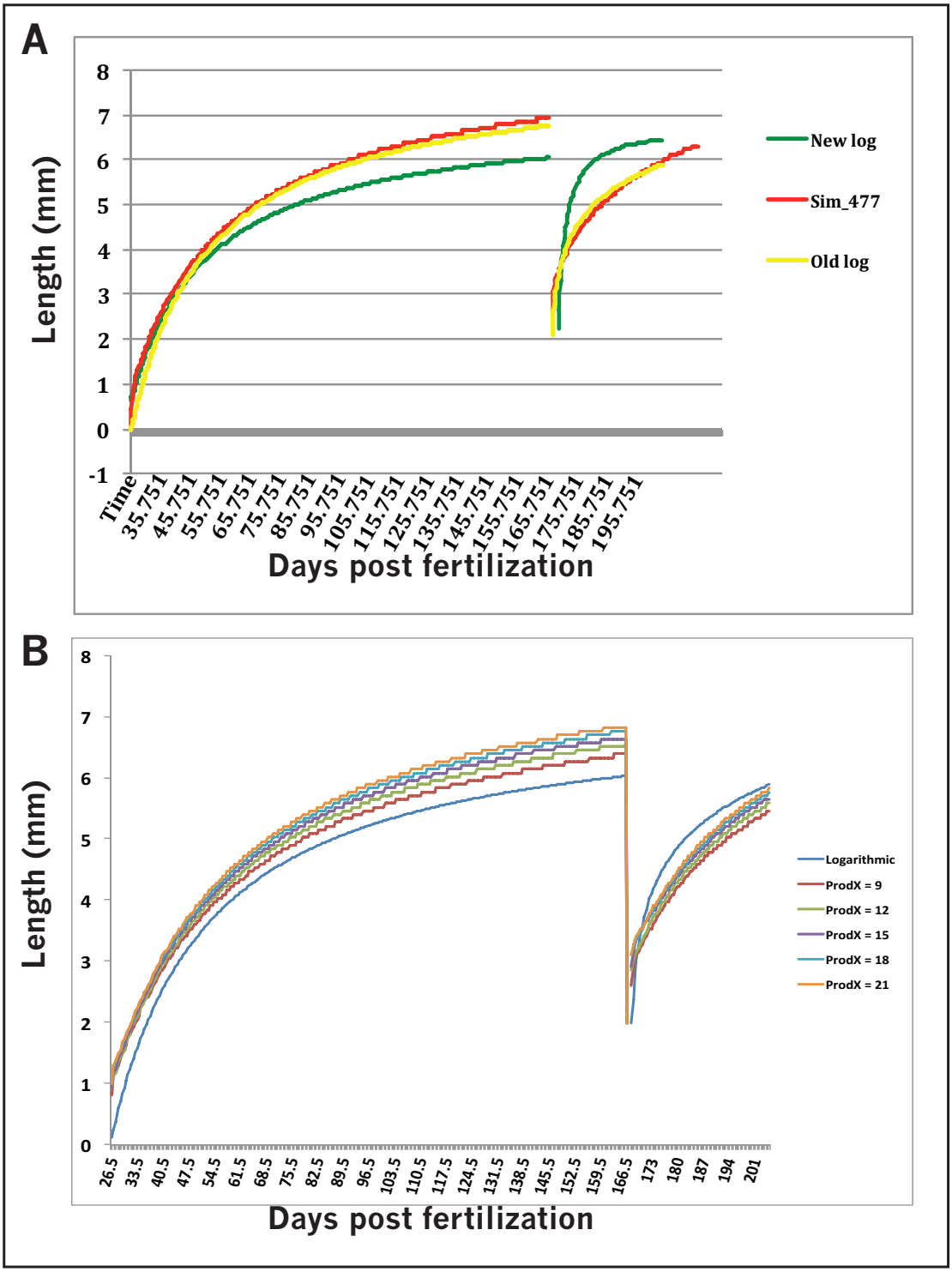

Figure 4.15 Fin growth simulation. **(A)** Comparison of curves for development (first series of curves on the left side) and regeneration (second series of curves shown on the right side of the graph). Yellow curve is the old logarithmic curve. Final length after regeneration did not regain pre-amputation length. Red curve is the output from the simulation with old parameter values. Green curve is the new logarithmic curve obtained from the proximal-distal amputation experiment used in this thesis. **(B)** Example of curve changes, obtained by altering the values of the parameter for morphogen "X" production. This morphogen controls the level of a secondary morphogen "G" for growth in the last compartment (see section 1.8.1). Each color represents a different level of production tested.

Parameter	Old Values	New Values	Observed Effect in Model Output
Initial production of morphogen "X" (ProdX)	21	12	Decreased fin length at the time of amputation.
Beta	0.001	0.001	Increases rate of regeneration growth, allowing fins to achieve pre-amputation length. Unfortunately, it also increases developmental growth, making impossible for the simulated fin to regain its pre-amputation size within realistic length and time. The old value was kept.
Morphogen "S"	2	95	Reduction of segment numbers as observed experimentally.
Diffusion of "S" (Ds)	0.3	0.92	Reduction of segment numbers as observed experimentally.
Compartment length	0.062	0.02	Reduction of the length of compartments representing individual cells. Greatly enhanced the effect of all other morphogens.

Table 4 List of parameter values used to optimize model calibration and the effects these changes made on the model. Ranges between these values were tested, and those that yield a lower RMSE were kept (see section 3.2.5: *calibrating model parameters*).

Chapter 5 - Discussion

5.1 Framework for Fin Data Extraction

Regeneration in teleost fins is a dynamic and complex process in both space and time necessary to achieve functional structures with specific patterns. We used a computational approach to provide new insights regarding zebrafish caudal fin development and regeneration. Previously, a theoretical model for caudal fin growth had been proposed (Rolland-Lagan et al., 2012). To validate this model, we collected data from a proximal-distal amputation experiment using a framework for fin data extraction (Rolland-Lagan *in prep*). In addition, it was necessary to test the growth model and compare it to the results of our experimental data, and calibrate its original parameters

We also improved the framework for data extraction by adapting an image warping method to allow the proper analysis of samples with anatomical differences specifically, differences in the number of rays. With this, we increased the flexibility of this method, which originally required samples with the same number of rays and samples grouped according to their size. By doing this we greatly reduced error due to lateral rays of using a non-homogeneous sample set. In addition, our method allowed organizing segment length regression data in function to distance from the base of the fin. This segment length regression data could lead to potential new methods of analysis based on assigning specific values to each individual segment and create visual fin maps.

With our results, we tested the previous model predictions through analysis of the regenerated segments. Modifications of theoretical models based on feedback from experimental results are the basis for building robust models in systems biology. Therefore these efforts contribute to this field to study development and regeneration in the zebrafish. Starting by incorporating growth rates to this theoretical model for fin growth previously obtained from developing fish, and calibrating them with results from experimental data will further unveil the mechanisms for joint patterning in regenerating fins, which are another essential component besides fin growth.

5.1.1 Data Extraction From Non-homogeneous Samples

Zebrafish can present anatomical differences in terms of the number of rays that a fin comprises. The framework for extracting and analysing fin segment patterns developed by Rolland-Lagan (*in prep*), was originally intended to work with datasets involving fish classified in caudal fin size classes, and with individuals possessing caudal fins composed of 18 rays (ray numbering starting from the cleft as -1 and 1 and ascending or descending to lobes up to -9 and 9). The result is a highly reproducible and homogeneous dataset to study spatial-temporal patterns in the developing or regenerating fin. However, because ray numbers can vary between individuals, it is not always possible to have available samples with the exact same number of rays.

For this reason, we adapted the framework to image fins of different sizes, digitize, extract segment data and analyse fins with variations in ray numbers. Raw data from this dataset initially showed large variation and large error bars in the lateral rays (rays number [-9, -8, 8, 9]). There were also some samples that showed unusual distribution of lateral rays (especially rays [-10, 10]) resulting in asymmetrically shaped fins with one of the lobes being skewed in comparison to the other lobe, thus adding even more variations to results. Consequently, data interpretation in regard to lobe shape, ray length, segment length, number of segments and position of bifurcations can be affected at the level of the most-lateral rays due to anatomical variability (Figure 4.2, Figure 4.4).

When we obtained the regression data of segment length as a function of the distance from the base, we observed that the ranges for coefficient of determination (R^2= 0.63 – 0.92) are lower compared to those ranges reported using homogeneous samples (R^2= 0.92 – 0.97). This result again reflects how variability in ray numbers can lead to such differences.

Although fish size is a better indicator of developmental stage than age (Iovine & Johnson, 2000), the results here show that classifying fish by “days post

fertilization" (dpf) still provides useful information about fin ray and segment patterns, as classifying fish samples according to fin lengths (Rolland-Lagan *in prep*). Therefore, having a robust framework is essential for imaging morpho-dynamic methods to analyse fin growth and patterns.

5.2 Likely Fin Visual Maps Based On Average Data

The amount of studies on detailed segment patterns is limited. It is known that the rate of regeneration is faster than ontogenic growth (Iovine et al., 2007) and that lobe rays regenerate faster than cleft rays (Lee et al., 2005).

Furthermore, genetic and functional analysis suggests that fin growth and joint patterning are related but can act independently. Indeed, it has been shown that the zebrafish *evx1* mutants have no joints but normal fin length (Shulte et al., 2011) and that the *lof* mutants possess long fins with normal segments (Iovine & Johnson, 2000). Furthermore it has been reported that inhibition of fin growth results in small fins with normal segments (Lee et al., 2005).

We opted for the use of a quantitative method to analyse fin bony segment data. This allowed us to obtain detailed segment pattern maps at different time-points during development and fin regeneration and, to compare segment lengths and positions within any given ray.

In order to generate visual maps for fin patterns and to compare them at different time-points before amputation and after regeneration, we had to validate ray and segment data. However, some inconsistencies were appearing as a result of having fish with non-homogeneous ray numbers. One option to solve this problem was to simply remove the most lateral rays, as they are most likely the problematic rays for analysis. This solution only aids in studying bifurcations, as bifurcation never occur in the most lateral rays (Murciano et al., 2002) but it does not correct the high variability in data from adjacent rays (see appendix 8.10). A second option was chosen instead, which consisted in re-arranging ray data in "ray-zones" based on their lateral-medial position, and then aligning the samples through image warping.

These rearrangements of ray data allowed the generation of the “likely fin maps”. Ray trends shown in our likely fin maps are consistent with the observations of longer segments in more proximal regions and that lobe rays possess more and larger segments than cleft rays (Goldsmith et al., 2006).

5.3 Fin Model

5.3.1 Development and Regeneration

Our experimental results show on average both proximal and distal amputation sub-groups reach the pre-amputation length at similar time (28 dpa), showing that the rate of regeneration is faster in fins following proximal amputation compared to those after distal amputation. This is supported by data available regarding regeneration rates in fins amputated in a proximal position in their ventral lobe and a distal position in their dorsal lobe of the same individual. In this study, both lobes regain their pre-amputation length at the same time (Lee et al., 2005).

Currently the morphogen driven model proposed by Rolland-Lagan et al. (2012) cannot produce regenerated rays with the same length as before amputation even at 50 dpa. This indicates that growth rate for regeneration needs to be increased.

One of the parameters that can contribute to achieving a proper length of the regenerates is the rate of increase of morphogen “X” production in function of time (beta); higher values of “beta” result in longer fin lengths after regeneration (section 4.3.1). The growth model is set to have faster growth rates during regeneration than during ontogenic growth (Iovine et al., 2007). The combination of high values of “beta” from the model, and faster growth rates during regeneration, eventually lead to regenerated fins to achieve the pre-amputation length in the simulation output.

However, this is achieved after an unrealistic amount of time of regeneration. Moreover, the shapes of the growth curves were far too different to the expected curve.

Altogether, these results indicated that the change of parameter values alone was not enough to yield the appropriate growth curve as well as the final fin lengths after development and regeneration. Experimental data previously used to calibrate this model were based on two different datasets of different fin lengths, in which the samples used to calibrate the ontogenic growth were larger than those used to calibrate the regeneration growth rate. Thus, calibration using the same samples is necessary to obtain the most accurate rates of growth at different stages of ontogeny and regeneration. The new group of fish (n=11) used to repeat the distal amputation experiment and to corroborate previous results at the plane of amputation, will be useful to further calibrate the growth model after these samples are fully digitized.

5.3.2 Bony Segment Patterns

In the model postulated by Rolland-Lagan et al. (2012), joint patterning is determined by the actions of morphogen "X" and morphogen "S". Morphogen "S" is produced at the joints and inhibits the formation of new joints in the vicinity until its concentration falls to a certain threshold, the level of production of "S" is controlled by concentration of morphogen "X"; thus these two effectively determine joint spacing and bony segment length.

After adjusting this model to generate the number of segments in accordance to that found in our experimental data analysis, we simulated fins cut at proximal (2 mm) and distal (4 mm) positions, then quantify the number of compartments (section 3.2.5), forming the segments before and after regeneration. The output of the simulation yields longer segments (in number of compartments) at the amputation zone, with two compartments longer for the proximal, and one more compartment for the distal amputation simulation.

The results from our experimental set showed that segments at the amputation plane have statistically significant longer segments after regeneration. This is supported by studies made in goldfish showing that the first regenerated segments are longer to segments at the same positions of non-amputated fins (Mari-Beffa et al., 1999). In addition, the likely fin map comparisons allow identifying the longer segments after proximal amputation.

Both experimental data and simulation results show a more pronounced increase in length of the segment located at the amputation plane after proximal amputation than the increase observed after distal amputation. In fact, segments at the distal amputation plane were not detected by visual map comparisons because the length increase was too small. Interestingly, the model of Rolland-Lagan et al. (2012) also predicted longer segments in the next few segments distal to the amputation plane (segments showed more compartments in comparison to before amputation). However, in our comparison maps, we observed that only the first segment at the amputation plane is longer.

A possible explanation for this observation could be that amputation triggers a peak of maximum production of morphogen "S", therefore requiring more time to decrease to the levels necessary to form the next joint (section 1.8.1), hence resulting in a larger first regenerated segment. Then, the levels of production of morphogen "S" increase proportionally to the concentration of "X" in the next joint as it normally does. This results in only larger segments at the amputation plane (first regenerated segment), but normal segments for the second and following segments more distally when comparing before amputation and after regeneration.

Altogether, the results from this thesis constitute a step in improving the model mechanism for segment pattern formation, specifically in the number of segments produced in the simulation and the changes in segment patterns after regeneration. By increasing the values of the hypothetical morphogens for joint spacing, the model was calibrated to generate the number of segments observed experimentally. In addition, my results indicate that only the first regenerated segment increases in size after regeneration, and this increase is higher if the amputation is at a proximal position than in a distal position.

5.4 Future Directions

5.4.1 Experimental Data

As previously mentioned, the systems biology approach requires the proposal of a theoretical model based from available data and then integration of new experimental data for validation followed by tests of variations performed on the system in an iterative process (Kholodenko et al., 2005). My work here constitutes one part of this approach. The result of this work is a new calibrated model that can produce accurate number of segments and address changes in segment length at the amputation plane after regeneration. Based on these results, changes in the mechanism of joint spacing right after amputation have to be introduced in the model in order to reproduced the longer segments at the amputation plane as observed experimentally. One potential change in the model would be increasing the concentration of the morphogen responsible for joint spacing (morphogen "S") in a single peak.

Another aspect of systems biology is testing variations in individual elements to evaluate how the whole system responds to specific changes. The use of zebrafish mutants could contribute to further testing the mechanisms involved in ray growth and bony segment patterning. In particular the long fin (*lof*) and another long fin (*alf*) mutants provide interesting cases to study segment length control, considering that both of these mutants result in long fins, but the *lof* mutant possess normal segments (Iovine & Johnson, 2000), while the *alf* mutant results in longer segments compared to the wild-type (Sims et al., 2009).

This can be achieved by extracting fin and segment data from these mutants during ontogenic growth as well as after amputation. Then compare the results to the output of the morphogen model growth model simulating *lof* and *alf* mutants. In their study, Rolland-Lagan and colleagues (2012) showed a "virtual mutant" that reflects the patterns of *lof* mutants (in arbitrary values) by highly increasing transport for morphogen "X". Experimental data could be used to validate the "virtual mutants"

using fin, ray and segment patterns obtained before and after regeneration with these mutants.

Taking into account the procedure used in this thesis to achieve the proper number of segments in the model, we would expect that increases in "X" transport rate alone might not be enough to simulate the *alf* mutant. As it was necessary to increase the parameters for "S" and diffusion of "S" (Ds) to reduce the number of segments to what is seen experimentally in wild-type fish. The "virtual mutant" for *alf* may require high levels of transport of "X", as well as lower levels of "S" and "Ds" compared to the levels shown in table 4.

Additionally, *evx1* mutants develop fins of normal length and have rays with no joints (Shulte et al., 2011). By highly increasing the production levels of "S" and setting its diffusion to zero it may be possible to reflect the phenotype of *evx1* (Ds has to be zero if we consider *evx1* as a candidate for "S", as *evx1* is a transcription factor and is located in the cell nucleus). The "virtual *evx1"* mutant would have to be tested if the same pattern (no joints, normal fin length) is conserved after fin regeneration.

Therefore these three mutants could help to unveil the mechanism that controls joint spacing and how this control can act independently of fin growth control in these cases.

5.4.2 Improvement of Computational Tools for Fin Data Extraction

Computational tools for extracting, quantifying and analysing data present the potential of processing considerable amount of information that otherwise would be impractical. Currently the digitizing process for fin data extraction relies on the manual identification of joints in every sample.

Colleague M.Sc. student Benoit Tremblay (2013) presented a method for automatic extraction of fin joint data, which requires limited assistance by the users during this step, thus reducing processing time for digitizing.

His proposed method was based on an algorithm to identify joints by marking the elements located inside the fin outline that fulfilled a threshold for joint criteria:

plane (shape), inside the fin outline, certain size (surface area) and parallel to horizontal axis. In order to work, the user only needed to manually digitize the first segment of each ray located at the base of the fin. The program would then use the length of these segments to search for new joints in a distal position.

He determined that the amount of time saved for digitizing three samples using the automatized method was 30 minutes (total time of manual digitizing of three samples was 65 min). To put it in perspective, this thesis required the digitizing of 102 fin samples to evaluate fin growth and segment patterns at 6 time-points. If more time-points were necessary for future analysis with a larger number of samples, the digitizing step would be highly time consuming to be performed manually. In addition, user error could be reduced in shorter segments provided that the custom programs can properly identify and discriminate joints from background noise.

It is important to note however, that he reported instances in which the program did not properly digitize the segments located at the amputation plane when dealing with regenerated fins. The reason is that these segments are longer and the program used the length of the previous (shorter) segment proximally to the amputation plane as reference for finding the next joint. The results found in my study for differences in length at the proximal amputation plane between B000 and A038, show in average that the regenerated segment length is 0.346 mm, but there were cases of segments as long as 0.416 mm. These measurements could then be applied to adjust the program when dealing with the amputation plane and solve this issue.

Also, this program automatizes the digitizing step, and does not include fin shape detection, assignment of nodes, tracking segments between time-points or generation of files for analysis, as described in the methods section (3.2.1, 3.2.2). All those steps still need to be performed. Benoit Tremblay (2013) proposes the integration of all programs into one single automatized program to increase the efficiency and reduce time consumption. This could provide a very useful addition in segment pattern analysis.

In addition to improvements on the digitizing step, the use of bony segment regression data (see section 4.1.2, appendix 8.5) obtained from this thesis could be

used to generate visual maps to analyse patterns and predict the location and length of individual segments within the fin. In this manner, our likely fin would be based on segment regression data, where each individual segment has assigned their own constant and slope from the linear regression equation in the form (Y = a + bX), at different times of development and regeneration. These data could possibly predict the length of every segment based on their distance from the base, when experimental data is not available for that specific developmental time-point.

This would require however, that the new regression maps be validated with experimental data and standard error maps before they can be used to predict segment lengths and locations with reliability. One first step will be to elaborate regression maps using the same specific time-points studied here (167 dpf, and 0, 28, 31, 35, 38 dpa) and to compare them with the likely fin maps obtained in this thesis.

Chapter 6 - Conclusions

In this thesis, we present an analysis of bony segment patterns from the zebrafish caudal fin following two different levels of amputation, using a computational approach. We tested a framework for extraction and analysis of fin patterns and adapted this framework to work with non-homogeneous samples which otherwise generate high variability and error.

Secondly, we tested the previous theoretical model prediction of changes in segment patterns after amputation. Likely fin maps made from average data were compared before proximal-distal amputations and after regeneration to identify changes in segment patterns. Statistical analysis confirms that both level of amputations leads to one larger segment at the plane of amputation while the model was predicting several larger segments. These results suggest that the event of amputation may generate an increase in concentration of the joint inhibiting substance from the model, controlling segment spacing.

We also optimized the original morphogen driven model to recreate accurate segment numbers based from experimental data. Finally we collected segment regression data that could be integrated into a new visual map method to analyse fin bony segment patterns.

Altogether these efforts contribute to provide different elements for developmental analysis and are part of the systems biology approach. We suggest that implementing these features to data extraction and analysis, in addition to new experimental data from specific mutants can result in a robust system for unveiling the poorly understood mechanisms controlling fin growth and segment patterning during regeneration.

Chapter 7 - Bibliography

Aboobaker A. (2011). Planarian stem cells: a simple paradigm for regeneration. *Trends in Cell Biology*, **21** (5): 304–311

Akimenko M.A., Marí-Beffa M., Becerra J., Géraudie J. (2003). Old questions, new tools, and some answers to the mystery of fin regeneration. *Developmental Dynamics*, **226**(2), 190-201.

Akimenko M.A., Johnson S.L., Westerfield M., Ekker M. (1995). Differential induction of four msx homeobox genes during fin development and regeneration in zebrafish. *Development*, **121**(2), 347-357.

Avaron F., Hoffman L., Guay D., Akimenko M.A. (2006). Characterization of two new zebrafish members of the hedgehog family: atypical expression of a zebrafish indian-hedgehog gene in skeletal elements of both endochondral and dermal origins. *Developmental Dynamics*, **235**(2), 478-489.

Becerra J., Junqueira L.C., Bechara I.J., Montes G.S. (1996). Regeneration of fin rays in teleosts: a histochemical, radioautographic, and ultrastructural study. *Archives of histology and cytology*, **59**(1), 15-35.

Becerra J., Montes G.S., Bexiga S.R., Junqueira L.C. (1983). Structure of the tail fin in teleosts. *Cell and Tissue Research,* **230**(1), 127-137.

Bellusci S, Grindley J, Emoto H, Itoh N, Hogan BL (1997) Fibroblast growth factor 10 (FGF10) and branching morphogenesis in the embryonic mouse lung. *Development,* **124**:4867–4878

Blum N., Begemann G. (2012). Retinoic acid signaling controls the formation, proliferation and survival of the blastema during adult zebrafish fin regeneration. *Development*, **139**(1), 107-116.

Brittijn S.A., Duivesteijn S.J., Belmamoune M., Bertens L.F., Bitter W., Bruijn J.D., Champagne D.L., Cuppen E., Flik G., Vandenbroucke-Grauls C.M., Janssen R.A., Jong I.M., Kloet E.R., Kros A., Meijer A.H., Metz J.R., Vandersar A.M., Schaaf M.J., Schulte-Merker S., Spaink H.P., Tak P.P., Verbeek F.J., Vervoordeldonk M.J., Vonk F.J., Witte F., Yuan H., Richardson M.K. (2009). Zebrafish development and regeneration: new tools for biomedical research. *The International Journal of Developmental Biology,* **53**:835-850.

Brockes J., Kumar A., (2002). Plasticity and reprogramming of differentiated cells in amphibian regeneration. *Cellular Biology*. **3**, 566–574

Broun M., Bode H.R. (2002). Characterization of the head organizer in hydra. *Development*, **129**(4), 875-884.

Dowis H.J., Sepulveda C.A., Graham J.B., Dickson K.A. (2003). Swimming performance studies on the eastern Pacific bonito *Sarda chiliensis*, a close relative of the tunas (family *Scombridae*) Swimming performance studies on the eastern Pacific bonito *Sarda chiliensis*, a close relative of the tunas (family *Scombridae*). *Journal of Experimental Biology*, ***206*** (16), 2749-2758.

Franz-Odendaal T. (2011). Induction and patterning of intramembranous bone. *Frontiers in Bioscience* ,**16**: 2734-46.

Felsenstein K.M., Candelario M., Steindler D.A., Borchelt D.R., (2014). Regenerative medicine in Alzheimer's disease. *Translational Research*, **163(4)**, 432-438.

Gardiner D.M., Endo T., Bryant S.V., (2002). The molecular basis of amphibian limb regeneration: integrating the old with the new. Semin. *Cell Dev. Biol*., **13**, 345 – 352.

Géraudie J., Monnot M.J., Ferretti P. (1995). Caudal fin regeneration in wild-type and long-fin mutant zebrafish is affected by retinoic acid. *The International Journal of Developmental Biology,* **39**(2):373-381.

Goldsmith M.I., Iovine M.K., O'Reilly-Pol T., Johnson S.L. (2006). A developmental transition in growth control during zebrafish caudal fin development. *Developmental Biology*, **296**(2), 450-457.

Goldsmith M.I., Fisher S., Waterman R., Johnson S.L. (2003). Saltatory control of isometric growth in the zebrafish caudal fin is disrupted in long fin and *rapunzel* Mutants. *Developmental Biology,* **259**: 303-317

Haas, H. J. (1962). Studies on mechanisms of joint and bone formation in the skeleton rays of fish fins. *Developmental Biology,* **5**, 1-34.

Hirashima T., Iwasa Y., Morishita Y. (2009) Mechanisms for split localization of *Fgf10* expression in early lung development. *Developmental Dynamics,* **238**, 2813–2822

Howe K., Clark M. D., Torroja C. F., Torrance J., Berthelot C., Muffato M., Plumb B. (2013). The zebrafish reference genome sequence and its relationship to the human genome. *Nature*, **496** (7446), 498-503.

Ingham, P. W., McMahon, A. P. (2001). Hedgehog signaling in animal development: paradigms and principles. *Genes & Development*, **15**(23), 3059-3087.

Iovine M.K., Johnson S.L. (2000). Genetic analysis of isometric growth control mechanisms in the zebrafish caudal fin. *Genetics,* **155**(3), 1321-1329.

Iovine M.K., Higgins E.P., Hindes A., Coblitz B., Johnson S.L. (2005). Mutations in connexin43 perturb bone growth in zebrafish fins. *Developmental Biology*, ***278***(1), 208-219.

Jain I., Stroka C., Yan J., Huang W.M., Iovine M.K. (2007). Bone growth in zebrafish fins occurs via multiple pulses of cell proliferation. *Developmental Dynamics*, ***236*** (9), 2668-2674.

Johnson S.L., Weston J.A. (1995). Temperature-sensitive mutations that cause stage-specific defects in zebrafish fin regeneration. *Genetics* **141**, 1583–1595.

Kholodenko B.N., Bruggeman F.J., Sauro H.M. (2005). Mechanistic and modular approaches to modeling and inference of cellular regulatory networks. *Systems Biology,* **143**.

Kicheva A., Cohen M., Briscoe J. (2012) Developmental pattern formation: insights from physics and biology. *Science* **338**, 210–212

Knopf F., Hammond C., Chekuru A., Kurth T., Hans S., Weber C. W., Weidinger G. (2011). Bone regenerates via dedifferentiation of osteoblasts in the zebrafish fin. *Developmental Cell*, **20**(5), 713-724.

Koshiba K., Kuroiwa A., Yamamoto H., Tamura K., Ide H. (1998). Expression of *msx* genes in regenerating and developing limbs of axolotl. *Journal of Experimental Zoology*, **282**(6), 703-714.

Laforest L., Brown C.W., Poleo G., Géraudie J., Tada M., Ekker M., Akimenko M.A. (1998). Involvement of the sonic hedgehog, patched 1 and *bmp2* genes in patterning of the zebrafish dermal fin rays. *Development*, **125**(21), 4175-4184.

Lee Y., Grill S., Sanchez A., Murphy-Ryan M., Poss K.D. (2005). *Fgf* signaling instructs position-dependent growth rate during zebrafish fin regeneration. *Development,* **132**(23), 5173-5183.

Li Y, Zhang H, Choi SC, Litingtung Y, Chiang C (2004). Sonic hedgehog signaling regulates Gli3 processing, mesenchymal proliferation, and differentiation during mouse lung organogenesis. *Developmental Biology* **270**:214–231

Matthews M., Trevarrow B., Matthews J. (2002). A virtual tour of the guide for zebrafish users. *Resource*, **31**, 34-40.

Marí-Beffa M., Murciano C. (2010). Dermoskeleton morphogenesis in zebrafish fins. *Developmental Dynamics*, **239** (11), 2779-2794.

Marí-Beffa M., Palmqvist P., Marín-Girón F., Montes G.S., Becerra J. (1999). Morphometric study of the regeneration of individual rays in teleost tail fins. *Journal of Anatomy*, **195**(3), 393-405.

Metzger R.J., Krasnow M.A. (1999) Genetic control of branching morphogenesis. *Science* **284**:1635–1639

Montes G.S., Becerra J., Toledo O.M., Gordilho M.A., Junqueira L.C. (1982). Fine structure and histochemistry of the tail fin ray in teleosts. *Histochemistry,* **75**(3), 363-376.

Murciano C., Fernández T.D., Durán I., Maseda D., Ruiz-Sánchez J., Becerra J., Akimenko M.A., Marí-Beffa M. (2002). Ray–Interray Interactions During Fin Regeneration of *Danio rerio*. *Developmental Biology* **252**, 214–224.

Nechiporuk A., Keating M.T. (2002). A proliferation gradient between proximal and *msxb* expressing distal blastema directs zebrafish fin regeneration. *Development,* **129**, 2607-2617.

Paznekas W.A., Boyadjiev S.A., Shapiro R.E., Daniels O., Wollnik B., Keegan C.E., Jabs E.W. (2003). Connexin43 (*GJA1*) mutations cause the pleiotropic phenotype of oculodentodigital dysplasia. *The American Journal of Human Genetics*, **72**(2), 408-418.

Poleo G., Brown C.W., Laforest L., Akimenko M.A. (2001). Cell proliferation and movement during early fin regeneration in zebrafish. *Developmental Dynamics,* **221**:380–390.

Poss K.D., Shen J., Keating M.T. (2000). Induction of *lef1* during zebrafish fin regeneration. *Developmental Dynamics*, ***219***(2), 282-286.

Poss K.D, Shen J., Nechiporuk A., McMahon G., Thisse B., Thisse C., Keating M.T. (2000). Roles for Fgf signaling during zebrafish fin regeneration. *Developmental Biology,* **222**: 347–358.

Poss K.D., Keating M.T., Nechiporuk A. (2003). Tales of regeneration in zebrafish. *Developmental Dynamics*, **226**(2), 202-210.

Quint E., Smith A., Avaron F., Laforest L., Miles J., Gaffield W., Akimenko M.A. (2002). Bone patterning is altered in the regenerating zebrafish caudal fin after ectopic expression of sonic hedgehog and *bmp2b* or exposure to cyclopamine. *Proceedings of the National Academy of Sciences*, **99**(13), 8713-8718.

Rolland-Lagan, A.G., Paquette M., Tweedle V., Akimenko M.A. (2012). Morphogen-based simulation model of ray growth and joint patterning during fin development and regeneration. *Development*, **139**(6), 1188-1197.

Rolland-Lagan, A.G., Amin M., Pakulska M. (2009). Quantifying leaf venation patterns: two-dimensional maps. *The Plant Journal*, **57**(1), 195-205.

Roselló-Díez A., Ros M.A., Torres, M. (2011). Diffusible signals, not autonomous mechanisms, determine the main proximodistal limb subdivision. *Science*, **332**(6033), 1086-1088.

Santamaria J.A., Mari-Beffa M., Santos-Ruiz L., Becerra J. (1996). Incorporation of bromodeoxyuridine in regenerating fin tissue of the goldfish *Carassius auratus*. *Journal of Experimental Zoology,* **275**, 300–307.

Santos-Ruiz L., Santamaria J.A., Ruiz-Sanchez J., Becerra J. (2002). Cell proliferation during blastema formation in the regenerating teleost fin. *Developmental Dynamics,* **223**, 262–272.

Salo E., Abril J., Adell T. (2009). Planarian regeneration: achievements and future directions after 20 years of research. *Developmental Biology,* **53**, 1317–1327

Schulte C.J., Allen C., England S.J., Juárez-Morales, J.L., Lewis KE. (2011). *Evx1* is required for joint formation in zebrafish fin dermoskeleton. *Developmental Dynamics*, **240**(5), 1240-1248.

Sims K., Eble D.M., Iovine M.K. (2009). Connexin43 regulates joint location in zebrafish fins. *Developmental Biology*, ***327***(2), 410-418.

Smith A., Zhang J., Guay D., Quint E., Johnson A., Akimenko M.A. (2008). Gene expression analysis on sections of zebrafish regenerating fins reveals limitations in the whole-mount in-situ hybridization method. *Developmental Dynamics,* **237**(2), 417-25.

Sullivan G.M., Feinn R. (2012). Using effect size-or why the P value is not enough. *Journal of Graduate Medical Education*, ***4*****(**3), 279-282.

Spemann H., Mangold H. (2001). Induction of embryonic primordia by implantation of organizers from a different species. *Developmental Biology*, **45**(1), 13.

Thummel R., Bai S., Sarras M.P., Song P., McDermott J., Brewer J., Goodwin A.R. (2006). Inhibition of zebrafish fin regeneration using *in vivo* electroporation of morpholinos against *fgfr1* and *msxb*. *Developmental Dynamics*, **235**(2), 336-346.

Turing A.M. (1952) The chemical basis of morphogenesis. *Philosophical Transactions of the Royal Society of London. Series B, Biological Sciences,* **237**:37–72

Tremblay B. (2013). Theoretical approaches to joint pattern formation in zebrafish caudal fins. B.Sc. Thesis. *University of Ottawa*. Canada

Tweedle V. (2012). Simulation model of ray patterning in zebrafish caudal fins. M.Sc. Thesis. *University of Ottawa*. Canada

Villalobos F.J., Hall A.J., Ritchie J.T., Orgaz F. (1996). OILCROP-SUN: A development, growth, and yield model of the sunflower crop. *Agronomy Journal*, **88**(3), 403-415.

Waddington C.H. (2011). Biological Processes in Living Systems: Toward a Theoretical Biology. *AldineTransaction* (Vol. 4).

Westerfield M. (1995). General methods for zebrafish care. *Westerfield, M: The Zebrafish Book: a Guide for the Laboratory Use of Zebrafish*, **1**-1.

White P., Brestelli J.E., Kaestner K.H., Greenbaum L.E. (2005). Identification of transcriptional networks during liver regeneration. *Journal of Biological Chemistry*, **280**(5), 3715-3722.

Wolpert L. (1969). Positional information and the spatial pattern of cellular differentiation. J*ournal of Theoretical Biology*, **25**(1), 1-47.

Wolpert L. (1972). Positional information and pattern formation. *Current Topics in Developmental Biology*, **6**, 183.

Wolpert L. (2002). Principles of Development. second edition, *Oxford University Press*, New York, (pp 15).

Zhang S., Zhang X.S., Chen L. (2008). Biomolecular network querying: a promising approach in systems biology. *Systems Biology*, ***2***(1), 5.

Zhang J., Jeradi S., Strahle U., Akimenko M.A. (2012). Laser ablation of the sonic hedgehog-a-expressing cells during fin regeneration affects ray branching morphogenesis. *Developmental Biology*, **365** (2), 424-433.

Zhou S, Degan S, Potts E.N., Foster W.M., Sunday M.E. (2009) *NPAS3* is a trachealess homolog critical for lung development and homeostasis. *Proceedings of the National Academy of Sciences of the United States of America,* **106**:11691–11696.

Chapter 8 – Appendices

8.1 Files of Extracted Fin Data

All data were stored in three excel files:

1) Whole fin: Contains data regarding total fin lengths, widths, areas, number of rays and total number of segments per sample at every extracted time-point divided per type of amputation.
2) Ray length data: Contains information from each ray classified according to assigned ray number during the tracking rays across time-points step. It shows the length of ray sections, total ray length obtained by measuring both longest branch as well as the mean length of all branches, the number of bifurcations.
3) Segment by ray data: Contains the segment patterns divided by ray number. Quantification of all segment data, such as total and average segment lengths, number of segments, and also the IDs assigned to each individual segment.

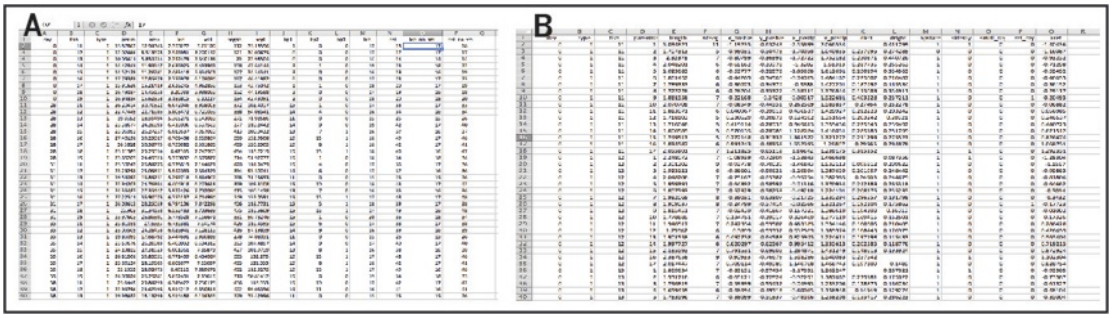

Figure 8.1 Management of extracted fin data. **(A)** Whole fin data. **(B)** Segment data arranged by section (data is still not ready to analyse based on appropriate ray order).

8.2 Measuring Segments at Amputation Plane Using ImageJ

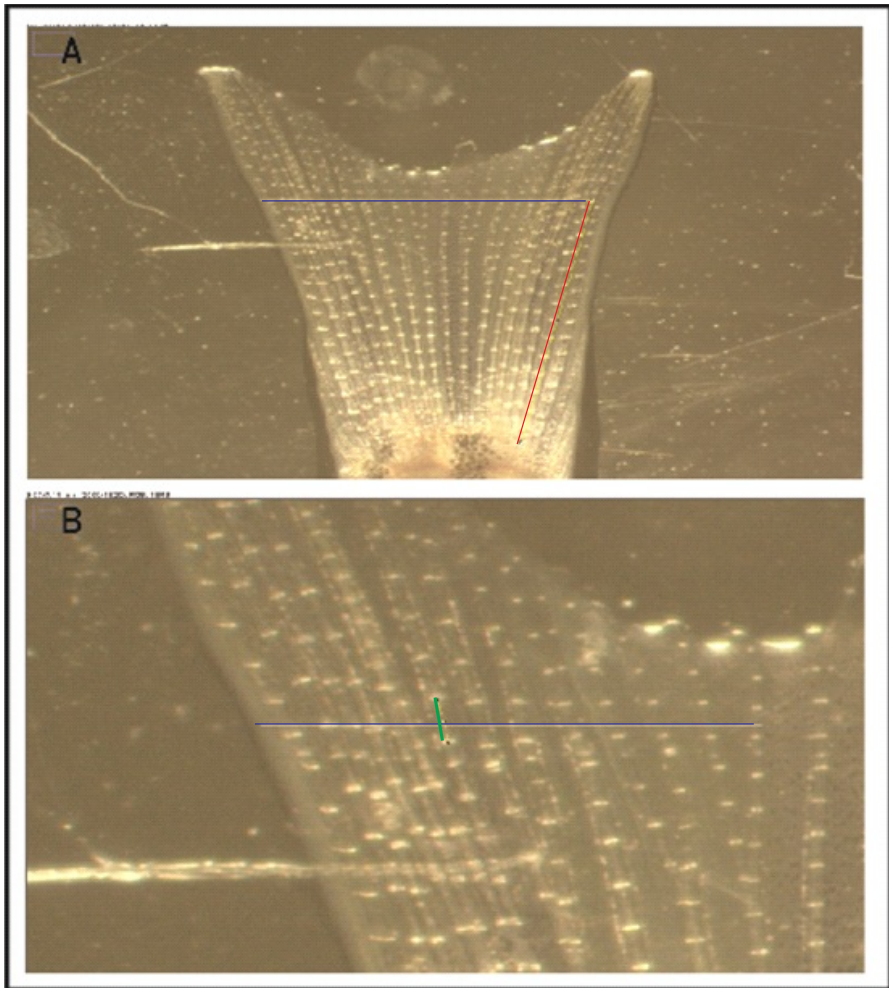

Figure 8.2 Determining Amputation Plane with ImageJ. **(A)** Identification of the amputation plane. **(B)** Measurement of individual segments located at the amputation plane

8.3 Stepwise Regression for Tested Parameters

Alpha-to-Enter: 0.001 Alpha-to-Remove: 0.001

Response is rmse on 4 predictors, with N = 375

Step	1	2	3	4
Constant	0.3429	-0.4668	-1.2521	-0.3339
beta	1.058	1.058	1.058	1.058
T-Value	12.42	14.25	16.42	19.39
P-Value	0.000	0.000	0.000	0.000
prodG		0.0810	0.0810	0.0810
T-Value		10.91	12.56	14.84
P-Value		0.000	0.000	0.000
prodX0			0.0357	0.0357
T-Value			11.07	13.08
P-Value			0.000	0.000
Dx				-0.1148
T-Value				-12.14
P-Value				0.000
S	0.233	0.203	0.177	0.149
R-Sq	29.27	46.41	59.72	71.19
R-Sq(adj)	29.08	46.12	59.40	70.88
Mallows Cp	537.5	319.4	150.4	5.0

Appendix 8.3 Stepwise regression for parameters as predictors of RMSE: Intial production of morphogen X (prodX0), Diffusion of morphogen X (Dx), Production of morphogen G (prodG) and increase of production of morphogen X in function of time (beta).

8.4 Types of Amputation

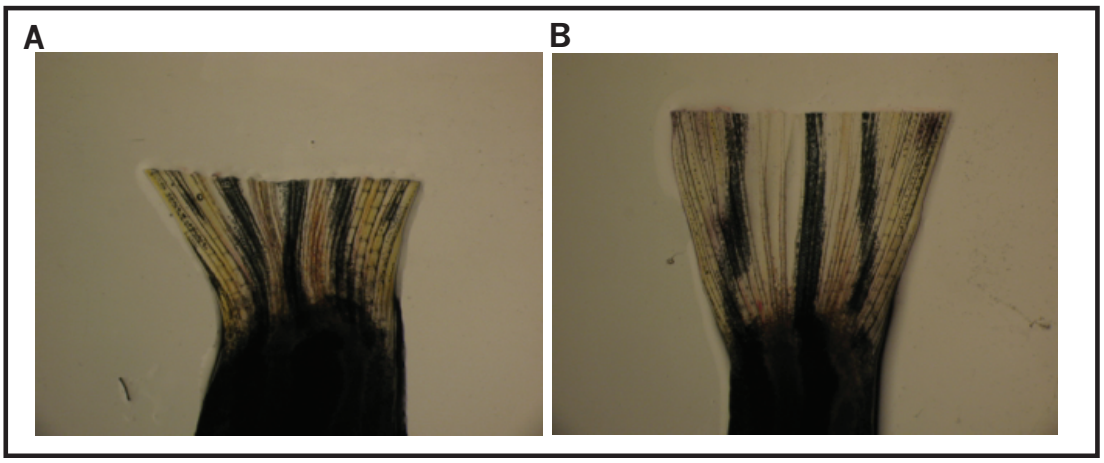

Figure 8.4 Amputation types. **(A)** Proximal amputation (2 mm) from fin base. **(B)** Distal amputation (4 mm) from fin base.

8.5 Segment Regression Data by Ray Number

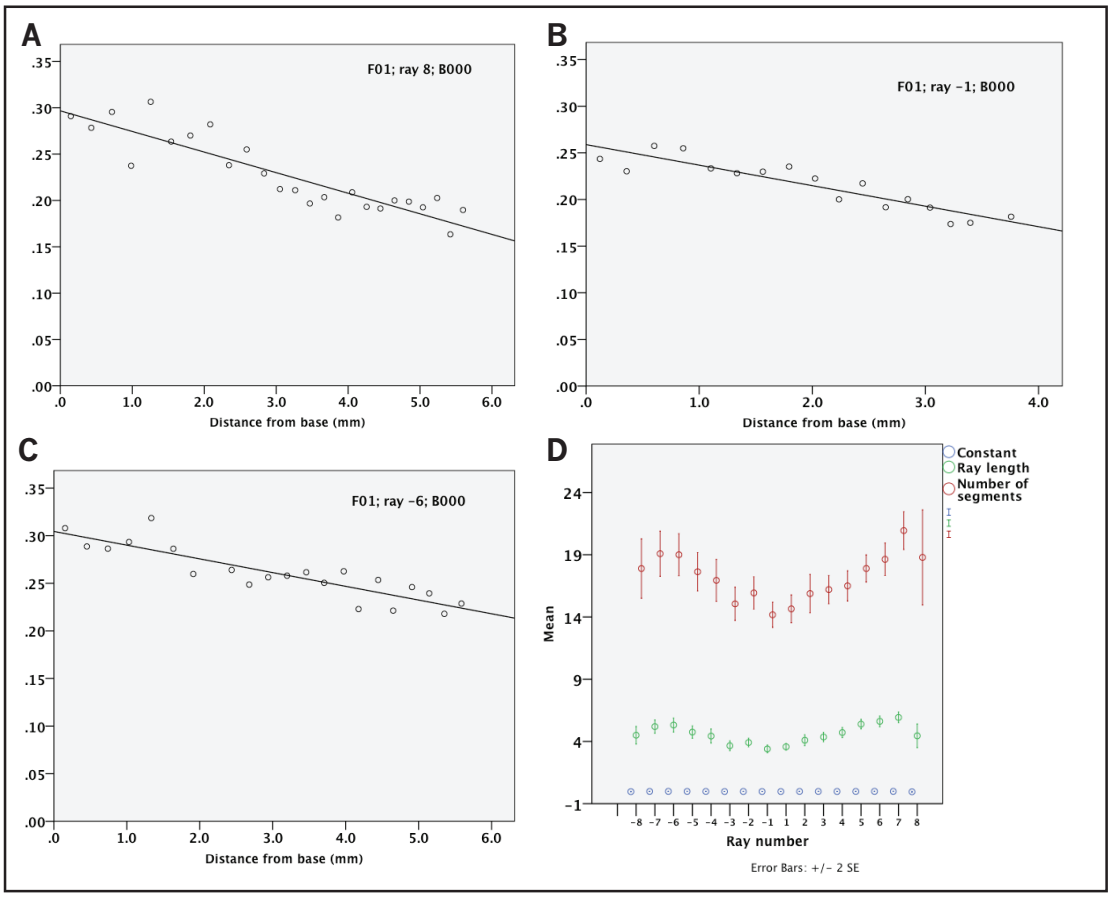

Figure 8.5 Differences in segment regression data before amputation as a result of ray numbering. **(A)** Changes in segment length of ray [8] in function to distance from base. **(B)** Changes in segment length of ray [-1] in function to distance from base. **(C)** Segment length in ray [-6] in function to distance from base. **(D)** Average number of segments per ray, mean ray length and length of first segments based on ray number.

8.6 Ray Data Re-arranged to the 17 Ray-zones

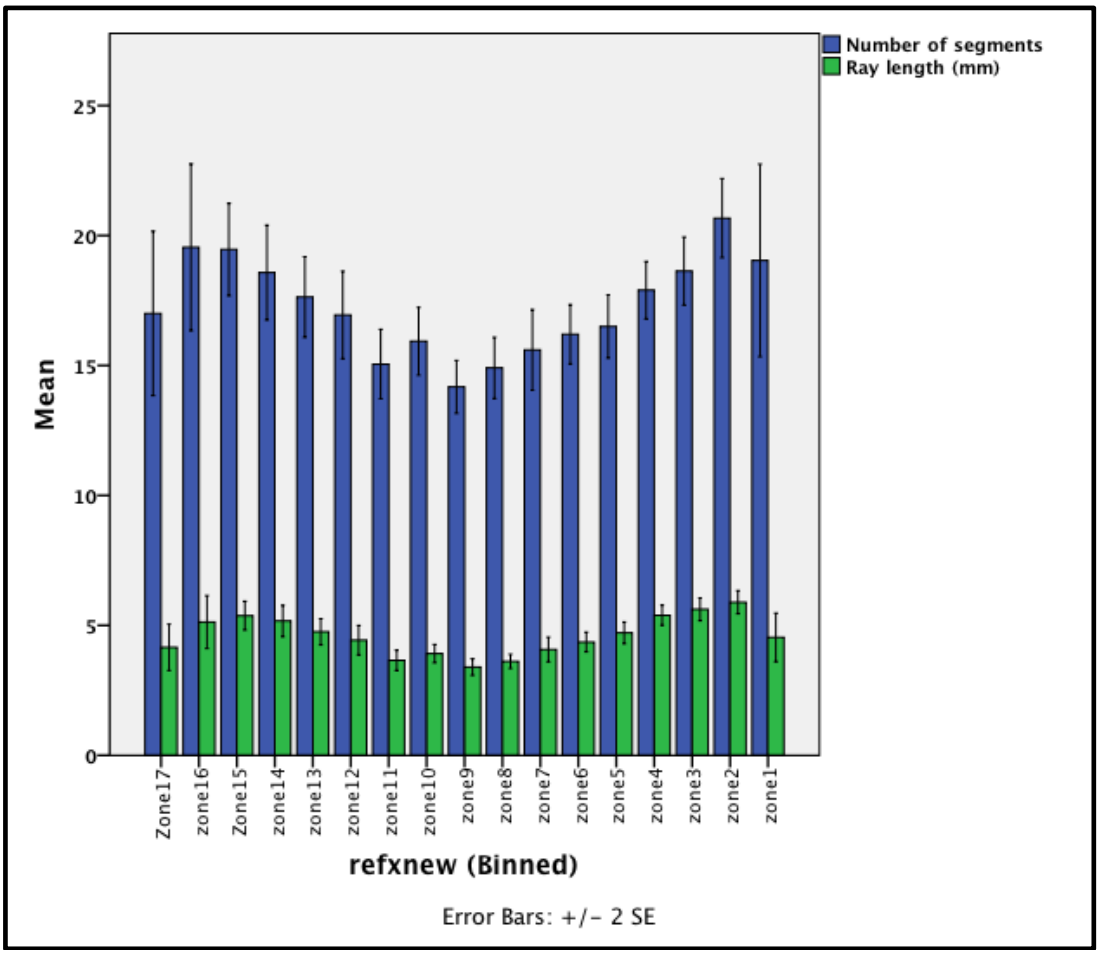

Figure 8.6 Ray data at B000 re-assigned to each ray-zone based on their lateral-medial position at the base of the fin.

8.7 Differences Between Ray Lengths Using Longest and Mean branches

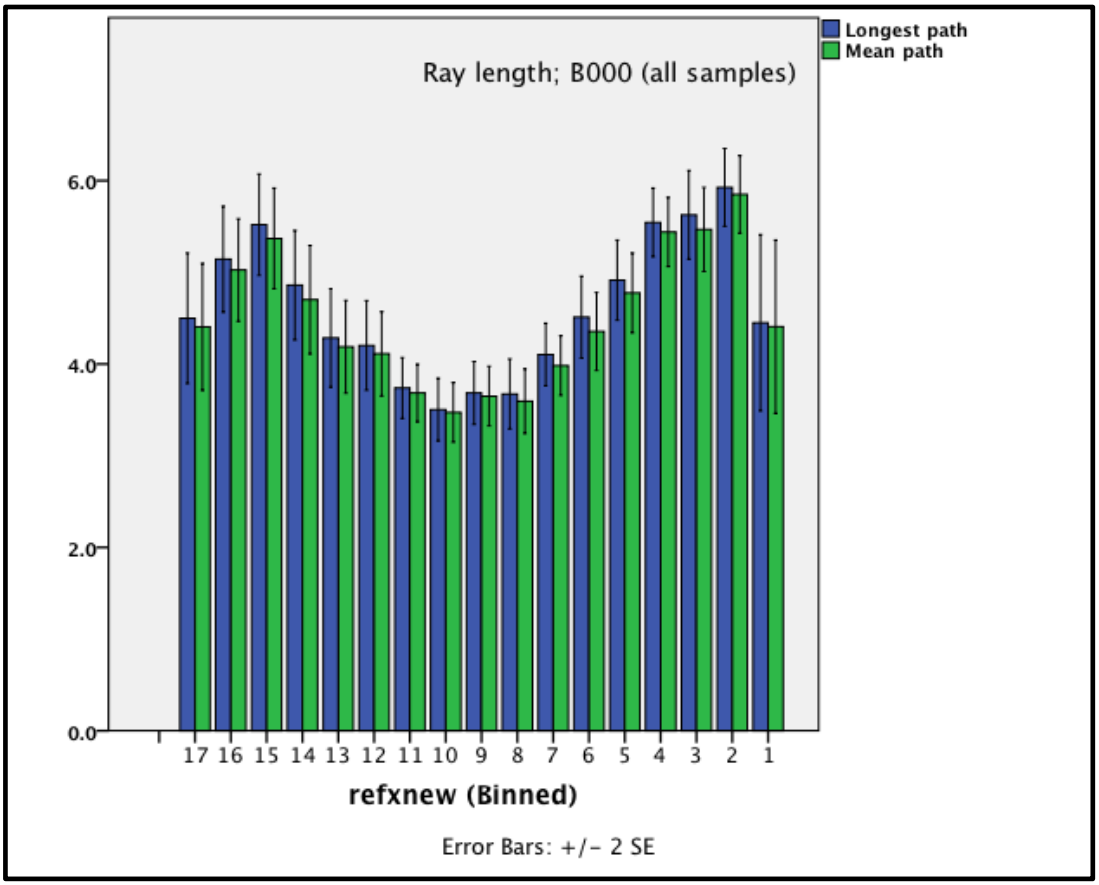

Figure 8.7 Mean rays length at B000 after re-arrange using the longest ray branch (blue) and the average value from all branches (green), when dealing with bifurcations.

8.8 Standard Error Maps

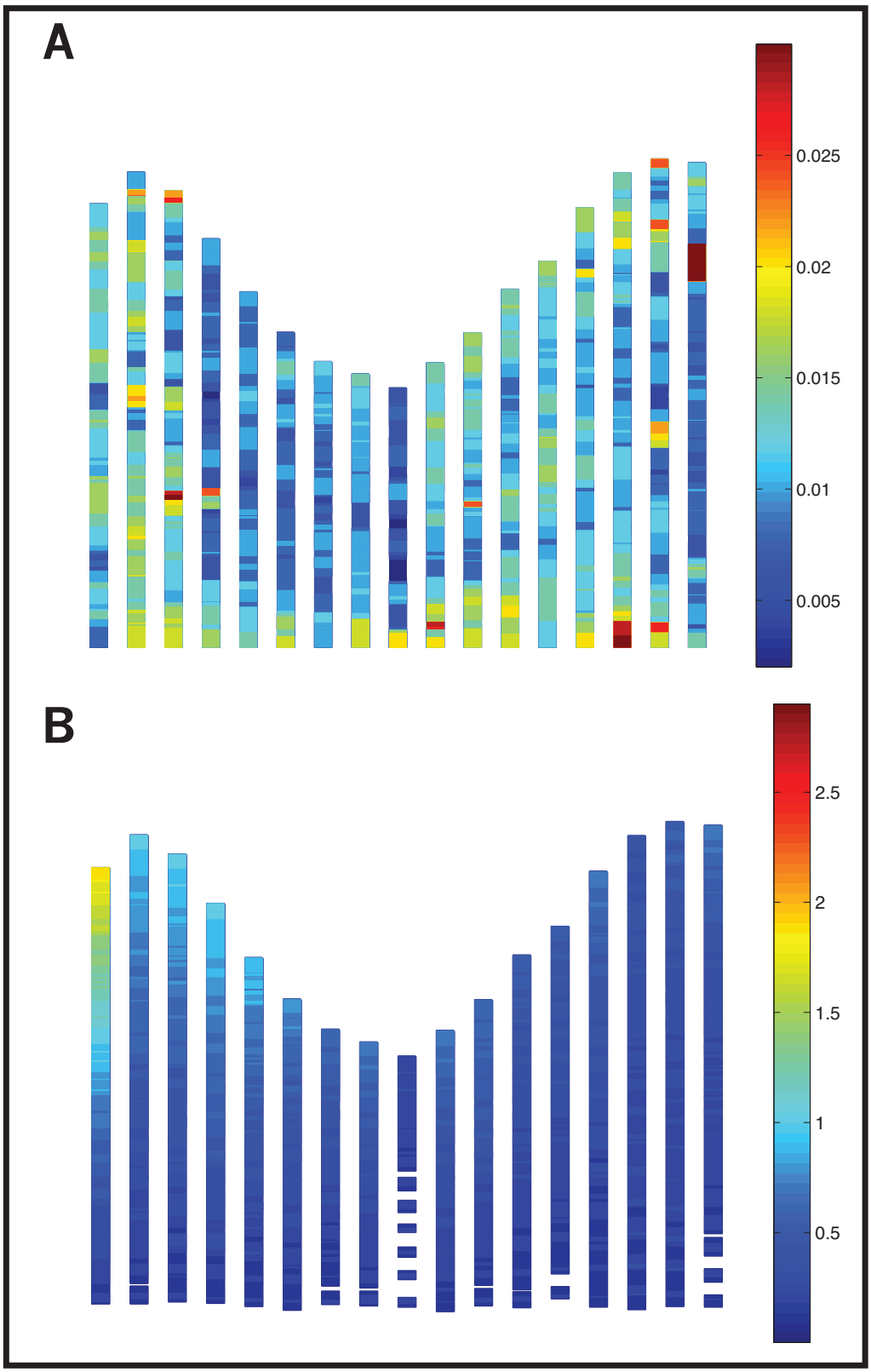

Figure 8.8 Standard error maps **(A)** Standard error of segments length (see figure 4.9A) **(B)** Standard error of segment positions based on their ID (see figure 4.9B).

8.9 Number of Segments in the Simulation Output

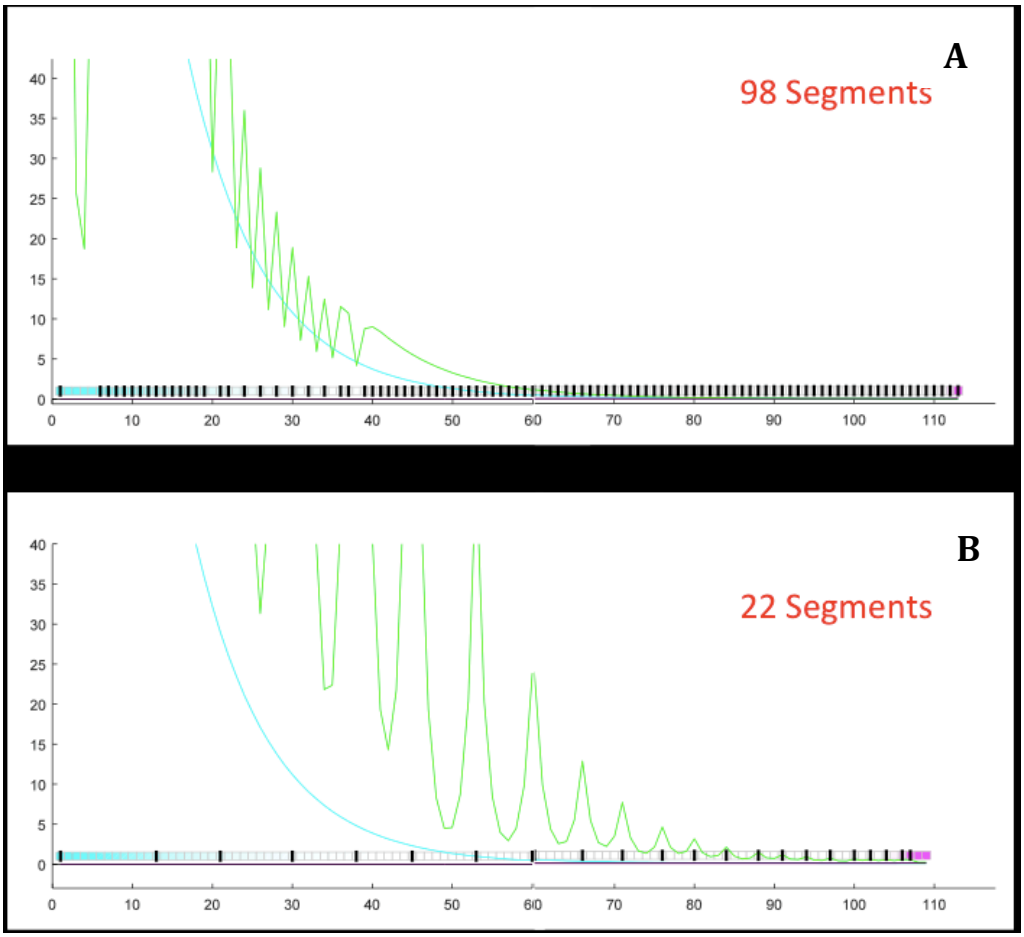

Figure 8.9 Simulation output of a single ray at 167 dpf with different parameter values for joint spacing control. **(A)** Simulation after 167 dpf using old parameter values for morphogens "S" and "Ds". **(B)** Simulation after 167 dpf with the increased values for morphogen "S" and "Ds" as reported in Table 4.

8.10 Comparison of Raw Data and Re-assigned Data in Positional Ray-zones

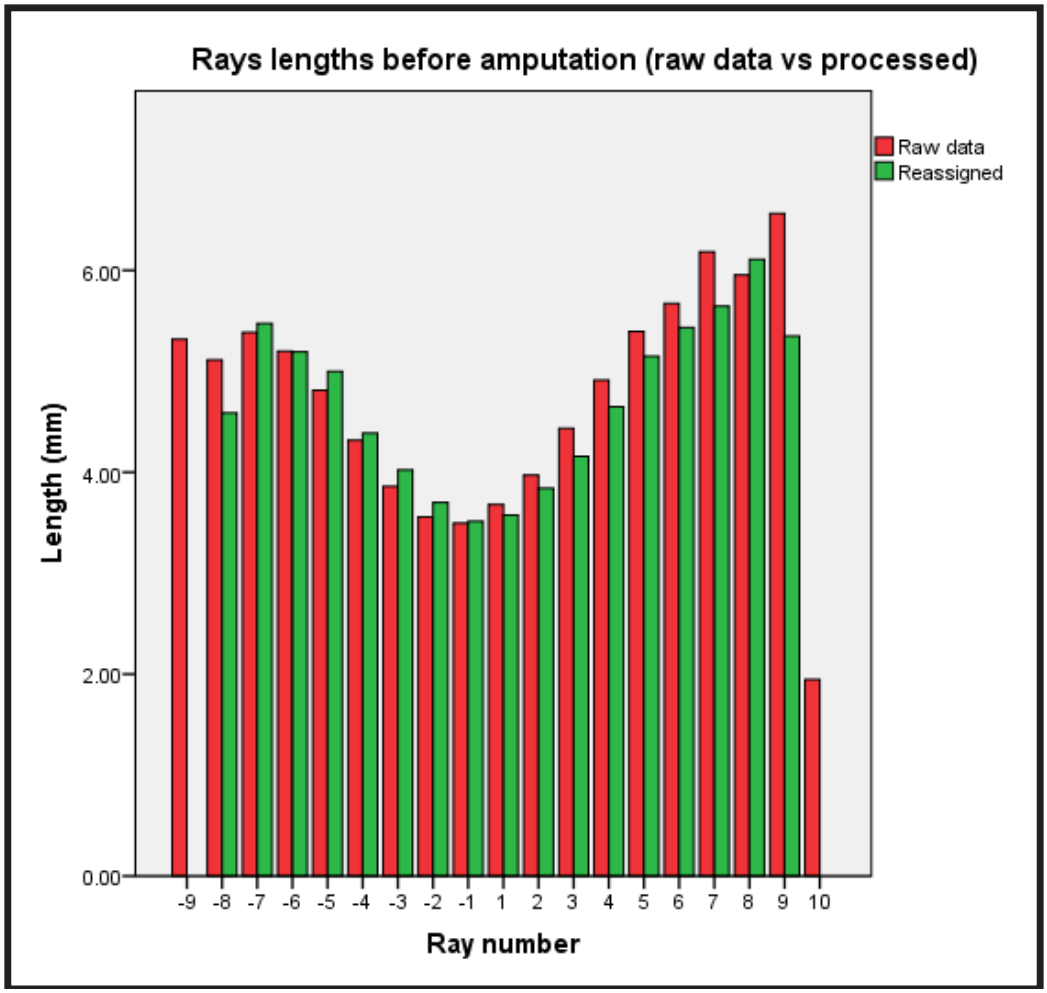

Figure 8.10 Comparison of ray length at B000 with ray data re-assigned (green) against raw data (red) without the most lateral rays [-10 & 11]. Removing these rays from analysis does not solve the high variability and error produced from ray number differences.